ISTANBUL TECHNICAL UNIVERSITY ★ GRADUATE SCHOOL OF SCIENCE ENGINEERING AND TECHNOLOGY

A NUMERICAL INVESTIGATION ON PASSIVE FLOW CONTROLS OF OPEN CAVITIES AT TRANSONIC SPEEDS

M. Sc. THESIS

Oğuzhan DEMİR

Department of Aeronautical and Astronautical Engineering

Aeronautical and Astronautical Engineering Programme

JUNE 2019

ISTANBUL TECHNICAL UNIVERSITY ★ GRADUATE SCHOOL OF SCIENCE ENGINEERING AND TECHNOLOGY

A NUMERICAL INVESTIGATION ON PASSIVE FLOW CONTROLS OF OPEN CAVITIES AT TRANSONIC SPEEDS

M. Sc. THESIS

Oğuzhan DEMİR
511161138

Department of Aeronautical and Astronautical Engineering

Aeronautical and Astronautical Engineering Programme

Thesis Advisor Assoc. Prof. Dr. Bayram ÇELİK
Thesis Co-Advisor: Assoc. Prof. Dr. Kürşad Melih GÜLEREN

JUNE 2019

İSTANBUL TEKNİK ÜNİVERSİTESİ ★ FEN BİLİMLERİ ENSTİTÜSÜ

AÇIK KAVİTELERİN PASİF KONTROLÜNÜN TRANSONİK AKIŞLARDA SAYISAL İNCELENMESİ

YÜKSEK LİSANS TEZİ

Oğuzhan DEMİR
511161138

Tez Danışmanı: Doç. Dr. Bayram ÇELİK
Eş Danışman: Kürşad Melih GÜLEREN

HAZİRAN 2019

Oğuzhan Demir, a M.Sc. student of ITU Graduate School of Science Engineering and Technology student ID 511161138, successfully defended the thesis/dissertation entitled "A NUMERICAL INVESTIGATION ON PASSIVE FLOW CONTROLS OF OPEN CAVITIES AT TRANSONIC SPEEDS", which he prepared after fulfilling the requirements specified in the associated legislations, before the jury whose signatures are below.

Thesis Advisor :	**Assoc. Prof. Dr. Bayram ÇELİK** İstanbul Technical University	.....
Co-advisor :	**Assoc. Prof. Dr. Kürşad Melih GÜLEREN** Eskişehir Technical University	.....
Jury Members :	**Prof. Dr. Mehmet ŞAHİN** İstanbul Technical University	.....
	Asst. Prof. Dr. Kemal Bülent YÜCEİL İstanbul Technical University	.....
	Assoc. Prof. Dr. Tolga YASA Eskişehir Technical University	.....

Date of Submission : 03 May 2019
Date of Defense : 11 June 2019

To my family,

FOREWORD

First of all, I would like present my gratitudes to my supervisors Assoc. Prof. Dr. Bayram Çelik and Assoc. Prof. Dr. Kürşad Melih Güleren for training me through my acamedic life in every aspect of aeronautical engineering. They have been significantly helpful and patient to me and pushed me to be a better engineer. I also feel indebted to my esteemed project colleagues Osman Mirza Demircan and Seyfettin Türk for their support and advices throughout the studies conducted in this thesis. It has been an honour to work with these two engineers.

I would like to thank Damla for all her love and support throughout the entire process.

I also would like to thank my colleagues Erdem Turan, Ahmet Serkan Altınok, Musa Onur Öztürkmen and Doruk Turgul, for their assistance and suggestions throughout the writing process of this thesis.

Lastly but most importantly, I would like to state that I will always feel indebted to my family because they were always with me and I always felt their presence at every moment of my life.

Studies within the scope of thesis were run on the National Center for High Speed Computing UHeM (http:(//en.uhem.itu.edu.tr/). This study is supported by the Turkish Aerospace Industries (https://tai.com.tr/en) under the grant of TM-2013. The autor(s) are grateful to the authorized staff for their support, funding and assistance with this study.

May 2019

Oğuzhan Demir
Aeronautical Engineer

TABLE OF CONTENTS

Page

ABBREVIATIONS

ABB	**:** Ayrık Burgaç Benzetimi
CFD	**:** Computational Fluid Dynamics
CTS	**:** Convective Time Scale
DES	**:** Detached Eddy Simulations
DILU	**:** Diagonal Incomplete Lower-Upper
DNS	**:** Direct Numerical Simulation
FFT	**:** Fast Fourier Transform
GAMG	**:** General Algebraic Multi-Grid
HAD	**:** Hesaplamalı Akışkanlar Dinamiği
HWA	**:** Hot Wire Anemometry
LDV	**:** Laser Doppler Velocimetry
LES	**:** Large Eddy Simulation
MILES	**:** Monotone Integrated Large Eddy Simulation
NVD	**:** Normalised Variable Diagram
OASPL	**:** Overall Sound Pressure Level
OpenFOAM	**:** Open source Field Operation and Manipulation
PBiCGStab	**:** Stabilized Preconditioned Bi-Conjugate Gradient
PISO	**:** Pressure-Implicit-Split-Operator
PIV	**:** Particle Image Velocimetry
PSD	**:** Power Spectral Density
RANS	**:** Reynolds Averaged Navier Stokes
RMS	**:** Root Mean Square
SA	**:** Spalart Allmaras
SIMPLE	**:** Semi-Implicit-Method-Of-Pressure-Linked-Equations
SPL	**:** Sound Pressure Level
SST	**:** Shear Stress Transport
TVD	**:** Total Variation Diminishing
UHeM	**:** National Center for High Performance Computing
URANS	**:** Unsteady Reynolds Averaged Navier Stokes
USAF	**:** United States Air Force

SYMBOLS

C_{DES} : DES model calibration constant
C_{μ} : Turbulence model constant
D : Depth of the cavity
E : Total energy
I : Turbulence intensity
L : Length of the cavity
L_t : Turbulent length scale
Ma_{∞} : Freestream Mach number
N : Number of gathered pressure data
P_k : Production term
$\widetilde{P}_k$: Modified production term
R : Universal gas constant
Re : Reynolds Number
S : Invariant measure of strain rate
S_C : Constant part of source term
S_P : Non-linear part of source term
S_S : Effective temperature
S_{ij} : Rate of strain tensor
S_{ϕ} : Source term for a general scalar
St_n : Strouhal Number for nth mode frequency
T : Temperature
T_0 : Reference temperature
U : Velocity
V_P : Control volume
W : Width of the cavity
f_n : n^{th} mode frequency
k : Turbulence kinetic energy
n : n^{th} Rossiter mode
p : Pressure

p_i : Instantaneous value of pressure

q_j : Heat flux

$\bar{s}_{ij}$: Strain rate tensor

u_i, u_j : Velocity vector

$\bar{u}_i$: Filtered velocity vector

t : Time

x_i, x_j : Spatial coordinate

y : Wall distance

σ_{ij} : Shear stress tensor

Δ : Maximum local grid spacing

∇ : Nabla operator

α : Phage lag constant

β^* : Turbulence model constant

γ : Specific heat ratio

κ : Thermal conductivity

κ_v : Phase delay constant

μ : Dynamic viscosity

μ_0 : Reference viscosity

ν : Kinematic viscosity

ν_t : Turbulent eddy viscosity

ρ : Density

ω : Turbulence specific dissipation rate

ϵ : Turbulence dissipation rate

ϕ : General scalar

LIST OF TABLES

Page

LIST OF FIGURES

Page

A NUMERICAL INVESTIGATION ON PASSIVE FLOW CONTROLS OF OPEN CAVITIES AT TRANSONIC SPEEDS

SUMMARY

Cavity flows have been an interesting subject since 1950's when the studies on internal weapon bays were first conducted. Since then, numerous experimental, theoretical and numerical researches have been performed on the subject. Despite the simple geometry, cavity flows have a complex and unsteady flow physics behind. Besides internal weapon bays, cavity flows may also be encountered in wheel wells, car sunroofs and windows, and so on.

A major problem that has been related to cavities is the generation of excessive noise and presence of severe pressure oscillations. In open cavities where the flow has the sufficient energy to bridge the cavity, a self-oscillation mechanism takes place. The flow that is separated from the cavity leading edge which forms a free shear layer along the cavity mouth region up until the cavity trailing edge, impinges on cavity aft wall and interacts with it, and eventually generates strong acoustic waves. These acoustic waves then travel upstream and interact with the vortices that formed because of the separation of the flow at cavity leading edge and with the free shear layer, resulting in an excitement of the flow. This feedback mechanism and acoustic interactions result in severe pressure oscillations, noise generation and vibration. Many studies conducted over time have shown that the aft wall of cavity, the main source of the sound, has non-negligible importance on these studies. In order to reduce the noise generated by cavity flows, numerous researches have been conducted over the years and continue to be done.

The fundamental aim of this thesis is to examine and comprehend the physics of cavity flows and at the same time endeavouring the reduction of noise generation and minimization highly oscillatory behavior of the flow. The methods applied to reduce the noise generation in the cavity flows are divided into two as passive and active control methods. Active flow control methods require an energy input to the system whilst passive flow control methods require no such input. Making various changes to the cavity geometry or adding/subtracting some external devices to/from the cavity are some of the well-known methods that may be categorized as passive flow control methods. Considering that the passive flow control methods have a wider area of usage than passive flow control methods, they have been emphasized in this thesis.

In the present thesis, firstly, a rectangular shaped cavity with no flow control mechanism is investigated. Following to that, various passive flow control methods such as reshaping cavity walls (front, aft walls), placing external devices to cavity upstream wall (spoilers, vortex generators), injecting/sucking flow passively to/from the cavity and combining some of the aforementioned methods are applied with the aim of reducing the noise generation.

Within the scope of the thesis, cavity flow analyses are conducted numerically. Simulations were carried out with a Finite Volume Navier-Stokes solver of the open-source software OpenFOAM® (Open source Field Operation and Manipulation). The compressible solver of OpenFOAM®, rhoPimpleFoam is used. The rectangular shaped cavity geometry has L/D ratio of 5 and W/D ratio of 1. The length of the cavity is specified as 0.508 meters and the depth and the width as 0.1016 meters. Freestream Mach number is taken as 0.85 which corresponds to a Reynolds number of ~$1x10^7$ based on the cavity length. A Detached Eddy Simulation (DES) method based on the $k-\omega$ Shear Stress Transport (SST) Unsteady Reynolds Averaged Navier-Stokes (URANS) turbulence model is used throughout the simulations. Transient analyses were conducted for a Courant number of less than unity with a time step of ~10^{-6} seconds. One convective time scale (CTS) is calculated as the passage of a flow particle through the cavity length and analyses are carried out for 50 CTS. Data of last 40 CTS are stored and used for the result of mean values. Probes are placed to cavity floor at ten different locations to measure the pressure history. The simulations were carried out using 200-280 cores in a parallel manner. The high number of required computational power, large number of grids and great number of configurations have obligated the use of parallelization.

Results of passive flow control methods are gathered and compared with both each other and with the original baseline cavity. Results of baseline cavity, that is named as clean cavity, are compared with the available experimental and numerical findings with the aim of validation. Discrete acoustic tones seen in cavity, called Rossiter modes, have been compared and similar results are found with the theoretical and experimental data. Mean longitudinal velocity profiles are compared with the available numerical data and satisfactory consistence is observed. Overall sound pressure level (OASPL) distribution on cavity floor was caught in general and the profiles are seen to be similar with a slight overprediction of ~5 dB than the experimental data. This overprediction is also seen in other numerical studies in the literature.

Once the validation of the current model is obtained, passive flow control methods are analyzed. Considering the aft wall being the main source of the noise generation, aft wall configurations have proven to be useful in terms of noise reduction. Spoiler and vortex generators have also been found to be efficient since they lift or deteriorate the incoming boundary layer. Inclining the cavity aft wall by 45° has reduced the OASPL distribution on cavity floor by ~10 dB since this inclination diverts the pressure waves outside of the cavity and prevent the strong excitations of the flow. Combined passive flow controls -applied in this study- where aft wall modifications are implemented simultaneously with spoilers have also been effective at noise reduction.

Results are also examined in terms of flow contours, isosurfaces and pressure histories. Mean contours of Mach, turbulence intensity, OASPL are inspected for and compared with each configuration. Instantaneous contours of flowfield are also given to provide a more detailed insight to unsteady nature of the cavity flow. Isosurfaces of Q-criterion colored by x-vorticity are presented to visualize the chaotic three dimensional behavior of the flow.

Applicability and success of open-source software for such challenging flows have been investigated within the scope of this thesis. It is also shown the open source software OpenFOAM®, with proper parallelization settings, might be an appropriate tool for problems that require high computing powers.

AÇIK KAVİTELERİN TRANSONİK HIZLARDA PASİF AKIŞ KONTROLÜNÜN İNCELENMESİ

ÖZET

Kavite akışları, 1950'lerden itibaren birçok alanda araştırmaya konu olmuş, aerodinamik ve aeroakustik alanlarında önemli bir yer edinen ve içinde birden çok disipline ait olgular barındıran bir akış tipi olma özelliğine sahiptir. Kavite akışı araştırmaları, 1950'lerde dâhili silah yuvalarının kullanımı fikrinin ortaya çıkmasıyla ile başlamış olup günümüzde halen devam etmektedir. Son zamanlarda, yeni nesil savaş uçaklarının radar kesit alanlarını azaltma, maruz kaldıkları aerodinamik sürükleme ve ısınmaları en aza indirgeme gereksinimleri gibi ihtiyaçlar sebebiyle kavite çalışmaları yeniden hız kazanmıştır. İlk zamanlarda çoğunlukla teorik ve deneysel olarak yürütülen çalışmalar, güçlü bilgisayar donanımlarının ve hesaplama yeteneklerinin ortaya çıkması sayesinde, günümüzde sayısal olarak da yürütülmektedir. Kavite akışları sadece dâhili silah yuvalarında değil, uçakların iniş takımları, kara araçlarının pencereleri ve açılır tavanları gibi birçok alanda pratik olarak görülebilmektedir.

Kavitelerin yarattığı en büyük sorunlardan birisi oluşan yüksek basınç salınımları ve gürültüdür. Kaviteler, açık ve kapalı olarak iki ana kategoriye ayrılmaktadır. Açık kavitelerde, öz salınım sebebiyle yüksek derecede gürültü oluşabilmektedir. Kavite hücum kenarından kopan ve serbest bir kayma tabakası şeklinde girdaplar üreterek ilerleyen akış, kavite firar kenarına çarpıp bu kenar ile etkileşime girerek güçlü akustik dalgaların oluşumuna neden olmaktadır. Oluşan akustik dalgalar yukarı akım yönünde ilerlemekte ve firar kenarından kopup gelen tabaka ve girdaplarla etkileşime girerek bu girdapları etkilemektedir. Bu geri besleme mekanizması ve akustik etkileşimler, yüksek basınç salınımlarına, gürültü ve titreşime yol açmaktadır. Zaman içerisinde yapılan birçok çalışma, kavitelerde temel ses kaynağı olan arka duvarın önemli bir role sahip olduğunu göstermiştir. Kavitelerin oluşturduğu gürültüyü azaltmak amacıyla yıllar içerisinde birçok araştırma yapılmıştır ve yapılmaya devam etmektedir. Yolcu uçaklarının iniş takımlarının kapaklarının açılması nedeniyle oluşan kaviteler 160 dB seviyelerinde ses oluşturabilmekte, bu ses ise pilotlar için yanıltıcı, yolcular için rahatsız edici olabilmektedir. Bomba ve füze dâhili yuvalarının oluşturduğu kaviteler ise yüksek basınç salınımları sonucu mühimmatın uçaktan güvenli ayrılmasını engelleyebilmekte, kavitenin çevresindeki yapıya ve sonuç olarak uçağa zarar verebilmektedir. Kavite akışları, geometrik olarak basit bir şekle sahip olmasına rağmen akışın düzensizliği sebebiyle zorlu bir fiziğe sahip bir problem olarak öne çıkmaktadır. Bu sebeple dikkatli bir şekilde ele alınmalı ve incelenmelidir.

Bu tez, kavite akışlarını incelemeyi, anlamayı ve kavite akışlarında ortaya çıkan gürültüyü en aza indirgemeyi amaçlamaktadır. Kavite akışlarında gürültü oluşumunu azaltmak için kullanılan yöntemler pasif ve aktif olarak ikiye ayrılmaktadır. Aktif kontrol yöntemleri sisteme harici bir enerji girdisi gerektirirken, pasif kontrol yöntemlerinde böyle bir ihtiyaç duyulmamaktadır. Pasif kontrol yöntemleri, kavite

geometrisine çeşitli değişkeler yaparak veya kaviteye harici cihazlar ekleyerek akışı kontrol etmeyi amaçlayan yöntemler olarak özetlenebilir. Aktif yöntemlerde ise akışa ve kaviteye dışarıdan müdahaleler ve bir enerji alış-verişi söz konusu olmaktadır. Pasif kontrol yöntemlerinin aktif yöntemlere göre kullanım alanının daha fazla olması sebebiyle, bu tez kapsamında pasif kontrol yöntemleri üzerine durulmuştur. Tez içerisinde, öncelikle temiz kavite olarak adlandırılan, herhangi bir akış kontrol yöntemi içermeyen ve dikdörtgensel bir şekle sahip olan bir kavite incelenmiştir. Daha sonra bu kavite geometrisi üzerinde çeşitli pasif kontrol yöntemleri kullanılarak oluşan gürültünün azaltılması hedeflenmiştir. Bu pasif kontrol yöntemleri, kavite duvarlarının (ön, arka) çeşitli değişkeleri, kavite öncesine dış kontrol cihazlarının yerleştirilmesi (spoyler, girdap üreteci), kaviteden geometrik değişkelerle pasif emme ve üfleme yapılmasının sağlanması ve bahsedilen pasif kontrol yöntemlerinden birkaçının birleştirilmesi olarak sıralanabilir.

Tez kapsamında kavite araştırmaları sayısal bir şekilde gerçekleştirilmiştir. Hesaplamalı Akışkanlar Dinamiği (HAD) yöntemi ile yürütülen sayısal analizler, açık kaynak kodlu bir yazılım olan OpenFOAM® ile yapılmıştır. OpenFOAM® yazılımının sıkıştırılabilir, dolaşık akışlar için tasarlanmış olan ve zamana bağlı çözümler elde edilmesini sağlayan basınç-tabanlı alt-çözücüsü rhoPimpleFoam kullanılmıştır. 3 boyutlu olarak yürütülen analizlerde, temel alınan kavitenin L/D oranı 5, W/D oranı 1 olarak belirlenmiştir. 0.508 metre uzunluğa, 0.1016 metre derinliğe ve 0.1016 metre genişliğe sahip olan kavite, 0.85 Mach serbest akış hızında ve yaklaşık $1x10^7$ Reynolds sayısında incelenmiştir. Reynolds sayısı, kavite uzunluğu temel alınarak hesaplanmıştır. Yürütülen analizler için $k-\omega\,SST$ URANS dolaşım modelinin temel alındığı bir Ayrık Burgaç Benzetimi (ABB) olan $k-\omega\,SSTDES$ yöntemi kullanılmıştır. Zamana bağlı olarak yürütülen analizler, Courant sayısı biri geçmeyecek şekilde yaklaşık olarak 10^{-6} saniye zaman adımında yürütülmüştür. Bir taşınımsal zaman ölçeği, bir akış parçacığının kaviteyi boydan boya geçtiği süre olarak hesaplanmış ve analizler 50 taşınımsal zaman ölçeği süresince yürütülmüştür. Son 40 taşınımsal zaman ölçeğine ait verilerin ortalaması alınarak sonuç için saklanmıştır. Analizler süresince kavite tabanında 10 farklı noktada basınç ölçümleri yapılmış ve basıncın zamana bağlı profilleri oluşturulmuştur. Analizler, gereken hesaplama gücünün fazlalılığı, kullanılan hücre sayısının çokluğu ve çok fazla konfigürasyonun ele alınması sebebiyle paralel bir şekilde, 200-280 çekirdek kullanılarak gerçekleştirilmiştir.

Elde edilen sonuçlar, gerek temel alınan temiz kavite ile gerek kendi aralarında karşılaştırılmıştır. Temiz kavite analizleri, doğrulama amacıyla deneysel veriler ve daha önce gerçekleştirilmiş olan sayısal çalışma verileri ile karşılaştırılmıştır. Temiz kavite konfigürasyonu için Rossiter modları olarak da adlandırılan akustik keskin tonlar deneysel ve teorik verilerle kıyaslanmış, yakın sonuçlar elde edilmiştir. Kavite içerisindeki boylamsal hız profilleri daha önceki sayısal sonuçlarla karşılaştırılmış ve benzer profiller yakalanmıştır. Kavite tabanındaki ortalama ses basınç tayf düzeyi (OASPL) dağılımı profili genel hatlarıyla yakalanmış fakat deneysel verilere göre ~5 dB daha fazla değerlerle karşılaşılmıştır. Bu durum, literatürdeki sayısal çalışmalarda da göze çarpmaktadır. Kavite çevresindeki akış, Mach, dolaşım yoğunluğu, OASPL gibi birçok yönden ortalamalar alınarak incelenmiştir. Zamana bağlı hız konturları sayesinde akışın salınımlı ve düzensiz yapısı ortaya konulmuştur. Anlık Q-kriteri eşyüzeyleri gösterilerek akışın üç boyutlu dönel kaotik yapısı sunulmaya çalışılmıştır. Kavite tabanındaki kontrol noktalarından alınan basınç verileri sayesinde basıncın zamana bağlı dolaşık salınım profilleri incelenmiştir. Kavite tabanındaki OASPL

dağılımları hesaplanarak her bir konfigürasyonun yaptığı iyileştirmeler göz önüne serilmeye çalışılmıştır. Bu aşamadan sonra, pasif kontrol yöntemlerine ait incelemeler yapılmaya başlanmıştır.

Kavite arka duvarının gürültü oluşumunda oynadığı rol düşünüldüğü zaman, en önemli iyileştirmelerin arka duvar geometrisinin değiştirildiği konfigürasyonlarda olması beklenmiştir ve nitekim öyle de olmuştur. Ayrıca, kavite önüne yerleştirilen spoyler tarzı cihazların sınır tabakanın hareketini değiştirip, bu tabakaya kavite hücum kenarından ayrıldıktan sonra bir yükseltme kazandırdığı ve kayma tabakasının arka duvarla etkileşimini azalttığı için gürültü oluşumunun azaltılmasında faydalı olduğu görülmüştür. Kavite arka duvarına 45° eğim verilmesi, oluşan akustik ses dalgalarını kavite dışına yönlendirdiği için kavite tabanındaki OASPL profilinde ortalama ~10 dB civarında iyileştirme sağlamıştır. Kavite önüne yerleştirilen spoyler ve girdap üreteci çalışmalarında ise yine benzer derecelerde iyileştirmeler sağlanmıştır. Arka duvar konfigürasyonları ile spoyler konfigürasyonlarının birlikte uygulandığı birleşik pasif kontrol yöntemlerinde ise yine ortalam 8-9 dB iyileştirmeler sağlanmıştır.

Tez kapsamında, açık kaynak kodlu çözücülerin kullanılabilirliği ve kavite akışı gibi zorlu bir fiziğe sahip olan problemlerde gösterdiği başarı sunulmaya çalışılmıştır. Ek olarak, açık kaynak kodlu OpenFOAM® yazılımının, doğru paralleştirme ayarları ile yüksek hesaplama gücü gerektiren problemlerde uygun bir araç olabileceği gösterilmiştir.

1. INTRODUCTION

The present study is dedicated to understand turbulent cavity flows at transonic regime. The focus of this numerical investigation is the reduction of noise generation and severe pressure fluctuations generated by the cavity via numerous passive control technique. Compressible Navier-Stokes solver of OpenFOAM®, rhoPimpleFoam, is used for numerical analyses throughout the thesis.

1.1 Motivation

Internal weapon bays are subject to intensive interest and research, especially in the field of aeronautics, since 1950's. They have numerous advantages such as reducing radar cross section or aerodynamic drag of a fighter. Whereafter supersonic regimes are achieved, the aerodynamic heating has become a major problem for aircraft operating at that flight regime. Additional to aerodynamic benefits, because vibrations encountered by an external weapon bay may go up to catastrophic levels and damage the aircraft, internal weapon bays are also effective in structural manner. Considering these major concerns, internal weapon bays are advantageous in many aspects. Over the years, enhancing technologies and new high-level requirements of the military operations which demand high speeds and low radar visibility have increased the interest in internal weapon bays. The flow over the internal weapon bays while dropping the bomb is termed as cavity flow. A typical internal weapon bay is shown in Figure 1.1.

Figure 1.1 : A typical internal weapon bay [1].

Cavity flows are seen not only on internal weapon bays of a fighter aircraft but also on car sunroofs or windows, measurement windows, wheel wells, escape hatches, and so on. Therefore, the range of study of cavity is not only limited to aeronautics applications.

Cavity flows, which were studied experimentally in earlier decades, are now subject to extensive studies that aim both innovating and validating new methodologies with the help of developing computing technologies.

Cavities, depending on their classification may create high discrete acoustic tones or high levels of noise or violent nose-pitching moments which affect the separation of a bomb/missile from the aircraft and potentially harm the structural integrity of the surroundings. Eventually, the safety and success of the desired operation may be obstructed. Aforementioned vibrations and high levels of noise must be investigated carefully and reduced.

1.2 Literature Survey

Various types of studies have been conducted concentrating on the cavity flow problems since 1940's [2-5]. Thenceforward, studies ranging from theoretical investigations to numerical investigations have intended to understand the nature of complex flow physics of cavities. Pressure fluctuations, acoustic resonance excitations, flow instabilities and noise generation are among the most points of interest that are emphasized in these researches.

In this section, an extensive literature survey about studies on cavities is presented. Throughout this survey, fundamental physics of cavity flow and classification will be conveyed. Thereafter, theoretical, experimental and numerical studies that exist in the open literature will be mentioned and briefly explained. A summary of selected studies in literature will be also given as tables.

1.2.1 Cavity Flows

Cavity flows are essentially divided into three categories according to the behavior of the shear layer: open, transitional and closed cavities, respectively. Early studies by Stallings and Wilcox [6] and Plentovich et al. [7] have aimed to define the boundaries of this main classification. Stallings and Wilcox [6] have extensively investigated the cavity classification at supersonic speeds from Mach number 1.5 to 2.86, and

Plentovich et al. [7] have studied the classification at subsonic speeds. Briefly, open cavities generally have L/D ratio of less than 10, which is a typical bomb bay. Closed cavities generally have L/D ratio of more than 13, which is a typical missile bay of a fighter. Transitional cavity is formed between these boundaries and the characteristic of the flow is neither open nor closed [8]. Two additional cavity types are present when the flow regime is supersonic: transitional/open and transitional/closed cavity. Transitional/open cavities have a similar behavior to open cavities. Transitional closed/cavities, on the other hand, have similar behavior to closed cavities. An open cavity is a type of cavity where the flow has enough energy to bridge the cavity and generated shear layer impinges on the cavity aft wall; whereas, a closed type cavity is a cavity where the flow does not have the sufficient energy to bridge the cavity, resulting in the impingement of the shear layer on the cavity floor and then separation before reaching to the cavity aft wall. Even though the L/D ratio has a great effect on the cavity type classification, it is not the only parameter. Other parameters such as W/D ratio or flow regime (subsonic, supersonic or hypersonic) have an impact on the cavity type classification. The results that are originally obtained from the study of Plentovich et al. [7] and modificated with the data of ESDU [9] have shown that the behavior of the pressure coefficient at the cavity floor was a representative of the cavity classification (Figure 1.2).

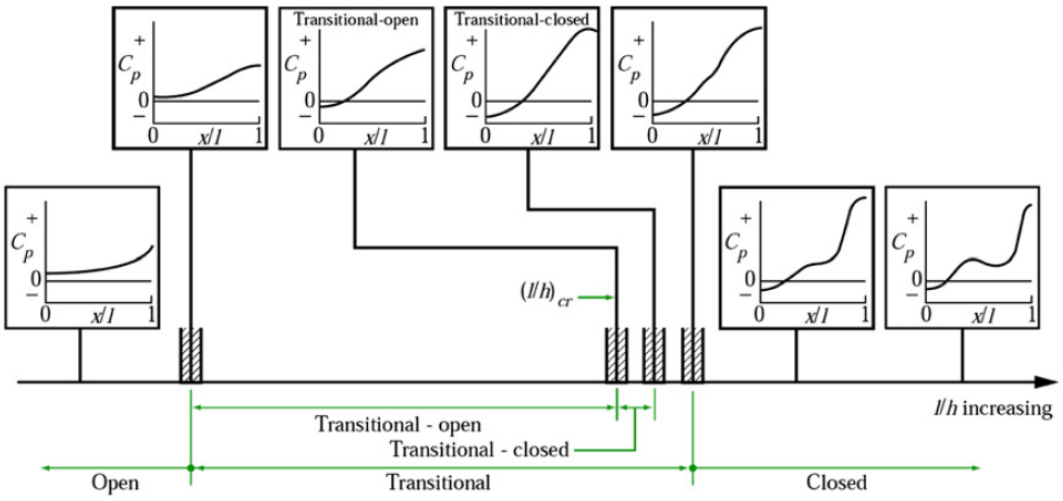

Figure 1.2 : Cavity floor pressure coefficient distribution at transonic and subsonic speeds, l/h is the L/D ratio [10].

As can be seen from Figure 1.2, for open cavities, pressure coefficient distribution shows a plateau profile up to 50% of the cavity floor and slightly increases towards aft edge. For transitional cavities, the plateau section is shorter and the increment is higher

for the pressure coefficient. The slope of the increment can change while moving from the front edge to aft edge, as shown in Figure 1.2. For closed cavities, the starting region has a plateau profile which goes up to 20% of the cavity, then an increase in pressure coefficient continues until a point close to cavity mid-zone. A second plateau region then occurs for a small portion of the cavity floor, finally another but a stronger increase in the pressure coefficient is observed.

The parameters that affect cavity classification such as W/D ratio or Mach number were investigated by Plentovich et al. [7] and an important result of that study was presented in Figure 1.3. It is clear that along with the L/D ratio, W/D ratio and Mach number are also important when the classification of a cavity is to be made. By examining Figure 1.3, it can be concluded that there are no exact boundaries between the cavity types and certainly L/D is not the only parameter that affects this classification.

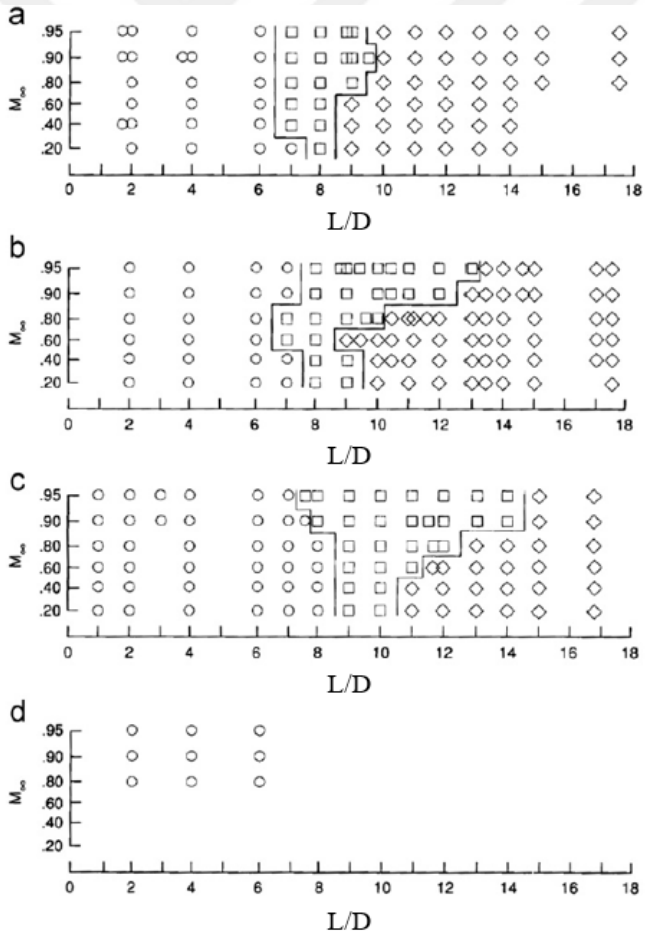

Figure 1.3 : Cavity type classification based on freestream Mach number and L/D ratio.o – open cavity; □ – transitional cavity; ◊– closed cavity. a) Width=2.40, Depth=2.40, W/D=1; b) Width=9.60, Depth=2.40, W/D=4; c) Width=9.60; Depth=1.20, W/D=8; d) Width=9.60, Depth=0.60, W/D=16. Units in inches [7].

Another distinction between open and closed cavities may be found in acoustic behavior of the flow in cavity environment. All types of cavities show a broadband spectrum in terms of pressure spectrum. Besides, for open cavities, discrete tones of high acoustic intensity exist, too [11]. The physical meaning of broadband spectrum is the natural fluctuations of the pressure that is generated by a turbulent shear layer [12]. For a better understanding of the spectrum differences of two different cavity types, study of Tracy and Plentovich [13] may be used as a good reference. Power Spectral Density (PSD) graphs of the mentioned study are given in Figure 1.4.

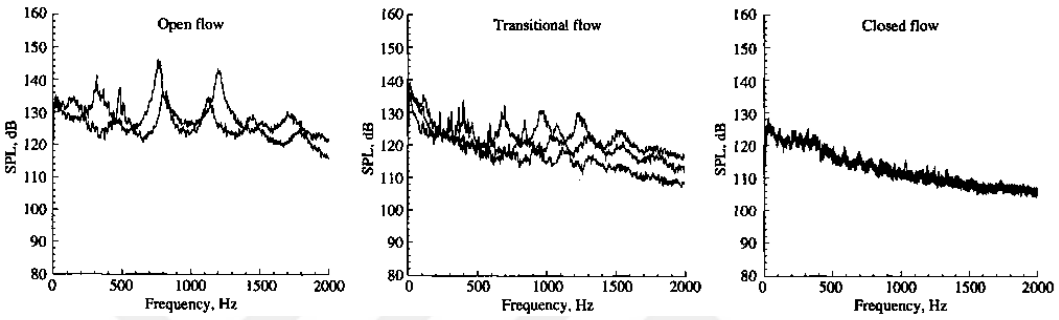

Figure 1.4 : SPL vs Frequency graphs of different types of cavities with different L/D ratios. Freestream Mach number is 0.9 [13].

It is obvious that for open cavities, discrete acoustic tones are very clear in the pressure spectrum, along with the broadband noise. For closed cavities, on the other hand, the discrete tones vanish and a smoother Sound Pressure Level (SPL) profile is present.

The shear layer, which forms over cavity caused by the separation of flow at the cavity leading edge, is of uttermost importance at the cavity classification. In open cavities, the shear layer has sufficient energy to bridge the cavity and impinges to the cavity aft wall or somewhere at the downstream of the cavity [7]. The generation of shear layer is the main governing parameter of noise generation in open cavities. Between the shear layer and the cavity, large circulation areas occur and this occurrence aids the pressure distribution to be in a plateau shape [10]. The impingement of the shear layer to the cavity aft wall creates severe acoustic tones and eventually cause the generation high levels of noise and vibration that can damage the structural integrity of the cavity or its surroundings. The schematic representation of open cavities is given in Figure 1.5. Typical open cavities are bomb bays (F-111 bomb bay), wheel wells of aircraft, measurement windows, and so on.

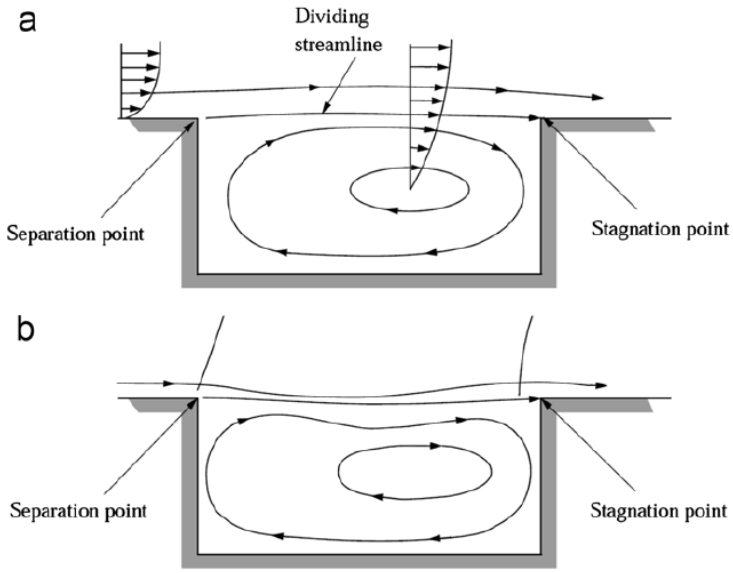

Figure 1.5 : Schematic representation of open cavity a) subsonic and transonic regime b) supersonic regime [10].

In open cavities, the shear layer has sufficient energy to bridge the cavity and reach the cavity aft wall without any impingement on the cavity floor. Since cavity flow is a time-dependent and highly unstable type of flow, the generated shear layer oscillates over the cavity and creates instabilities. After the separation of freestream flow from the cavity leading edge, these instability waves start to occur periodically. These instability waves form so-called Kelvin-Helmholtz vortices that are generated by Kelvin-Helmholtz instability. A representative demonstration of Kelvin-Helmholtz instabilities seen in clouds is given in **Figure 1.6**.

Figure 1.6 : Kelvin-Helmholtz instabilites seen in clouds [14].

The main source of this vortex generation is the velocity difference between the freestream and the cavity zone. Izawa [15] have illustrated the feedback mechanism

schematically in his study as shown by Figure 1.7. This feedback mechanism occurs as a result of the shear layer formation.

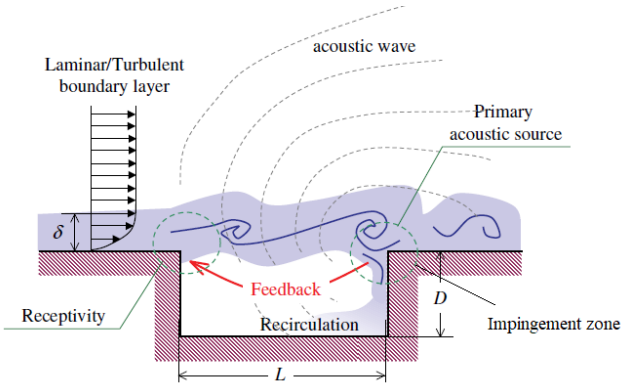

Figure 1.7 : Schematic representation of shear layer and feedback mechanism for an open cavity [15].

The shedding of vortex occurs when the flow separates at the cavity leading edge and starts to spread downstream, eventually impinges on the aft wall of the cavity which is shown as impingement zone in Figure 1.7. The impingement of the shear layer and vortices to the cavity aft wall generates a pressure wave which travels upstream that is indicated as the feedback. The impingement region, basically the aft wall, is therefore the main source of the generated pressure waves and acoustics. Generated acoustic waves interact with the oncoming shear layer and at the impingement zone and excite the shear layer at resonant frequency which forces the flow in an acoustic manner, called acoustic forcing.

In supersonic regimes, since the waves do not propagate upstream, pressure waves may only be seen in the lower part of the cavity.

The acoustic discrete tones that were mentioned earlier while explaining the broadband spectrum is also called narrow-band tones. The broadband noise part of the spectrum is basically the contribution of low-energy noise by freestream, shear layer and turbulent fluctuations [10]. The acoustic discrete tones, also known as Rossiter modes [16], are generated as a result of interaction of shear layer with generated vortices, walls and combined interactions.

The feedback mechanism explained previously creates acoustic waves, which causes the noise. The noise generation is investigated in terms of SPL and PSD. SPL may be described as the deviation of local pressure from the equilibrium atmospheric pressure [17]. In other words, it is an indication of generated noise caused by a source. It is

measured in decibels (dB). Experimentally, it can be measured using SPL meter. In numerical studies, such as this thesis study, it is calculated using the deviation of unsteady pressure. OASPL [18] is the integrated SPL all over the resolved frequencies and used to notate the noise generation. In this study, noise is calculated in terms of OASPL as shown in equation 1.1.

$$OASPL\ (dB) = 20\log_{10}(\frac{p_{rms}}{p_{ref}}) \tag{1.1}$$

where p_{rms} is the root mean square (RMS) of pressure. The standard for the minimum perceivable sound p_{ref} has the value of 2x10^{-5} Pascals. The RMS of pressure may be defined as

$$p_{rms} = \frac{1}{N}\sum_{i=1}^{N}\frac{(p_i - p_{mean})^2}{N} \tag{1.2}$$

In equation 1.2, N indicates the number of pressure data gathered, p_{mean} indicates the mean value of pressure throughout the measurement and p_i indicates the instantaneous value of pressure. Mean value of pressure can be calculated as

$$p_{mean} = \frac{1}{N}\sum_{i=1}^{N} p_i \tag{1.3}$$

Fast Fourier Transform (FFT) also applied to the gathered pressure data for the aim of obtaining PSD. PSD indicates the RMS of pressure versus frequency and gives an insight about the frequency content within the overall spectrum. Discrete acoustic tones, so called Rossiter modes, can be seen by inspecting the PSD graphs. In this study, PSD investigations of baseline cavity geometry are performed in order to ensure the validity of the numerical setup.

In closed cavities, the shear layer does not have sufficient energy to bridge the cavity and impinges on the cavity floor at some point along the cavity floor. Further downstream, a second separation occurs and the flow re-attaches/impinges on the cavity aft wall, as shown in Figure 1.8.

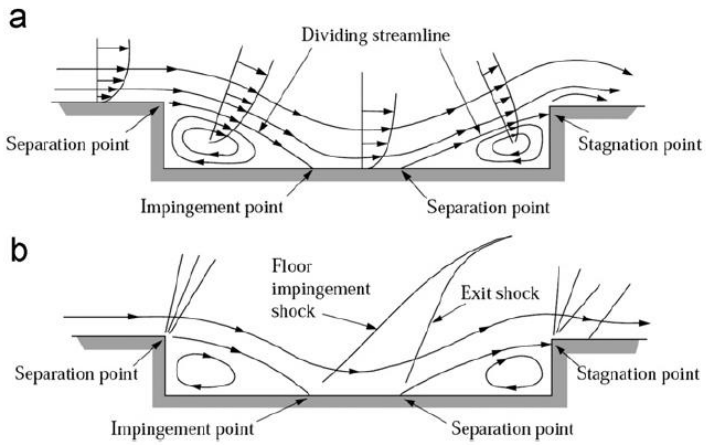

Figure 1.8 : Schematic representation of closed cavity a) subsonic and transonic regime b) supersonic regime [10].

The lack of a feedback mechanism results in no acoustic tone generation, but the severe oscillatory behavior of pressure coefficient along the cavity floor might create large nose-pitching moments and higher drags than open cavities [19]. Due to the lack of these acoustic tones, SPL generated by closed cavities are generally lower than open cavities [11]. The flow also tends to behave more steady-like as the L/D or closeness of the cavity increases. As for the vortex generation, as it can be seen from Figure 1.8, two separate circulation regions occur inside the cavity, one is near the leading edge, one is near the trailing edge. Charwat et al. [20] have named these circulation areas as separation wake and recompression wake. Obviously, the separation wake refers to the region that is close to cavity upstream while the recompression wake is the one that is close to cavity downstream.

In supersonic regime, the flow behavior is generally the same except for the λ shaped shock formation which is generated by expansion waves and oblique shock waves occurred inside the cavity (Figure 1.8). Closed cavities are mainly used for missile bays.

Transitional cavity is a special type of cavity where the behavior of flow is neither open nor closed. Flow physics is generally more complicated than pure open or closed cavity flows, due to the unpredictable nature of the flow. For instance, the acoustic discrete tones or severe pressure fluctuations that are seen in open cavities and large pitching moments that are seen in closed cavities are seen in transitional cavities in a concurrent way. As a result of this problem, studies concerning transitional cavities were not frequently seen, contrary to open or closed ones. Henderson et al. [21] have

studied transitional cavities in subsonic and transonic regimes and extended the knowledge about the transition in cavities.

In transonic cavities, there exist two vortices where one is generated by the interaction of shear layer with the aft wall and the other is generated in a similar manner to the closed cavities. The schematic representation of transonic cavities are shown in Figure 1.9.

a

b

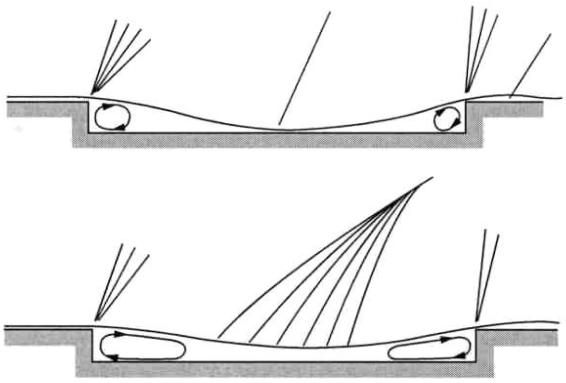

Figure 1.9 : Transitional cavity types [8].

1.2.2 Theoretical and Experimental Studies

Theoretical studies about cavity flows have been intensely conducted after the second half of the 20th century, starting with the inspirational study of Rossiter [22] who defined the frequency of the acoustic domain with an empirical formula. Several authors thereafter [22-24] conducted studies that aim to modify and enlarge the Rossiter's formula.

Theoretical studies that focus on the prediction of the resonant frequencies and amplitudes in cavities have been conducted along with the experimental studies [22,23].

The most notable study regarding the theoretical investigation of cavity flows is conducted by Rossiter [22]. In his study, a semi-empirical formula was derived that can be used to predict the frequencies of the acoustic tones inside the cavity, for cavities that have L/D ratio greater than 1. Assuming that the acoustic radiation is a result of vortex generation, the resonant frequency corresponding to the nth mode is given in equation 1.4.

$$St_n = \frac{f_n L}{U_\infty} = \frac{n - \alpha}{Ma_\infty + 1/\kappa_v}, \quad n = 1,2, \ldots, \tag{1.4}$$

where St_n stands for Strouhal number corresponding to n^{th} mode frequency, and α and $\kappa_v$for average convection speed of disturbances in shear layer and phase delay, respectively.

Rossiter [22] stated that the total time of the flow cycle is a summation of time needed for the generated vortices to convect downstream and time needed for acoustic waves to travel upstream. A study conducted by Shaw and Shimovetz [24] has revealed that the phase delay term, hence the frequency, was affected by the variation of L/D ratio.. They have also stated that this dependence and variation to phase delay term vanishes for higher frequency modes. Rossiter's formula has been used to predict the frequencies of cavities in the range of 0.4-1.4 Mach. For a wider use, Rossiter's formula has been updated as shown in equation 1.5.

$$f_n = \frac{U_\infty}{L} \frac{(n - \alpha)}{\frac{Ma_\infty}{\sqrt{1 + \frac{\gamma - 1}{2} Ma_\infty^2}} + \frac{1}{\kappa_v}} \tag{1.5}$$

where γ is the specific heat ratio of the working fluid.

Another widely addressed approach is presented by Tam and Block [23] to calculate the acoustic field inside a cavity. Additional parameters that are not included in the Rossiter's formula, such as shear layer thickness, L/D ratio and effects of external acoustic waves are taken into consideration in this theoretical study. Three dimensional effects were ignored as well as the mean flow inside the cavity. Main assumption that was followed in this study was that a line source located at the cavity aft edge was the source of the acoustic waves. The schematic view of their assumption can be seen in Figure 1.10.

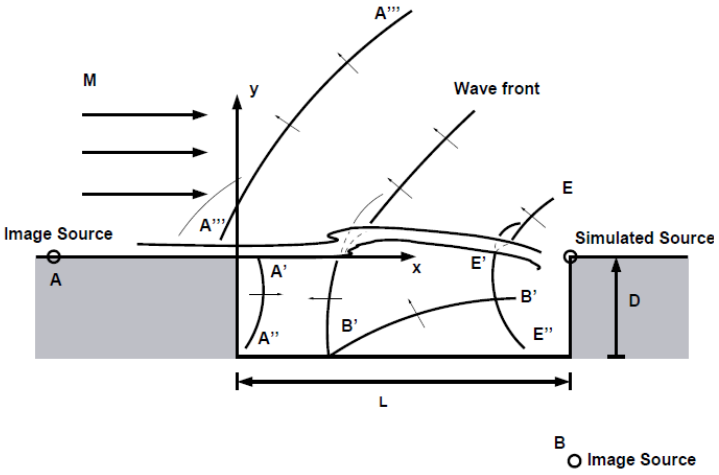

Figure 1.10 : Schematic representation of cavity flow as suggested by Tam and Block [23].

A recent theoretical study conducted by Alvarez et. al. [25] has proposed a different approach where no empirical constants are used. They have predicted the dispersion at cavity edges and united it with a procedure that takes the propagation of the disturbances in the central zone of cavity into consideration. By doing so, they have ended up with a general description of the cavity acoustic field.

To sum up briefly, theoretical models proposed by different authors and studies are good at predicting the frequencies but are inaccurate to predict the amplitudes [26].

Experimental studies concerning cavity flow investigations have attracted the attention of researches since 1940's. First studies were mostly military-related weapon bay investigations [4,5]. Early studies by Roshko [27], Krishnamurty [28] and Rossiter [29,30] have pioneered the studies about cavity flows. They have investigated the behavior of rectangular cavities with varying L/D and W/D ratios, in both subsonic and supersonic speeds. SPL and frequency investigations based on Rossiter's formula [22] have been conducted by Ross et al. [31-34] for both clean cavities and store separation situations. In time, experimental studies about cavity flows have been increased and become more sophisticated with the use new-generation measurement techniques such as Particle Image Velocimetry (PIV), Laser Doppler Anemometry (LDA), and so on [35,36]. One of the most famous cavity case, M219 cavity -also the baseline study of the present thesis- was also investigated by Ross [37] and Nightingale et al. [38].

Before the enhanced powerful computing technologies, most of the reliable studies, other than theoretical ones, were conducted experimentally. As mentioned before, studies relating to cavities trace back to 1940's [2,3]. First known detailed study on cavities focused on rectangular, circular and grooved cavities over a wide range of L/D ratios. Importance of L/D ratio and oncoming boundary layer are investigated and it was deduced that the drag coefficient value has a dependence on cavity length and boundary thickness [3].

During early 1950's, with the increased need of investigation of bomb bays, studies related to understanding unsteady pressure in cavities were increased. These studies were mostly carried out by military-related companies such as English Electric and Boeing for the aim of examination of weapon bays and its surrounding environment, installed on various aircraft [4,5]. An important and pioneering study about the investigation of drag in cavity found that the viscosity is not the only source of drag phenomenon; and fluctuations of pressure and its periodicity were also additional facts playing important roles in the increase of drag [27]. A broad range of cavity geometries at various freestream speeds were investigated in that study. It was stated that the formation of vortices in cavity was mainly due to deflection of shear layer. Studies of Roshko [27] has been one of the mostly cited and replicated studies since then. In another study conducted in the same year, acoustic radiation of sound waves in cavities were visualized for the first time [28]. In that study, it was found that the radiated field was stronger when the incoming boundary layer was laminar. Additionally, an intensity level of 160 dB was reached during experiments where freestream Mach number was 0.8. Karamcheti [39,40] has used schlieren photography, interferometry and Hot-Wire Anemometry (HWA) technique in his studies to investigate rectangular cavities both in subsonic and supersonic speeds. As a result of his studies, he stated that the acoustic field was dependent mainly on three parameters, cavity dimensions, type of oncoming boundary layer and free-stream Mach number, respectively. He defined a term called minimum cavity length at which shear layer no longer spans the cavity opening and therefore no longer impinges on downstream wall of cavity which results in the inexistence of acoustic field. Considering his findings, it was stated that the measured frequency in acoustic field was inversely proportional to cavity length, as expressed in equation 1.5.

$$f = (Ma)\frac{\alpha}{L} \tag{1.6}$$

where α is the proportionality constant and (Ma) is a function of Mach number. This formulation was the first attempt to analytically calculate frequencies. Additional to these pioneering studies, a vast number of experimental researches that have been conducted since 1950's are summarized in Table 1.1.

The most notable and respected studies of cavity flows were provided by Rossiter [16, 22, 29, 30, 41] where plenty of comprehension for understanding the flows over cavities were gathered. The first known classification of cavities are made by Charwat et al. [20] and Rossiter [22] who have concluded that cavities are mainly classified in three categories, open, closed and transitional, respectively. Both studies asserted that pattern of the flow and shear layer has a sturdy dependence on L/D ratio of cavity and on the term critical L/D ratio which defines the transition between open and closed type cavity. Rossiter [22] suggested that the transitional cavities should be avoided especially in weapon bays because of a possible occurance of buffet phenomenon. He stated that for certain maneuvers of aircraft, type of cavity (weapon bay) due to flow type may change to open where unsteady behaviour of pressure is dominant which may eventually harsh the weapon or surrounding structure.

Further analysis of pressure fluctuations and acoustic field paved the way for a better understanding of cavity flow mechanisms. As a result of widescale measurements of cavity flows for different L/D ratios at different Mach numbers, Rossiter [16] have discovered both broadband and narrowband noise spectrum exist in unsteady pressure field. He stated that the existence of broadband frequencies in shallow cavities were mostly due to randomly fluctuation pressures. On the other hand, for deep cavities, alongside with the broadband noise, discrete acoustic tones were also appeared. A typical noise spectrum inside a cavity is presented in Figure 1.11.

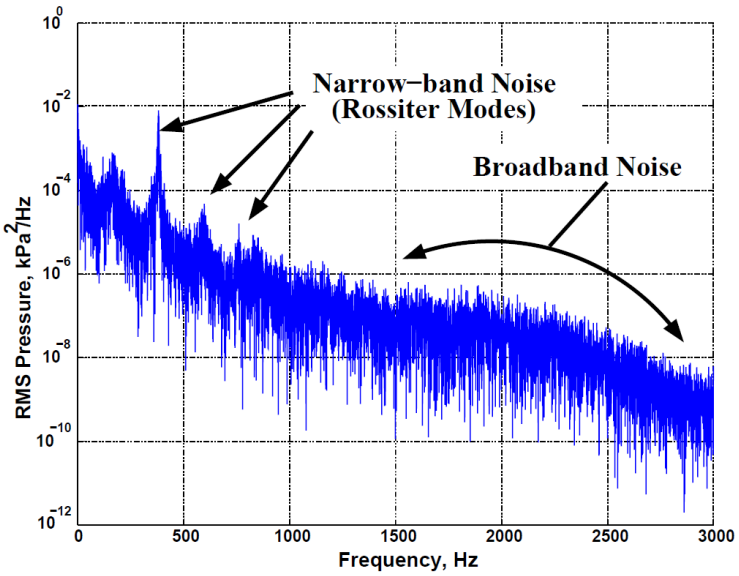

Figure 1.11 : A typical noise spectrum graph inside a cavity [22].

An empirical formula to predict the frequencies of the acoustic tones in cavity derived by Rossiter [16] based on edge-tone analogy [42] for shallow cavities was given above in equation 1.4. This relation has been extensively used as a benchmark for numerical studies since then. Ever since the pioneering studies of Rossiter, the modes in cavity are known as Rossiter modes. Another precursor side of these studies were that for the first time, a device (a spoiler upstream of the cavity) to suppress oscillations in cavity was used. Rossiter [16] also concluded that the cavity width has a small effect on pressure fluctuations but considerable effect on SPL magnitude. Studies conducted during 1960's by Rossiter has led the way for more complex and comprehensive researches investigating acoustic resonance in cavities [43,44]. Heller and Bliss [44] have conducted an experiment using water table visualization at which they have demonstrated the pressure waves travelling upstream of the cavity. It is stated that the front wall of the cavity is a reflecting wall whereas the aft wall is the is the source of the acoustics and noise generation. In order to describe the various behaviors of flow encountered in cavity, wave interaction mechanism concept which is basically the shear layer oscillation cycle is used. They have concluded that the waves generated at cavity aft wall was propogating outward as compression waves. Rockwell and Naudascher [43] have used a vortex interaction mechanism definition to describe and explain the shear layer motion in cavity. They have stated that the vortex formations inside the cavity were the driving parameters of shear layer instabilities.

In 1980's, with the increasing need of faster, more maneuverable and lower radar cross-sectioned aircraft, researches about flow over weapon bays are densed. Especially experimental studies considering store release and separation were in demand. Stallings Jr. [45] and Blair Jr. and Stallings Jr. [46] have investigated the main characteristics of store separation at supersonic regimes and have come to conclusion that the profile of separation was more desirable when the type of cavity is deep rather than shallow. Two famous experimental studies by Gharib and Roshko [47,48] were performed for an axisymmetric cavity using water as working fluid for low speed regimes. They stated that with the increasing L/D, impingement of the shear layer on downstream edge was vanished and also an enormous rise in the magnitude of drag was observed. This drag increase was due to violent fluctuations of flow. They named this behavior as wake mode since it evoked the wake behind a bluff body.

Researches about cavities, particularly about store separation, have continued to increase in 1990's. Remarkable contributions by Ross et al. [31-34] have carried the literature a step forward about the understanding of the cavity flows. They have conducted numerous wind tunnel studies of cavities and store separations. For the purpose of suppressing acoustic resonance generated by cavities, they have used different methods such as changing the cavity geometry, using spoilers, injecting mass, and so on so forth.

More recent experimental studies which use enhanced measurement techniques such as PIV [36, 49, 50] and Laser-Doppler Velocimetry (LDV) [35] have taken the knowledge about cavities much further than ever. Turbulence and velocity related parameters have become analysable in detail only with minor errors using such methods which provide a better perception on these type of flows.

M219 cavity case -one of the famous test cases in the literature- has been extensively used for validation of both experimental and numerical studies in recent years. Basically, the cavity cross-section has an orthogonal structure and surrounded by a flat plate. The M219 case is used by Ross et. al. [31-34, 36, 37] and Nightingale et al. [38] to provide data over an enormous range of cavity geometries and Mach numbers. Nightingale et al. [38] have studied a cavity which has a length of 20 in. and width and depth of 4 in. embedded into a flat plate rig. In this study, a variety of control methods to suppress the acoustic waves and decrease the noise levels were applied. As being the reference experimental study used in the present thesis, details of this study will be

provided in proceeding chapters. Some of the experimental studies on clean cavities where no control method is applied are listed in Table 1.1.

Table 1.1 : Experimental studies of clean cavities (Originally taken from [10]).

Study	Geometric Features		Freestream Conditions		Method Details
	L/D	W/D	Mach	Re	
Krishnamuty [28]	1-4	39.96	0.4-1.5	$0.25\text{-}1.47\text{x}10^5$	Hw, Sch
Rossiter [16, 22, 29, 30]	1-10	0.25-2.5	0.4-1.2	$1\text{-}1.6\text{x}10^6$	Dpt, Sh
Heller et al. [51]	4-7	1.3-2.3	0.8-3	0.8-8.3	Spt, Mic
Stallings and Wilcox [6]	1-24	0.5-5	1.5-2.86	$2\text{x}10^6$	Sch, Dpt
Baysal and Stallings [52]	6-16	5	1.5	$8.3\text{x}10^4$	Spt
Tracy et al. [53,54]	4.4-20	0.97-4.4	0.2-0.9	$1.9\text{-}94\text{x}10^6$	Spt, Dpt
Plentovich et al. [7]	1-17.5	1-16	0.2-0.95	$0.2\text{-}18\text{x}10^6$	Spt
Stallings et al. [55]	6.7-17.5	2, 4	0.2-0.95	$5.3\text{-}16\text{x}10^6$	Spt
Tracy and Plentovich [8]	1-17.5	1-16	0.2-0.95	$02\text{-}18\text{x}10^6$.	Dpt
Forestier et al. [56]	0.42	1	0.8	$8.5\text{x}10^5$	Dpt, Sch, Ldv
Ritchie et al. [49]	5	2.5	0.82	N/A	PIV
Kegerise et al. [57]	2, 4	0.7, 1.3	0.2-0.6	$1.5\text{x}10^6$	Dpt, Sch
Ukeiley et al. [58]	5.6, 9.0	2	0.6, 0.75	$2.4\text{-}3.2\text{x}10^4$	Dpt
Ünalmış [59]	6	3	2, 5	N/A	Dpt
Chandra and Chakravarty [60]	0.25-6.25	0.3-3.75	1.5	$5\text{-}25\text{x}10^6$	Dpt
Nightingale et al. [38]	5	1	0.6-1.35	$6.5\text{x}10^6$	Dpt, PIV
Zhuang et al. [61]	5.16	0.87	2	$2.8\text{x}10^6$	Dpt, Sh, PIV
Hirahara et al. [62]	1, 2	1.25	0.5-0.85	$3\text{-}4\text{x}10^5$	Dpt, Sch, PIV
Malone et al. [63]	4	4	0.2-0.65	$0.6\text{-}2\text{x}10^5$	Dpt

Hw: Hot-Wire, Sch: Schlieren, Dpt: Dynamic Pressure Transducer, Sh: Shadowgraph, Spt: Static Pressure Transducer, Mic: Microphone, Ldv: Laser Doppler Velocimetry, PIV: Particle Image Velocimetry, N/A: Not Available

1.2.3 Computational Studies

Expensive requirements of high speed wind tunnels and real-flight tests, and the lack of accuracy of theoretical models have pushed researches to seek for alternative methods, such as CFD investigations. The progress in high-speed and high-performance computers had led the way for numerical fluid mechanics studies. Cavities, with their relatively simple geometry and complex physics, have become one of the most attracting problems in the CFD field. Since CFD methods make both high spatial and temporal resolution possible, they are preferred by researchers especially in late history instead of wind tunnel experiments where some major drawbacks concercing the resolution quality [10]. Earliest numerical studies considering turbulent cavity flows were using URANS technique that has small requirements and fast solutions [64]. Numerous studies have been conducted using various turbulence

modeling techniques such as $B-L$ [12], $k-\epsilon$ [65], $k-\omega$ [66]. Shih et al. [65] have concluded that the SPL predictions using URANS were a bit higher than the value it should normally be. Due to the insufficiency of URANS techniques to capture the unsteadiness and highly oscillating behavior of the cavity flow, more sophisticated techniques that are able to resolve smaller scales in the flow such as Large Eddy Simulation (LES) and/or DES were introduced [26]. Nayyar [26], in his doctoral dissertation, has studied open cavities and weapon bays extensively using different modeling techniques of CFD (URANS, DES; LES). Larcheveque et al. [67] have studied the M219 cavity using LES and provided lots of quantitative data for the further investigations. Their results for SPL and normalized velocity profile were satisfactory and well-suited with the experimental data of Ross [37]. Peng and Leicher [68] have implemented the DES methodology to cavity flow problem and have found satisfactory results both quantitatively and qualitatively. They have well-predicted the OASPL distribution on cavity floor and the pressure contour of their study concentrating on the cavity zone have shown an expected behavior of the flow. Lately, Atalay [69], Elsayed [70], Freitas [11] and Omer [71] have conducted widescale investigations about cavities in their master dissertations. More compact and detailed information about the development in numerical side of the cavity investigations can be found at Lawson and Barakos [10].

With the advent of high-speed and high-performance computers, researches about the cavity have shifted to numerical studies. Also, relatively simple geometries of rectangular cavities and complex flow physics makes the cavity case one of the most intriguing problems in fluid dynamics field. CFD studies about cavity flow has increased day by day with the developing computing capabilities. Even though the relatively-low cost was the major advantage of the CFD, after numerous validation studies, other advantages of CFD has become prominent. Time dependent data of wind tunnels achieved using classical techniques such as Kulite pressure transducers has high temporal resolution but low spatial resolution; whereas, more expensive and recent methods such as PIV, on the other hand, have high spatial resolution, but low temporal resolution. CFD methods offer both high spatial and temporal resolution that overcome this major drawback of wind tunnel investigations [10].

First CFD studies were Reynolds Averaged Navier-Stokes (RANS) and URANS studies with simplified mathematical theories in background where computational

requirements were relatively small compared to techniques such as DES or LES. RANS simulations were barely preferred since the flow inside the cavity has an unsteady nature that needs to be taken into consideration in simulations. As with the new developments in the area of CFD (such as complicated newly developed models of URANS; DES and LES), researchers have extended their studies by using these sophisticated methods. Figure 1.12 represents the modeling levels in the CFD community. As moving from bottom to top, accuracy and reputability of study increases from RANS to Direct Numerical Simulation (DNS), but also computational cost starts to gain an exponential increment.

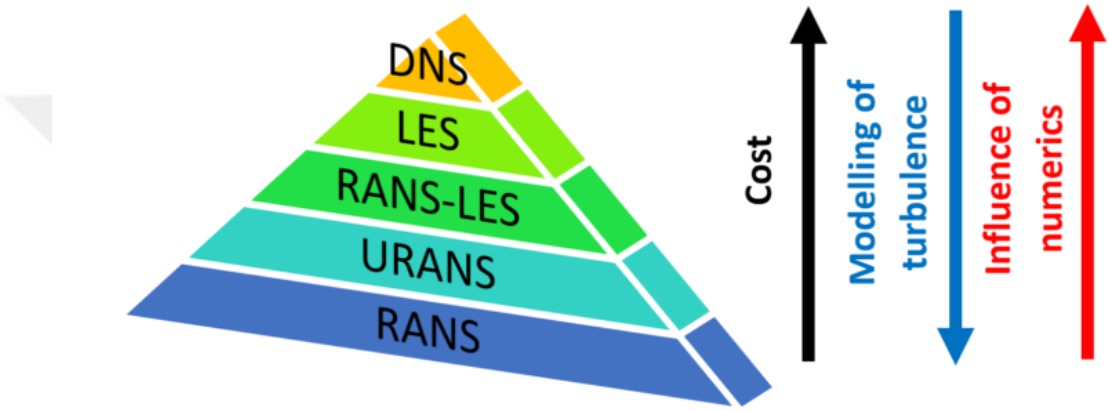

Figure 1.12 : Modeling levels in CFD [72].

Various numerical studies ranging from URANS to LES are reviewed in this section for the cavity flows. A vast number of selected numerical studies that have been conducted since 1950's are given in a summarized form in Table 1.2.

The least expensive and simplest numerical studies concerning the cavity flows were conducted using the URANS technique. The basic methodology of URANS is modeling the flow as a combination of two components, mean flow and and a random flow component, respectively. This kind of approach makes it possible to average the flow and setting a partial differential equation set based on Navier-Stokes equations. Knowing the mean flow and modeling the fluctuating terms form the basis of URANS method. Major drawback of this technique is being too dissipative and suppressing most of the oscillations in the flow. SPL estimation and wave propagation in URANS can be poor but the frequencies in the domain are generally predicted well [73]. URANS computations are generally conducted in supersonic regime where equations are hyperbolic and waves that propogate upstream does not exist. But as a side note, it

should be known that there are also studies that use URANS in transonic, high-subsonic regime [11].

URANS computations have started in 1980's with the development of Smith-Cebeci [74] and Baldwin-Lomax [75] models. Hankey and Shang [64], the first known study to use CFD as an investigation tool for cavity flows, have used zero equation Cebeci-Smith model to simulate a two-dimensional supersonic open type cavity flow. They have well-predicted the mean velocity and pressure compared to experimental findings; whereas, SPL was poorly predicted. Also, both frequencies in the domain and corresponding magnitudes of the frequencies were predicted well. The other commonly favoured Baldwin-Lomax algebraic model was used in numerous studies as well [12,76,77]. Rizzetta [12] have studied three-dimensional flow at a Mach number of 1.5 for a cavity with L/D ratio of 5.07 and W/D ratio of 2.67. Some crucial findings of this study are that the observed flow nature in the cavity was two-dimensional but three-dimensional effects has come to existence in the presence of a vortex near the front wall. Three-dimensional results have also showed a good aggreement with experimental data for pressure distribution at the cavity floor. As a conclusion of this study, it was seen that a detailed eddy-viscosity model was necessary to observe the details of the self-sustained oscillation inside the cavity.

The inability of the simple models to capture all the flow physics have played an important role on the initiation of the more complex turbulence models such as $k-\epsilon$ [78] and $k-\omega$ [79] models. Earliest studies related to two-equations turbulence models were mostly conducted in the supersonic regime [65-66,80-82]. Shih et al. [65] have investigated supersonic cavities using $k-\epsilon$ model and obtained satisfactory results in terms of both SPL prediction, mean pressure and velocity values and periodic shedding of vortices. Although SPL was slightly overpredicted, the correlation of overall trend of SPL distribution have showed promise about the usage of such turbulence models in supersonic cavity investigations. Zhang et al. [66,80-81] on the other hand, have used the $k-\omega$ model and conducted extensive research about the supersonic cavity flows. Henderson [82] has investigated transitional two-dimensional cavities and found satisfactory results with the experimental data in his dissertation.

Studies related to hypersonic cavity flows have been conducted by Morgenstern and Chokani [83]. In hypersonic regime, cavity flows are simpler than the supersonic regime and the flow can be treated as laminar which makes the use of turbulence

models redundant. The simplicity of equations in supersonic and hypersonic flows vanishes when the case is transonic. The most complex and computationally expensive cavity studies are the studies where the incoming flow is transonic [26]. Strong coupling of the shear layer, vortex structures and acoustic field makes the flow very complex. Transonic cavity investigations have started to increase in late 1990's and still increasing. Henderson [82] and Lawrie [84] conducted URANS simulations for open cavities ranging from high subsonic to low supersonic velocities.

Generally, URANS models tend to predict larger scales with lower frequency discrete acoustic tones well, but fail to maintain the same accuracy in smaller scales and higher frequencies. The existence of various acoustic tones and enormous number of turbulent scales may make it difficult for URANS methods to investigate the cavity flows in a detailed manner [10]. Stanek et al. [85] have limited the eddy viscosity value at each time step to a value that is higher than the produced in the incoming boundary layer. To gain a satisfactory behaviour from URANS simulations, a limitation to eddy viscosity level produced by the model was set. Unless the limitation was used, the level of dissipation produced by the model was too much for the cavity to provide the oscillatory motion. Therefore, major drawbacks of URANS simulations have led researches to implement more sophisticated simulation techniques [10].

DNS techniques being too expensive and impracticable and URANS techniques being too dissipative, studies using methods more sophisticated than classical URANS have started to appear in literature. Despite the considerably good performance of URANS, especially for cavity flows, techniques such as LES are required for more comprehensive investigations to understand the flow physics accurately. The rationale behind the LES is to resolve the large, energy containing eddies while modelling the sub-grid scale eddies which are smaller. This approach gives a better approximation of flow behaviour where large vortices exist in the current problem such as cavity flow [86]. However, near wall requirements of LES are similar to those of DNS which makes the usage of this implementation harder. A suggestion to overcome this drawback from [87] and [88] which involves the usage of wall modelling as in URANS implementations has been approved by the authorities and widely adopted since then. LES simulations are computationally more expensive than URANS and DES but cheaper than DNS. With the developing computational technologies, LES at moderate Reynolds numbers are becoming more and more prevalent [11].

Some of the most known pioneering studies of cavity flows using LES are performed by Smith et al. [89], Larcheveque et al. [90], Rizzetta and Visbal [91] and Forestier [56]. Forestier [56] have conducted numerical studies using LES technique in a transonic deep cavity where Reynolds number was $8.6x10^5$. He observed that, by validating their study with experimental data, LES may be used for moderate Reynolds number for cavity problem. Larcheveque et al. [90] have used a variation of standard LES called MILES (Monotone Integrated Large Eddy Simulation) which uses no sub-grid scale model. In those studies, a cavity of L/D and L/W ratio of 0.42 at high subsonic regime was investigated and results were compared with experimental data. They have made a deduction that their results were in a good aggreement with experiments. Then, they have introduced a new empirical relation to compute the aforementioned lag-phase term over the Rossiter's widely-known formula.

Rizzetta and Visbal [91] have simulated an open cavity that has a L/D ratio of 5 where freestream Mach number was 1.19. The grid used in their study was consisting of over 20 million cells and no wall function on solid boundaries were implemented. They have stated that it would not still be possible to resolve all the fine-scale turbulent structures at the same Reynolds number. Therefore, they have reduced the Reynolds number by an order of 10. The magnitude of Reynolds number used in experiments was $3.01x10^6$ whereas magnitude of Reynolds number used in numerical simulations was $2x10^5$, based on cavity length. They have observed that the fine-scale turbulence structures were three dimensional even though dominant flow physics were two dimensional. Comparisons with experimental data have shown that first (dominant) acoustic modes were in good agreement except that they were slightly lower, which could be due to the relatively low Reynolds number of the numerical simulations.

Larcheveque et al. [67] have also investigated the well-known M219 cavity in their studies where Reynolds number was $7x10^6$. Comparison with experimental findings of Ross [37] were satisfactory in terms of PSD. Their detailed investigations have revealed that a Kevin-Helmholtz instability was generated near the cavity front edge by a recirculation vortex. Comparisons related to cavity floor and velocity profiles were also made as with the PSD spectra and showed a good agreement, as well.

One of the most known alternative methods between URANS and LES is DES where a hybrid analogy is applied to the problem and both methods are used partially. Due to highly dissipative nature of URANS and resource requiring nature of LES, hybrid

methods such as DES are very common in CFD community. DES analogy was first proposed by Spalart et. al. [92] where it was suggested that the use of one-equation Spalart-Allmaras (SA) turbulence model in conjuction with a LES model was an advantegous approach to the problems that require high resources. Briefly, DES is a hybrid method which uses URANS near the boundary layer and LES in the regions away from the solid boundaries. Other DES methods which use $k-\omega\ SST$ turbulence model [93] and $k-\epsilon$ turbulence model [94] are also very common.

Suitability of DES for cavity flows are investigated by Mendonça et al. [95] and the results obtained were in good agreement with experiments. It was seen that the poorness of URANS methods was to predict the background broadband noise contribution. Hamed et al. [96] have also conducted numerical simulations where DES methodology is followed based on $k-\omega\ SST$. They have obtained similar results with Mendonca et al. [95] and have underlined the inefficacy of URANS for predicting the broadband noise.

Peng and Leicher [68] investigated M219 cavity numerically, using 6 million unstructured cells and modeled not just the flat plate but full geometry of the model that is used in the wind tunnel experiments of Nightingale et al. [38], which can be seen in Figure 1.13. In their study, they have used two numerical approaches, S-A DES and another hybrid RANS/LES, respectively. OASPL obtained by DES simulations was closer to the experimental data for cavity floor. However, DES simulations have overpredicted the OASPL by a magnitude of ~5 dB. Time-averaged pressure coefficient contours have also showed that a large vortex structure was present in the mid region of cavity (Figure 1.13).

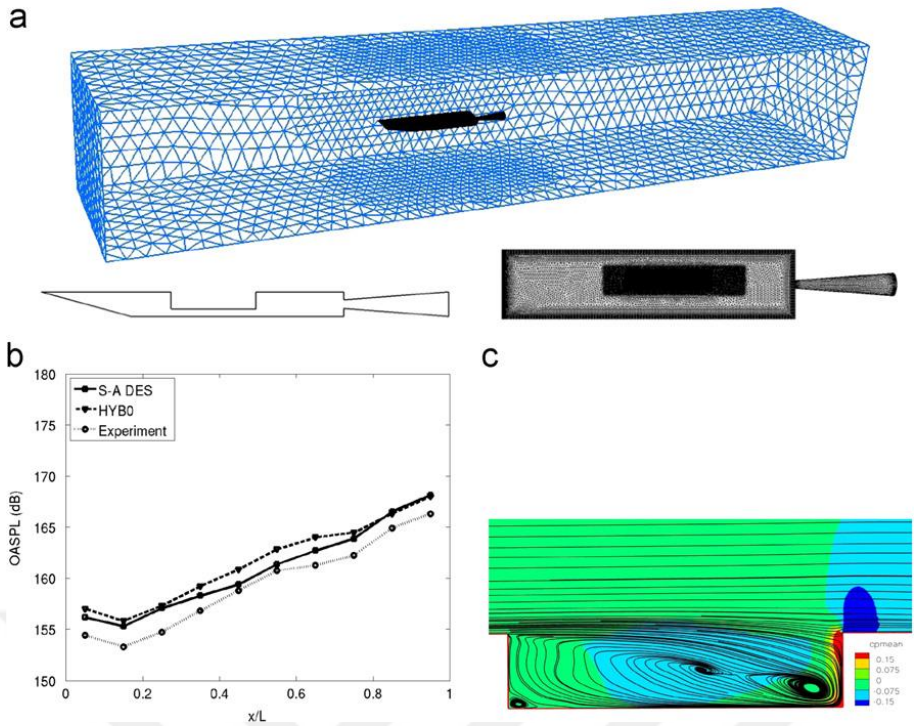

Figure 1.13 : Computational domain and unstructured grid (a), OASPL comparions with experiments (b), pressure coefficient contour of cavity region (c) [68].

Other numerical studies that used DES implementation for the cavity investigation that need attention are Ashworth [97], Lawson [98] and Togiti [99-100].

The most direct method of solving Navier-Stokes equations is called DNS. In DNS, all of the turbulent scales are resolved in the grid domain and no modeling is required. That being the most remarkable advantage of the DNS; however, it has also many disadvantages considering the computational requirements and expenses of the simulations. DNS requires a very fine grid and very small time step to resolve all of the flow quantities. Thus, it has limited applicability in reality and currently limited to low-Reynolds number problems. In addition to fine grid requirements, it is also necessary to use higher order specialized discretization schemes in DNS to minimize the dispersion and diffusion errors [10]. There are a few studies using DNS to investigate cavity flows [73,101-104] but the majority of the cavity coterie suggest the use of URANS or DES/LES.

Table 1.2 : Numerical studies of cavity flow (originally taken and updated from Lawson and Barakos (2011))

Study	Geometric Features		Freestream Conditions		Turbulence Modeling
	L/D	W/D	Mach	Re	
Hankey and Shang [64]	2.25	2D	1.5	$1.17x10^6$	B-L (URANS)
Baysal and Stallings [52]	6, 12, 16	2D	1.5	$8.33x10^4$	B-L(URANS)
Rizzetta [12]	5.07	1.0	0.9	$5.60x10^6$	B-L(URANS)
Lamp and Chokani [77]	4.33	2D	1.75	$9.21x10^6$	B-L(URANS)
Smith et al. [89]	4.5	1	1.2	N/A	SM+WF (LES)
Hamed et al. [101]	2	2D	0.6-1.1	$3x10^3$	DNS
Gloerfelt et al. [102-104]	2	2D	0.7	$4.1x10^4$	DNS
Arunajatesan et al. [105]	5.6	1	0.6	$1.45x10^7$	URANS+LES
Larcheveque et al. (90]	0.42	0.42	0.8	$0.86x10^6$	MS+WF
Mendonça et al. [95]	5	1	0.85	N/A	DES
Larcheveque [67]	5	1	0.85	$7x10^6$	MS+WF
Nayyar [26]	5	1	0.85	$1x10^6$	$k-\omega$ (URANS), SM + WF (LES), DES
Rizzetta and Visbal [91]	5	0.5	1.19	$0.2x10^6$	SM
Lai and Luo [106]	5	1	0.85	$1.36x10^6$	LES
Levasseur [107]	5	1	0.85	$7x10^6$	SM+WF
Peng and Leicher [68]	5	1	0.85	$7x10^6$	DES
Lawson and Barakos [98,108]	5	1	0.85	$1x10^6$	DES

B-L: Baldwin-Lomax, SM: Smagorinsky Model, WF: Wall Function, MS: Mixed Scale, N/A: Not Available

1.2.4 Flow Control Types

It is known that the cavity flow has a challenging physics and creates a harsh aeroacoustic environment. Phenomena occuring in cavity flows, such as high SPL, large pitching moments and pressure oscillations, may harm the structural integrity and prevent appropriate release of the store from the weapon bay or the complete flight system. Therefore, numerous studies to improve the cavity environment and to suppress the undesirable flow phenomena, both experimental and numerical, have been conducted since 1950's [4]. Noise levels around a cavity may reach up to ~160 dB which is extremely harmful to human ear and flight system structure [11].

First known studies that had an attempt to control the cavity flow are conducted by Norton [4] and Rossiter [16, 22]. Both Norton and Rossiter have suggested the use of

spoilers ahead of the cavity for the aim of changing the Reynolds number of the boundary layer, suppressing the pressure oscillations and eventually decrease the noise level. Rossiter [16] have performed widescale wind tunnel experiments and investigated the flow in many aspects. He stated that by keeping the geometrical relations constant (constant L/D and W/D) but slanting cavity walls, a reduction in cavity pressure oscillations and in SPL could be achieved. Even though a satisfactory reduction in SPL was achieved, acoustic frequencies and similar vortex generations were observed.

As the studies have increased and cavity flow physics have comprehended better, it was seen that the main source of the cavity noise is the interaction of the shear layer with the cavity aft wall, specifically cavity with aft up-corner. For instance, in an open cavity, a feedback loop generated from the oscillatory behavior of shear layer and from the acoustic waves that are sourced from the cavity aft wall and travel upstream is the main reason of noise. Various studies have aimed to suppress this feedback loop and to control (to reduce) the oscillatory behavior to decrease the noise level generated by cavity [26].

It is well known that the interaction of shear layer and cavity aft wall should be minimized in order to mitigate the acoustic field of the cavity. To mitigate the acoustic field and reduce the excessive noise, shear layer might be thickened so that the impact on aft wall is minimized. Shaw and Shimovetz [24] have suggested that any mechanism that make the shear layer bridge the cavity and attach at a point downstream of the aft corner, may vanish the feedback mechanism and the acoustic resonance. Thus, lifting or thickening the shear layer may decrease the intensity of impact between the shear layer and cavity aft wall, resulting in a reduction in noise level [98,105].

Lamp [77] and Arunajatesan [105] have observed that the increasing the energy of shear layer is also an alternative to reduce the noise level. The more smaller coherent vortex structures the flow has, the more reduction in noise generation.

Geometrical modifications of the cavity such as slanting the cavity walls (especially aft wall) or changing their shape, may also be useful in terms of noise and oscillation reduction. Smoothing the impingement of shear layer to cavity aft wall may create smaller oscillations in pressure and lower-magnitude acoustic waves [98, 105].

Basically, there are two types of cavity flow control, active and passive flow control, respectively. Active flow control requires additional energy input to the system throughout the flight, whereas passive flow control does not require any energy input [109]. Furthermore, active flow control is also divided into two categories, open-loop and closed-loop control systems, respectively. Closed-loop control corresponds to a system that has a feedback loop controlling the system or signal [110]. In closed-loop systems, efficiency of the system is higher since the adjustments may be provided instantly. Such a feedback mechanism does not exist for open-loop flow control systems [11]. Some of the common active flow control methods are jet blowings, passive devices implemented with a feedback mechanism (oscillating flaps), electro-mechanical actuators, piezoelectric flaps and mass injection [10]. Passive flow control may be summarized as the geometrical modifications of the cavity or addition of external devices to the system such as spoilers, vortex generators, flaps, fences, resonance tubes and so on [10].

A brief summary of active and passive control studies is given in [10,109,111]. Additionally, a brief table that summarizes some of the passive control studies is also presented in Table 1.3.

Active flow control methods has been extensively reviewed and investigated by Colonius [86] and Cattafesta et al. [109,111]. Since the present study deals with passive flow control of the cavity, the reader should refer to these studies for additional detailed information about active flow control studies.

Passive flow control methods of cavity are generally comprised of manipulation of cavity geometry or usage of an external device (such as vortex generator, spoiler, fence, and so on) or changing the behaviour of the upstream boundary layer which eventually alters the flow in cavity [112]. Various types of spoilers have been investigated by Rossiter [16] in subsonic speed regime and he stated that the use of a spoiler before the cavity may decrease the intensity of pressure fluctuations and acoustic instabilities.

Internal weapon bays of the famous United States Air Force (USAF) fighter F-111 were investigated by Shaw et al. [113] using a 1/20.4 scaled model with different types of spoilers. As a result of this study, they have concluded that for open cavities, the broadband acoustic level was reduced; however, the impact on the high amplitude

tones were insufficient for Mach 0.9. These inefficacies were suppressed when the freestream Mach number was increased to 1.2. The frequencies were also vanished for the case where freestream Mach number was 1.2. The same fighter model (F-111) was used by Smith et al. [114] to examine the effectiveness of a transverse rod spoiler rather than a flat spoiler. They have observed that both the location and diameter of the rod are important in the suppression of cavity noise. Maximum efficiency from rod was gained when the diameter to boundary layer thickness ratio was around 0.35 and the top edge of the rod were at the same level with the boundary layer outer edge.

Lawson and Barakos [98] have studied the effect of slanting the cavity aft wall since the major noise source of the cavity flow is the interaction of the shear layer with the aft wall. They have conducted numerical analyses of passive flow controls for spoilers, transverse rods and slanted walls. They have seen that all of the applied flow control methods have reduced the generated noise and eventually SPL. The lowest SPL was measured for the case where cavity aft wall was slanted. However, acoustic tones were still present with lower magnitudes.

Vortex generators are known to be effective at mitigating the pulsation effects of a cavity flow [115]. Stream wise vortices, orthogonal to the vortex that is formed in the midst of the cavity, are created by these vortex generators [116]. Recent studies [71,117] have shown that delta and curved spoilers are found to be very effective on suppressing acoustic resonance but highly dependent on their specific dimensions. Another interesting study on the modification of upstream wall of the cavity [112] has indicated that dimpled surfaces can also be used as a passive control method.

Detailed review of passive flow control methods can be found in [10,109,118].

Table 1.3 : Passive control studies of cavity flows (originally taken and updated from [98])

Study	Method	Geometric Features		Freestream Conditions		Details
		L/D	W/D	Mach	Re	
Charwat et al. [20]	Experimental	N/A	N/A	N/A	N/A	Sw
Rossiter and Kurn [41]	Experimental	N/A	N/A	0.3-2	$2.68x10^6$	Fts
Shaw et al. [113]	Experimental	6.79, 10.27	N/A	0.7-2	N/A	Sw, Sts; Tr
Wilcox [119]	Numerical	4.4-17.5	N/A	1.5-2.86	N/A	Pf
Baysal et al. [120]	Numerical	4.5	N/A	0.95	$8x10^6$	Sw, Fts
Sarno and Franke [121]	Experimental	2	0.3	0.6-1.5	1-$3.6x10^6$	Fts
Stallings et al. [55]	Experimental	6.7-17.5	2, 4	0.2-0.95	5.4-$12.6x10^6$	Pw
Ross and Peto [31]	Experimental	5, 10	1, 2	0.85-1.35	$6.5x10^6$	Sw, Sts
Zhang and Edwards [66]	Numerical	3	2D	1.5-2.5	$0.45x10^6$	Fts
Arunajatesan et al. [122]	Numerical	5.6	1	0.6	$1.47x10^7$	Tr
Smith et al. [114]	Experimental	4.8, 7.27	1.9, 2.9	0.9, 1.5	N/A	Tr, Fts
Ukeiley et al. [58]	Experimental	5.6, 9.0	2	0.6, 0.75	1-$3x10^5$	Tr, Fts
Nayyar [26]	Numerical+Experimental	5	1	0.85	$1x10^6$	Sw, Fts
Nightingale et al. [38]	Experimental	5	1	0.85	$6.5x10^6$	Tr, Fts, Sw, Sts
Comte et al. [123]	Numerical	0.42	1	0.85	$8.6x10^5$	Tr
Ashworth [124]	Numerical	5	1	0.85	N/A	Sts
Lawson and Barakos [98]	Numerical	5	1	0.85	$1x10^6$	Tr, Fts, Sw, Sts
Omer [71]	Numerical+Experimental	1, 1.67	0.33	0.45	N/A	Fts, Tr, Vg
Saddington [118]	Numerical	5	2	0.71	$1.31x10^7$	Sw, Pw
Wang [112]	Numerical	6.67	16	0.07	N/A	Uwd

Sw: Slanted wall, Fts: Flat top spoiler, Sts: Saw-tooth spoiler Tr: Transverse rod, Pf: Porous wall, Vg: Vortex generator, Uwd: Upstream wall dimple, N/A: Not available

1.3 Purpose of Thesis

The purpose of this thesis is to investigate the cavity flows numerically in a turbulent and compressible flow region at transonic speeds where the flow physics is highly complex. It is also aimed to decrease pressure oscillations and noise levels as much as

possible using various passive flow control techniques. Numerical analyses have been conducted for Mach number of 0.85 and Reynolds number of $1x10^7$ based on the cavity length. It is a known fact that the flow is highly unsteady and oscillatory in this regime. Therefore, examinations must be done with caution. Opensource software OpenFOAM® is used throughout the thesis and parallelization of high-computing power requiring analyses are run using the substructure of UHeM (National Computing Center). An open cavity with a L/D ratio of 5 and W/D ratio of 1, which is also known as M219 cavity, is taken as the baseline cavity geometry and numerical analyses are based on this case. Firstly, validation of the generated model is performed comparing the results of M219 clean cavity case which is a simple rectangular shaped cavity with existing experimental and numerical data. Passive flow control methods such as modificating cavity walls (front/aft), placing spoilers ahead of the cavity, combined methods, and so on are then applied to M219 clean cavity case for the aim of preventing severe pressure oscillations and generated noise. Numerical analyses are conducted using $k-\omega\ SST$ turbulence model-based version of DES technique.
Applied passive flow control methods are compared with the M219 clean cavity case by inspecting the OASPL distribution at cavity floor, flow variation inside cavity, turbulence and OASPL intensities and other findings in detail.

1.4 Thesis Organization

A general information about cavities and literature survey related to cavities since 1950's were given in Chapter 1.

Equations that govern the flow, numerical discretizations and modeling of turbulence used in the present thesis study will be presented in Chapter 2.

Chapter 3 is organized as follows. Firsly, M219 cavity which is the base study of this thesis will be examined and following to that the problem statement and list of applied passive flow control methods along with their description is given.

Computational details such as the generation of geometry, grid and numerical setup in OpenFOAM® will be given in Chapter 4. General simulation directory structure of OpenFOAM® will also be provided. Details concerning how the simulation was set, what types of settings were done and which parameters were used will be explained.

Chapter 5 will be the chapter where all results were presented, starting from validation. Results of applied passive control methods will be given thereafter. Applied passive

control methods will be compared both with the M219 clean cavity configuration and with each other in terms of pressure oscillations, OASPL generation to clearly investigate the impact on noise generation. An overall comparison of each configuration will also be provided along with the computational consumption details.

Chapter 6, where conclusions of the present thesis study will be given in a summarized way, will be the last chapter of the dissertation. Discussions of the results will also be conducted in this chapter.

2. GOVERNING EQUATIONS AND NUMERICAL DISCRETIZATION

Governing compressible Navier-Stokes equations of the flow, turbulence modeling and the finite volume discretization implementation in OpenFOAM® will be provided in this chapter.

2.1 Governing Equations

Numerical computations conducted in this thesis study were performed via compressible flow solver rhoPimpleFoam which is one of the many solvers of open-source CFD software OpenFOAM®. The aim of this section is to give an insight of the governing equations discretized and solved by rhoPimpleFoam. Details of the used turbulence model and the general solution procedure of the equations are also given.

There are a few compressible flow solvers in OpenFOAM. Among them, rhoPimpleFoam is suitable for solving turbulent flows in a time-dependent manner. rhoPimpleFoam is a transient, pressure-based, turbulent flow solver for compressible fluids by its definition in OpenFOAM® source code [125] shown in Figure 2.1.

```
Application
    rhoPimpleFoam

Description
    Transient solver for turbulent flow of compressible fluids for HVAC and
    similar applications.

    Uses the flexible PIMPLE (PISO-SIMPLE) solution for time-resolved and
    pseudo-transient simulations.
```

Figure 2.1 : rhoPimpleFoam definition in source code.

Governing equations of the present problem are conservation of mass (continuity equation), momentum (2nd law of Newton) and energy (1st law of thermodynamics), respectively. Additional to conservation of these three flow parameters, a turbulence modeling is also implemented in order to consider the turbulence effects.

By taking [126] as reference, some major assumptions are made such as:

- The flow is in continuum regime and Newtonian flow assumption is valid.
- The flow is in compressible region.

- The flow is in thermodynamic equilibrium, perfect gas assumption is valid.
- No reaction or phase change occurs in the flow.

Governing equations of flow are given in partial differential form in equation 2.1-2.4.

$$\frac{\partial \rho}{\partial t} + \frac{\partial (\rho u_j)}{\partial x_j} = 0 \tag{2.1}$$

$$\frac{\partial (\rho u_i)}{\partial t} + \frac{\partial (\rho u_i u_j)}{\partial x_j} + \frac{\partial p}{\partial x_i} = \frac{\partial \sigma_{ij}}{\partial x_j} \tag{2.2}$$

$$\frac{\partial (\rho E)}{\partial t} + \frac{\partial [(\rho E + p) u_j]}{\partial x_j} = \frac{\partial (\sigma_{ij} u_i)}{\partial x_j} - \frac{\partial q_j}{\partial x_j} \tag{2.3}$$

$$p = \rho R T \tag{2.4}$$

where t indicates temporal coordinate, x_i indicates spatial coordinate and u_i indicates the velocity vector.

The term ρE is the multiplication of total energy by density and is given in equation 2.5:

$$\rho E = \frac{p}{\gamma - 1} + \frac{1}{2} \rho u_i u_i \tag{2.5}$$

where R represents the universal gas constant.

Shear stress tensor shown in equation 2.2 has the following algebraic expansion given in equation 2.6:

$$\sigma_{ij} = 2\mu(T) S_{ij} - \frac{2}{3} \mu(T) \delta_{ij} S_{kk} \tag{2.6}$$

S_{ij} being the rate of strain tensor written as in equation 2.7,

$$S_{ij} = \frac{1}{2} \left(\frac{\partial u_i}{\partial x_j} + \frac{\partial u_j}{\partial x_i} \right) \tag{2.7}$$

Dynamic viscosity in equation 2.6 is defined as a function of temperature using Sutherland's law with three coefficient given in equation 2.8.

$$\mu(T) = \mu_0 \left(\frac{T}{T_0} \right)^{3/2} \frac{T_0 + S_S}{T + S_S} \tag{2.8}$$

where μ_0 is the reference viscosity having the value of 1.7894x10^{-5} kg/m/s, T is the static temperature, T_0 is the reference temperature having the value of 273.11 K, S_S is an effective temperature in Kelvin, having the value of 110.56 K.

Heat flux q_j appeared in equation 2.3 is calculated as in equation 2.9

$$q_j = -\kappa \frac{\partial T}{\partial x_j} \tag{2.9}$$

where κ is the thermal conductivity of the fluid.

2.2 Turbulence Modeling

The phenomenon known as turbulence is a distinct fluid behavior that was first discovered more than 500 years ago [127]. Figure 2.2 is a sketch of Da Vinci where his first impressions on the turbulence are presented.

Figure 2.2 : A rigid obstacle in flowing water creating wake turbulence, sketched by Leonardo Da Vinci in 1509 [128].

A more detailed explanation of turbulence and turbulent flow is as follows [129]:

"At values of the Reynolds number above Re_{cr} where instabilities in flow come to existence, a complicated series of event takes place which eventually leads to a radical change of the flow character. In the final state the flow behaviour is random and chaotic. The motion becomes intrinsically unsteady even with constant imposed boundary conditions. The velocity and all other flow properties vary in a random and chaotic way. This regime is called turbulent flow." (p. 41).

A typical velocity versus time graph for a turbulent flow is given in Figure 2.3.

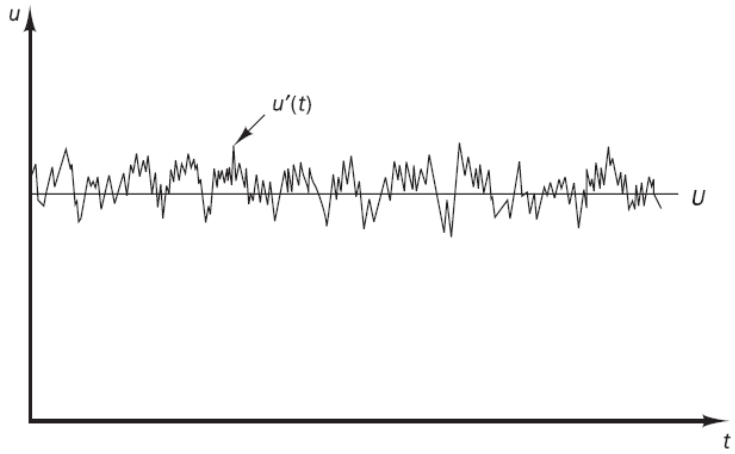

Figure 2.3 : Velocity versus time measurement of a specific point in a turbulent flow [129].

The current problem is in compressible region and turbulence effects are inevitable considering the high Reynolds number and complex flow physics. The most extensive method to examine the turbulence in a flow is DNS, but since solving the problem using DNS is impracticable, a modeling of turbulence is required. Therefore, DES implementation based on $k-\omega\ SST$ turbulence model is followed for all numerical analyses conducted on this thesis. Details of this turbulence modeling is given in the following section.

2.2.1 DES

The original DES implementation was proposed by Spalart et al. [92]. The main idea was to use RANS for near-wall treatments and LES for outside of the wall. The DES modification of the well-known RANS turbulence model implemented in OpenFOAM is called $k-\omega\ SSTDES$ [131].

Specific turbulence dissipation rate (ω) in terms of turbulent kinetic energy (k) and turbulent dissipation rate (ϵ) are given in equation 2.10:

$$\omega = \frac{\epsilon}{\beta^* k} \tag{2.10}$$

where $\beta^* = C_\mu$ is a turbulence model constant with the value of 0.09.

In $k-\omega\ SSTDES$ model, transport equation for turbulent kinetic energy is given below in equation 2.11.

$$\frac{\partial(\rho k)}{\partial t}+\frac{\partial(\rho k U_i)}{\partial x_i}=\tilde{P}_k-\beta^* k\omega F_{DES}+\frac{\partial}{\partial x_i}\left[(\mu+\mu_t\sigma_k)\frac{\partial k}{\partial x_i}\right] \quad (2.11)$$

The term F_{DES} is what differs DES implementation from the base RANS model of $k-\omega\ SST$.

The transport equation for specific turbulence dissipation rate is written in equation 2.12.

$$\frac{\partial(\rho\omega)}{\partial t}+\frac{\partial(\rho\omega U_i)}{\partial x_i}=\alpha\rho S^2-\rho\beta\omega^2+\frac{\partial}{\partial x_i}\left[(\mu+\mu_t\sigma_\omega)\frac{\partial\omega}{\partial x_i}\right]-2(1-F_1)\sigma_{\omega 2}\frac{1}{\omega}\frac{\partial_k}{\partial x_i}\frac{\partial_\omega}{\partial x_i} \quad (2.12)$$

where $S=\sqrt{2s_{ij}s_{ij}}$ is the invariant measure of the strain rate. Strain rate tensor of the velocity can be computed as follows by equation 2.13:

$$s_{ij}=\frac{1}{2}\left(\frac{\partial U_i}{\partial x_j}+\frac{\partial U_j}{\partial x_i}\right) \quad (2.13)$$

The first blending function F_1 can be computed as shown in equation 2.14 [131].

$$F_1=tanh(\eta^4),\qquad \eta=min\left[max\left(\frac{\sqrt{k}}{\beta^*\omega y},\frac{500\nu}{y^2\omega}\right),\frac{4\sigma_{\omega 2}k}{CD_{k\omega}y^2}\right] \quad (2.14)$$

where y is the nearest distance to wall.

$CD_{k\omega}$ term in η formulation is defined as in equation 2.15,

$$CD_{k\omega}=max\left(2\rho\sigma_{\omega 2}\frac{1}{\omega}\frac{\partial k}{\partial x_i}\frac{\partial\omega}{\partial x_i},10^{-10}\right) \quad (2.15)$$

The turbulent eddy viscosity is defined by equation 2.16:

$$\nu_t=\frac{\mu_t}{\rho}=\frac{a_1 k}{max(a_1\omega,SF_2)} \quad (2.16)$$

where a_1 is the square root of β^*. F_2 is the second blending function which is formulated as in equation 2.17,

$$F_2 = tanh(\zeta^2), \quad \zeta = max\left(\frac{2\sqrt{k}}{\beta^* \omega y}, \frac{500\nu}{y^2 \omega}\right) \tag{2.17}$$

where y is the wall distance.

A limiter of turbulent kinetic energy production exists on the SST model in order to prevent the build-up of turbulence in stagnation regions. The limiter is defined as shown by equation 2.18-19:

$$\tilde{P}_k = min(P_k, 10 \cdot \beta^* \rho k \omega) \tag{2.18}$$

$$P_k = \mu_t \left(\frac{\partial U_i}{\partial x_j} + \frac{\partial U_j}{\partial x_i}\right) \frac{\partial U_i}{\partial x_j} \tag{2.19}$$

In the DES formulation of this turbulence model, the function F_{DES} is implemented in the dissipation term of turbulent kinetic energy transport equation via equation 2.20:

$$F_{DES} = max\left(\frac{L_t}{C_{DES}\Delta}, 1\right) \tag{2.20}$$

where L_t is the turbulent length scale and calculated as $L_t = \sqrt{k}/\,(\beta^* \omega)$; Δ is the maximum local grid spacing which is defined as $\Delta = \max(\Delta x, \Delta y, \Delta z)$ and C_{DES} is a calibration constant with the value of 0.61.

In the case of a sufficiently fine grid, the term F_{DES} goes beyond the value of 1 which will in turn reduce turbulent kinetic energy and viscosity and make the problem unsteady. Therefore, when the local grid is sufficiently fine so that the turbulence can be resolved, DES model will decrease the amount of modeled turbulent shear stress and will switch to LES methodology for that region.

The value of blending function F_1 varies between 1 and 0; in regions close to wall, the value is 1 and the model switches to $k - \omega$, whereas in regions outside of the boundary layer the value becomes 0 and the model switches to $k - \epsilon$. Additional to blending function, constants that are placed in the formulation are also blended. The blending of model constants are done as presented in equation 2.21.

$$\chi = F_1 \chi_1 + (1 - F_1)\chi_2 \tag{2.21}$$

where χ is a general notation for β and α parameters. Another way of blending the model constants is given in equation 2.22:

$$\frac{1}{\psi} = F_1 \frac{1}{\psi_1} + (1 - F_1) \frac{1}{\psi_2} \tag{2.22}$$

where ψ is a general notation for σ_{kj} and σ_{wj} constants.

Values of model constants are given in Table 2.1 [131]:

Table 2.1 : Model constants of SST turbulence model.

Model constant	Value
α_1	5/9
α_2	0.44
β_1	3/40
β_2	0.0828
$1/\sigma k_1$	0.85
$1/\sigma k_2$	1
$1/\sigma_{\omega 1}$	0.5
$1/\sigma_{\omega 1}$	0.856

2.3 Finite Volume Method and Numerical Discretization

OpenFOAM software uses a Finite Volume Method (FVM) procedure to calculate the flow properties [132]. In the FVM, the basic procedure is to divide the domain into cells called control volumes. It is the numerical method that converts partial differential forms of governing conservations equations into algebraic equations over finite control volumes. As the first step of FVM procedure, the numerical domain is discretized into control volumes. After the discretization of the numerical domain, each partial differential equation is converted to algebraic equations. The obtained set of algebraic equations are then solved via linear system solvers to compute the necessary parameters for each element/control volume.

Let us consider the conservation law for the transport of a general scalar in an unsteady flow in partial differential form as shown by equation 2.23[133]:

$$\frac{\partial}{\partial t}(\rho\phi) + \nabla \cdot (\rho U \phi) = \nabla \cdot \left(\rho \Gamma_\phi \nabla \phi\right) + S_\phi \tag{2.23}$$

In equation 2.23, the first term denotes the temporal derivative, second term denotes the convection, third term denotes the diffusion and the fourth term denotes the source term. By integrating over control volume and applying Gauss theorem for each term, volume integrals are transformed into surface integrals as shown in equation 2.24-25.

$$\int_{V_P} \frac{\partial}{\partial t}(\rho\phi)dV + \int_{V_P} \nabla \cdot (\rho U\phi)dV = \int_{V_P} \nabla \cdot \left(\rho\Gamma_\phi \nabla\phi\right)dV + \int_{V_P} S_\phi(\phi)dV \quad (2.24)$$

$$\int_{V_P} \frac{\partial}{\partial t}(\rho\phi)dV + \oint_{\partial V_P} dS \cdot (\rho U\phi) = \oint_{\partial V_P} dS \cdot \left(\rho\Gamma_\phi \nabla\phi\right) + \int_{V_P} S_\phi dV \quad (2.25)$$

Prior to giving details of discretization of terms, the arbitrary control volume/cell used for the transformations is illustrated in Figure 2.4.

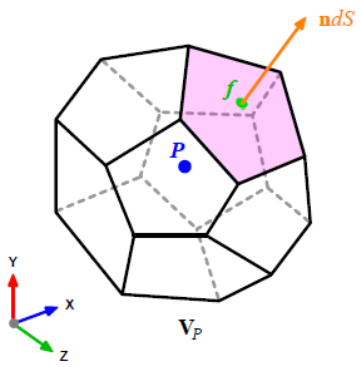

Figure 2.4 : An arbitrary control volume used for FVM [133].

In Figure 2.4, the control volume of volume V is denoted as V_P, centroid of the control volume as P, current face of the control volume as f, face area vector normal to face f as $\mathbf{n}dS$.

2.3.1 Convective Terms Discretization

Discretization of convective terms are performed as in equation 2.26 using Gauss theorem:

$$\int_{V_P} \nabla \cdot (\rho U\phi)dV = \oint_{\partial V_P} dS \cdot (\rho U\phi) = \sum_f S_f \cdot (\rho U\phi)_f \quad (2.26)$$

2.3.2 Diffusive Terms Discretization

Discretization of convective terms are performed as in equation 2.27 using Gauss theorem:

$$\int_{V_P} \nabla \cdot \left(\rho\Gamma_\phi \nabla\phi\right)dV = \oint_{\partial V_P} dS \cdot \left(\rho\Gamma_\phi \nabla\phi\right) = \sum_f S_f \cdot \left(\rho\Gamma_\phi \nabla\phi\right)_f \quad (2.27)$$

2.3.3 Source Term Discretization

Discretization of convective terms are performed as in equation 2.28 using Gauss theorem:

$$\int_{V_P} S_\phi(\phi) dV = S_C V_P + S_P V_P \phi_P \tag{2.28}$$

where S_C is the constant part and S_P is the non-linear part of the source term.

After the necessary discretizations, the following semi-discrete equation shown in equation 2.29 for transport of a scalar is obtained.

$$\int_{V_P} \frac{\partial}{\partial t}(\rho\phi) dV + \sum_f S_f \cdot (\rho U \phi)_f = \sum_f S_f \cdot \left(\rho \Gamma_\phi \nabla \phi\right)_f + S_C V_P + S_P V_P \phi_P \tag{2.29}$$

where the second term denotes the convective flux and the third term denotes the diffusive flux. Once the spatial discretizations are performed, the temporal discretization is applied to the equation 2.29.

2.3.4 Temporal Discretization

Discretization of temporal derivative is performed using one of the common time discretization schemes such as Crank-Nicolson or Euler implicit. The resulting form of the semi-discrete transport equation is given in equation 2.30.

$$\begin{aligned} \int_t^{t+\Delta t} \left[\left(\frac{\partial}{\partial t}(\rho\phi) \right)_P V_P + \sum_f S_f \cdot (\rho U \phi)_f \right] dt \\ = \int_t^{t+\Delta t} \sum_f S_f \cdot \left(\rho \Gamma_\phi \nabla \phi\right)_f dt + \int_t^{t+\Delta t} S_C V_P + S_P V_P \phi_P \end{aligned} \tag{2.30}$$

3. PROBLEM DEFINITION

3.1 M219 Cavity Description

M219 cavity configuration which has an orthogonal cavity cross-section is a well-known case in cavity investigations and taken as reference in numerous studies [26, 67, 82, 95, 9ü8, 134]. The M219 cavity setup has been extensively used by Ross [31-34, 36, 37] and Nightingale et al. [38] to give an insight of the cavity flow phenomena. Experimental study by Nightingale et al. [38] is taken as the reference experiment in the present study and is detailed in the following paragraphs.

The original setup of the case is a cavity embedded into a flat plate which is given in Figure 3.1.

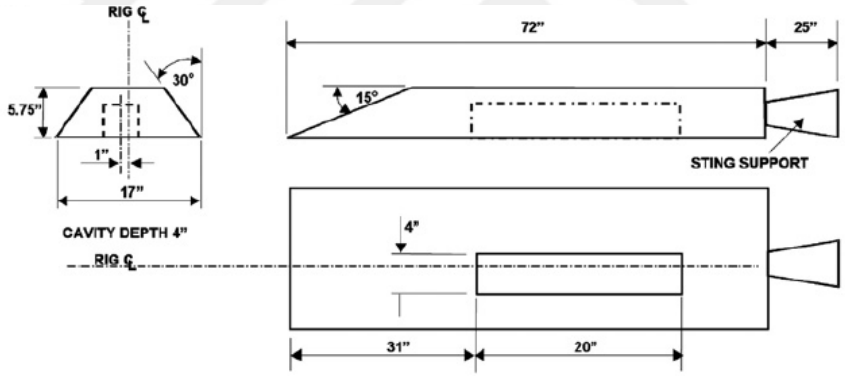

Figure 3.1 : Schematic representation of M219 cavity setup, units in inches [38].

It must be realized that the centerline of the cavity is not the centerline of the cavity rig but an offset of 1 inch (0.0254 m) is of the case. A vast number of configurations (different L/D ratios, cavity depth or lengths, and so on) are investigated by Nightingale et al. [38] but most of the investigations and tests are conducted for a cavity which has the specifications given in Table 3.1.

Table 3.1 : Cavity dimensions and freestream Mach number for the study of Nightingale et al. [38].

L (m)	D (m)	W (m)	L/D	W/D	Mach Number
0.508	0.1016	0.508	5	5	0.85

Various passive control methods are also applied such as slanting the walls, placing devices to upstream of cavity, and so on. A summary of applied passive control methods are given in Figure 3.2.

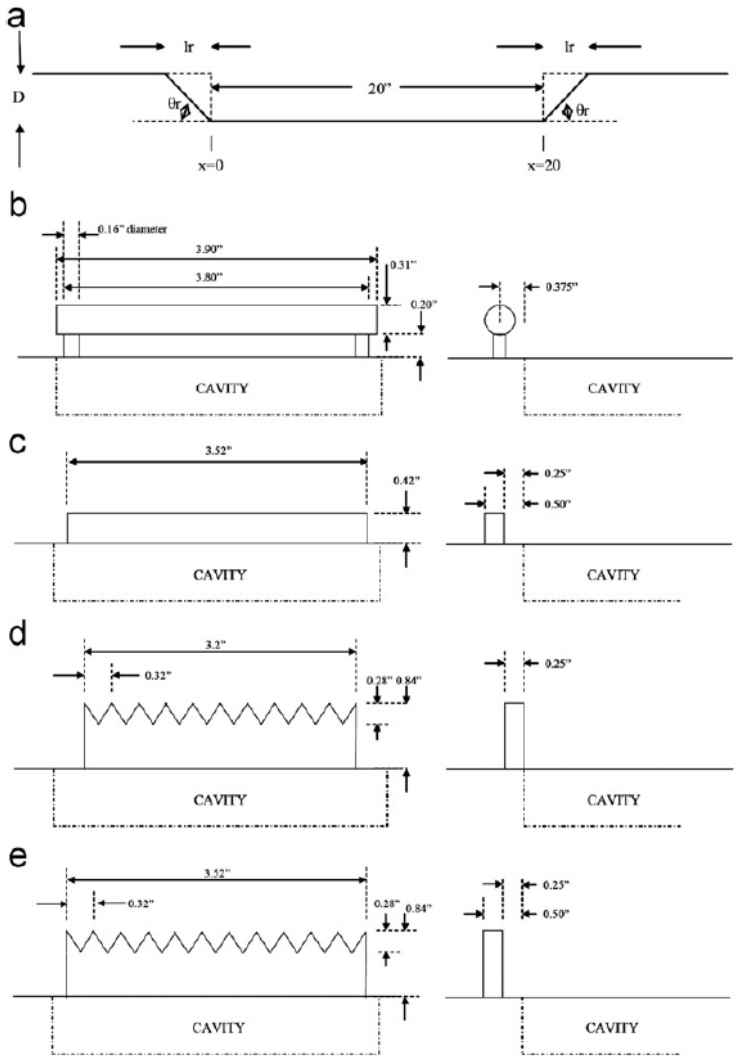

Figure 3.2 : Applied passive flow control methods to M219 cavity by Nightingale et al. [38]. a) M219 slanted walls b) M219 transverse rod c) M219 flat top spoiler d) Saw-tooth spoiler type 1 e) Saw-tooth spoiler type 2 [38].

Although the tests were ranging from 0.6 to 1.35 Mach, only the results of 0.85 Mach tests are considered here. By using pressure transducers, several data from cavity floor were gathered. The positions of pressure transducers placed at cavity floor of M219 clean cavity configuration are shown in Figure 3.3. Pressure transducers were sampled at a rate of 6 kHz for 3.4 s [10].

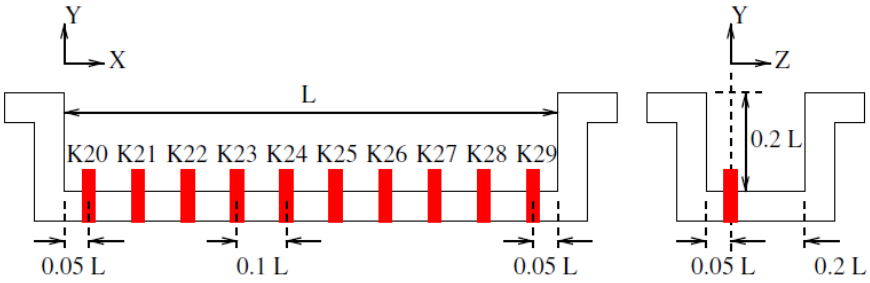

Figure 3.3 : Position of pressure transducers placed at the cavity floor [10].

Pressure transducer placed at the 0.95 x/L of the cavity floor (K29) is taken as the reference measurement point for PSD investigations. OASPL distributions of clean cavity and applied passive control methods at cavity floor of experimental study is given in Figure 3.4. It is seen that by implementing a control method, OASPL has been reduced by about 5 dB.

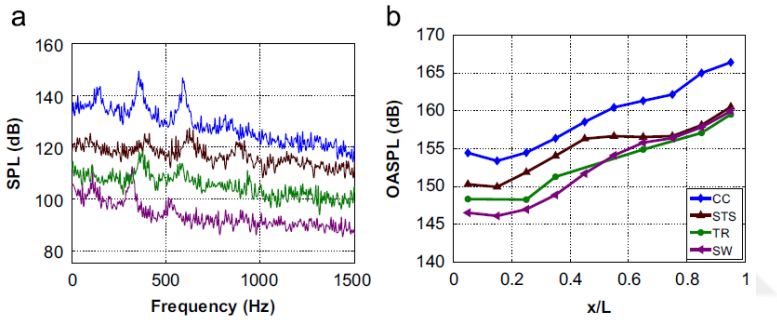

Figure 3.4 : Spectral analysis of cavity floor, experimental study of Nightingale et al. [38]. a) SPL vs. Frequency measured at 0.95 x/L of the cavity floor. b) OASPL distribution at cavity floor. CC-clean cavity, STS-saw-tooth spoiler, TR-transverse rod, SW-slanted aft wall [10].

The numerical study that is taken as the reference is the study of Larcheveque et al. [67]. In their study, they have conducted numerous LES simulations for the three dimensional M219 cavity for a Reynolds number of $7x10^6$. Extensive comparisons with the available experimental data are made and a satisfactory level of accuracy was achieved.

The numerical domain that is used in Larcheveque [67] is shown in Figure 3.5. Knowing the strong existence of pressure waves generating from the interaction of the shear layer with the cavity aft wall, non-reflecting boundary conditions were used in outer boundaries. The boundaries were put far away from the cavity in order to minimize the adverse effects. An upstream wall is placed before the cavity just as in the experimental setup, for the aim of mimicing a thin boundary layer. Symmetry boundary conditions are also put to the both sides of the cavity in spanwise direction.

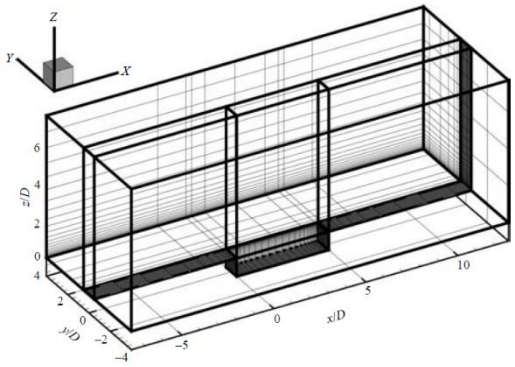

Figure 3.5 : Isometric view of the numerical domain that is used in Larcheveque et al. [67].

Main aim of the study was to investigate the shear layer formation and related phenomenon. Prior to shear layer examinations, mean profiles of longitunal velocity, vertical velocity, turbulent energy and cross-Reynolds stress are computed on the centerline and given in Figure 3.6. Mean longitudinal velocity profiles that are plotted in Figure 3.6(a) are used for the comparison with the present thesis study.

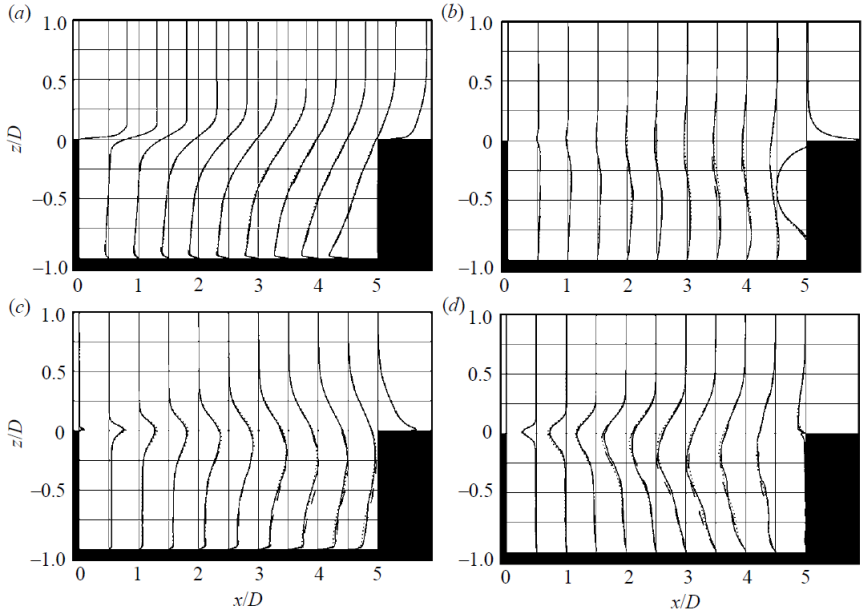

Figure 3.6 : a) Mean longitudinal velocity (b) Mean vertical velocity (c) urbulent energy (d) cross-Reynolds stress profiles [67].

3.2 Proposed Configurations for Noise Reduction

M219 clean cavity that was explained briefly in previous sections, where no passive/active control method is of the case, is the baseline problem of the present study. Various passive flow control methods in order to suppress the pressure

oscillations and reduce the OASPL generation are applied. Applied flow control methods are tabulated in Table 3.2.

The problem statement of the present study is as follows:

- Understanding the physics of the cavity flow and making an effort to improve the flow environment when a cavity is present.
- Investigating the unsteady behavior of three-dimensional cavities where the flow is compressible, transonic (0.85 Mach) and turbulent.
- Supressing the pressure oscillations encountered in cavity flows.
- Reducing the noise generated by cavities.

In order to achieve the desired goals, M219 clean cavity configuration (M219CC) is first taken into consideration and analyzed as the baseline geometry. Thereafter, various passive flow control methods are configured and applied to the baseline geometry. The original L/D ratio of 5 and W/D ratio of 1 are kept constant throughout the applied configurations as well as the freestream flow conditions. As it can be examined in Table 3.2, passive flow control methods related to reshaping cavity walls (aft, front), injecting/sucking the flow to/from the cavity passively, placing a spoiler or different types of vortex generators on the upstream of the cavity are applied. Additional combined configurations such as placing a spoiler on the upstream wall of the cavity whilst slanting the cavity aft wall are also implemented.

Table 3.2 : Performed passive flow controlled cavity cases throughout the present study.

Configuration	Notation	Brief Description
M219 Clean Cavity	M219CC	Clean cavity configuration with no flow control
Aft Wall Configurations	PAW1	45° inclination of aft wall
	PAW2	45° semi-inclination of aft wall
	PAW3	Stair-shaped aft wall
	PAW4	Spline-shaped aft wall
Front Wall Configurations	PFW1	22.5° inclination of front wall
	PFW2	45° inclination of front wall
Passive Injection-Suction Configurations	PIS1	Passive injection to front wall
	PIS2	Passive suction from aft wall
Spoiler Configurations	PSP1	Rectangular bar shaped spoiler at front edge of cavity
	PSP2	Rectangular bar shaped spoiler at 0.25D upstream of cavity
	PSP3	Rectangular bar shaped spoiler at 0.5D upstream of cavity
	PSP4	Wedge-shaped spoiler at front edge of the cavity
Vortex Generator Configurations	PVG1	Cylindrical shaped vortex generators upstream of the cavity
	PVG2	Triangular prism shaped vortex generators upstream of the cavity
	PVG3	Rectangular prism shaped vortex generators upstream of the cavity
	PVG4	Delta shaped vortex generators upstream of the cavity
Combined Configurations	PC1	Combination of PAW1 and PSP1
	PC2	Combination of PAW1 and PSP3

4. COMPUTATIONAL DETAILS

Details of geometry and grid generation, numerical domain and boundary conditions, OpenFOAM® setup and solution methodology will be given in this chapter.

4.1 Geometry Generation

The numerical domain of the present study is constructed using CATIA V5. Similar to the existing numerical studies [26, 84, 85, 98] a solution domain consists of upstream, sidestream and downstream walls is found to be suitable. Additional distances are put to the numerical domain to ensure that the mis-evolution and alteration of the flow caused by the numerical boundary conditions are negligible. The schematic representation of the numerical domain is given in Figure 4.1.

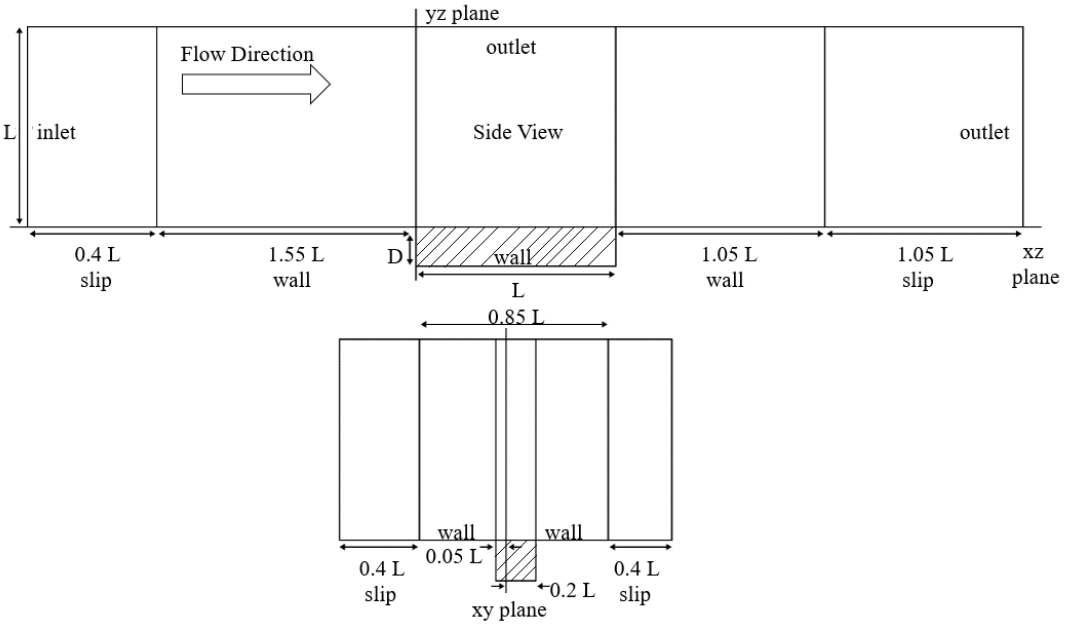

Figure 4.1 : Schematic representation of the outline of the numerical domain.

The dimensions in Figure 4.1 are shown relatively to the length of the cavity (L) which is 0.508 meters. An upstream wall of 1.55 L which is sufficiently long in terms of generating a fully developed boundary layer and a downstream wall of 1.05 L are created to mimic the wall specifications of the reference experimental study. The overall span of sidestream walls contiguous to the cavity is arranged as 0.65 L in order

to complete the similarity of geometric conditioning with the experimental cavity rig of Nightingale et al. [38] which was already shown in Figure 3.1. Additional extentions to the upstream, sidestream and downstream of the cavity rig are also created to minimize the undesired effects of the farfield boundary conditions to the cavity. The height of the numerical domain is arranged as the same with the cavity length that is 0.508 meters. Shaded region in Figure 4.1 represents the cavity region.

4.2 Grid Generation

The generation of the grid is performed via the mesh generation software Pointwise R18. Throughout the study, a structured grid methodology is applied except for the vortex generators cases.

A structured grid with hexahedral elements are generated for each case by following the log-law of the wall [129]. The dimensionless wall distance parameter y^+ is calculated prior to analyses and kept within the limits of log-law layer as 300 for upstream wall of the cavity for all computations. Additional y^+ independence studies are also conducted prior to the analyses of passive flow control techniques. Several reasons lie behind the decision of the value of y^+ being in log-law layer, such as the implementation of wall functions, large-scale coherent structures governed cavity flow physics [11,90] and the need of reducing the total number of cells, since more than 40 different configurations and tests were analyzed and limited available amount of CPUs were of the case. Proper wall functions are used for each cases in order to model flow near the walls.

Constructed three dimensional structured grid on M219CC is shown in Figure 4.2. Generated grids for each configuration that are given in Table 3.2 are presented sequentially in Appendix A.

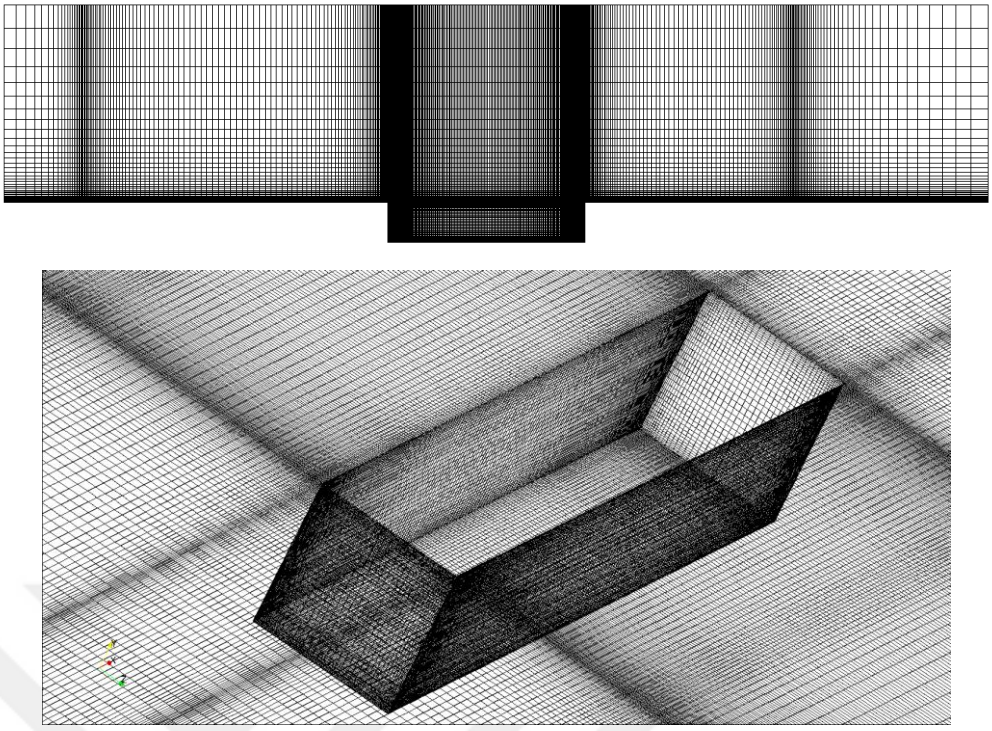

Figure 4.2 : Structured grid of the M219CC domain, side view (top) and close-up cavity region view (bottom).

An extensive grid convergence analysis is conducted by taking M219CC as the base case with different grid densities and different dimensionless wall distance parameter y^+ values. Details of the grid convergence study is given in Table 4.1.

Table 4.1 : Grid convergence study details.

Case Name	Overall Cell Count	Cells in Cavity Zone	First Layer Thickness (m)	y^+ on upstream wall
Coarse (C1)	1323000	135000	8.83×10^{-4}	300
Medium1 (M1)	3136000	320000	8.83×10^{-4}	300
Medium2 (M2)	3136000	320000	2.94×10^{-4}	100
Medium3 (M3)	3136000	320000	8.83×10^{-5}	30
Fine (F1)	6125000	625000	8.83×10^{-4}	300
Very Fine (VF1)	10584000	1080000	8.83×10^{-4}	300

The ratio of cells within the cavity zone to overall cells on the numerical domain is kept constant as ~10% for each test case. C1 grid consists of 1.33M cells while 135K of those cells are within the boundaries of the cavity zone. M1 case consists of 3.14M cells and nearly 10% of the cells are in the cavity zone. Overall cell count between M1, M2 and M3 cases are kept constant whilst the minimum wall spacing is changed from 8.83×10^{-4} m to 8.83×10^{-5} m by taking into consideration the log-law of the wall. F1 and VF1 cases are the condensed versions of C1 and M1. Cavity close-up side

views of grid convergence study cases are presented in Figure 4.3. Arrows pointing the edges of the cavity show where the coarsening or refinement is performed.

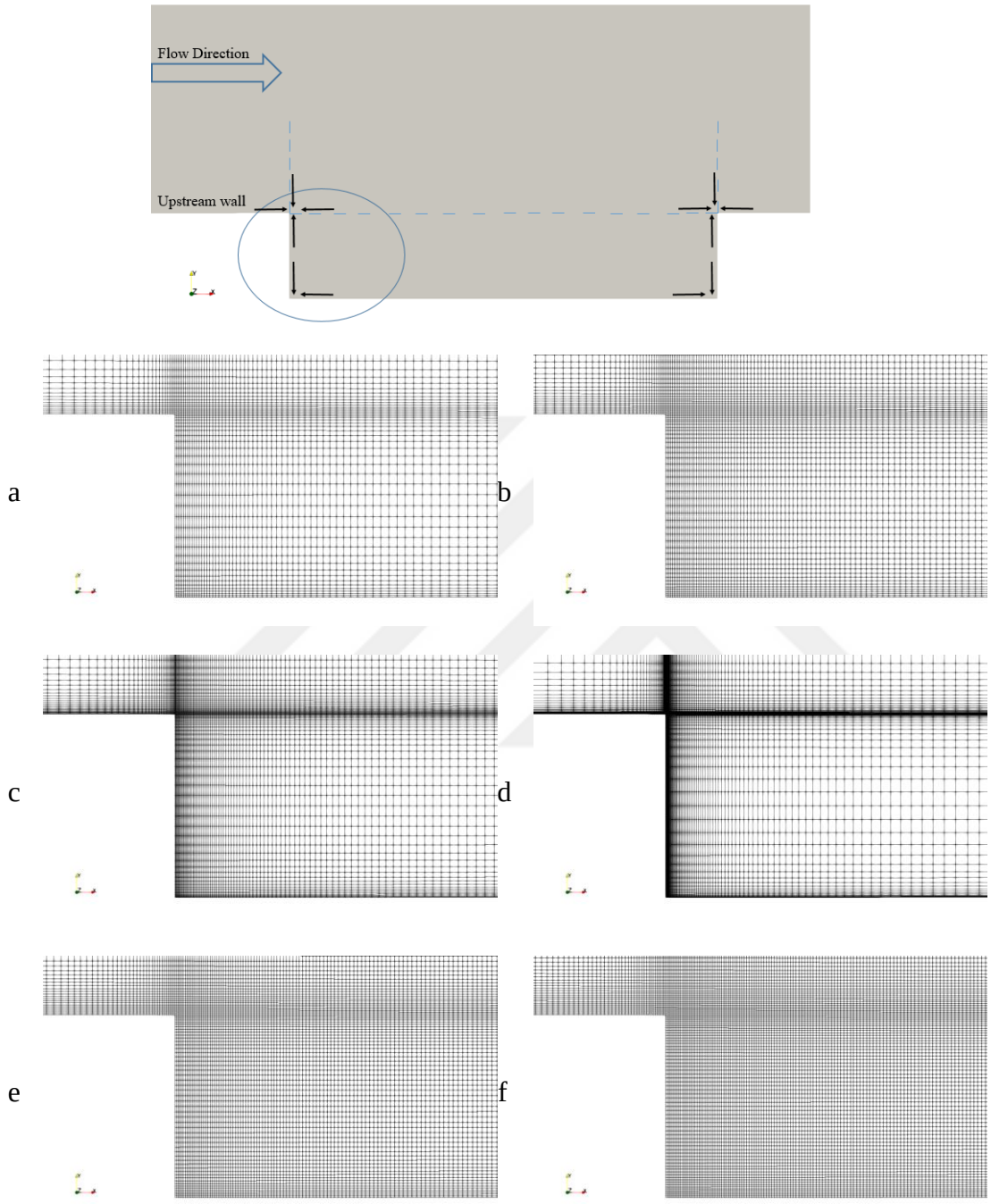

Figure 4.3 : Cavity region close-up side views of grid convergence study cases: a) C1 b) M1 c) M2 d) M3 e) F1 f) VF1.

Effects of refinement and coarsening as well as changing the first layer thickness in the grid will be discussed in the results section.

4.3 Solution Methodology

4.3.1 OpenFOAM Simulation Directories

Numerical analyses of this present study are conducted via the open-source engineering software OpenFOAM®. OpenFOAM® is an open source software written in C++ language that is capable of solving numerous engineering problems ranging from CFD to electromagnetics.

First steps of OpenFOAM® are taken in 1993 when Henry Weller has started to develop a closed-source software with Hrvoje Jasak who has completed his doctoral dissertation on the development of basis of the current OpenFOAM® [135]. In 2004, ESI-OpenCFD company has released OpenFOAM® as an open source software [136]. Since then, OpenFOAM® which is extensively capable of handling complex problems of CFD has been widely used by fluid dynamics community all around the world and continuously being developed by numerous researches. Software details of OpenFOAM® can be found in [125].

Three main directories are needed to perform a simulation in OpenFOAM®. Inside these main directories, there can be various sub-directories. Aforementioned main directories are as follows:

- ***0*** directory
- ***constant*** directory
- ***system*** directory

0 directory contains initial and boundary conditions of the problem and is essential for the initialization of the problem and for the appointment of necessary boundary conditions.

constant directory basically contains essential files about the mesh, turbulence modeling, transport and thermochemical properties of the working fluid(s).

system directory where arrangements related to discretization and solution methods of the governing equations are made is the keystone of the main solution folder. Numerical methods to discretize the governing equations, solver settings, linear equation solver settings are performed in this directory.

Structure tree of a general case in OpenFOAM® is shown in Figure 4.4.

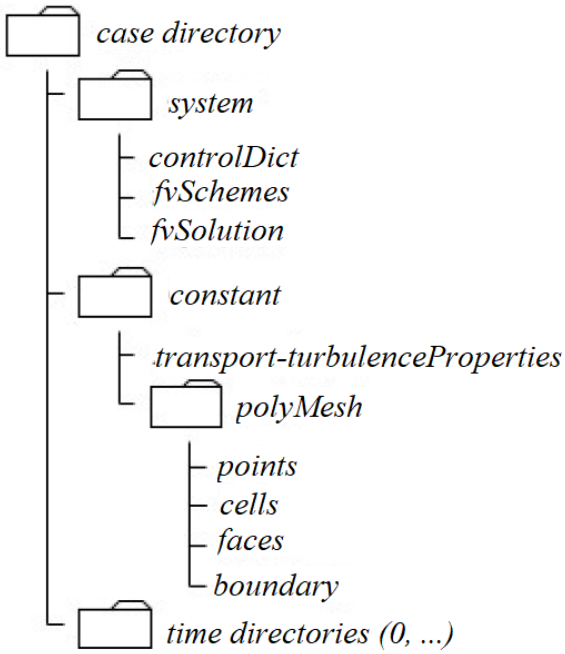

Figure 4.4 : Typical case structure of a simulation in OpenFOAM® [125].

4.3.2 Cavity Simulation Setup

First of all, a template case directory is created for the simulations. Sub-directories of case folder (***0***, ***constant*** and ***system***) are created in a way such that the desired problem is defined properly. In this section, boundary conditions, wall functions that are required to model the boundary layer near the wall, physical properties of the fluid, turbulence model specification, solver specification, discretization and linear system solver arrangements as well as the other details of the simulations will be provided.

Numerical domain along with the boundary conditions were presented in Figure 4.1. The inlet is a general Dirichlet type boundary, whereas the outlet is a general Neumann type boundary. In Dirichlet type boundary condition, a fixed value constraint for a variable is applied; whereas in Neumann type boundary condition, the gradient normal to the boundary of a variable at the boundary is specified as zero. The walls are set to be adiabatic to satisfy the criterion that the net heat flux across the wall boundary is zero. In OpenFOAM®, in ***0*** directory, parameters that are listed in Table 4.2 are emposed as necessary parameters for simulations to be run. This parameters are thermal wall function for turbulent thermal diffusivity, turbulence kinetic energy, turbulence viscosity, specific turbulence dissipation rate, static pressure, static temperature and velocity, respectively.

Table 4.2 : Emposed boundary conditions.

Parameter	Notation in OpenFOAM®	Unit
Thermal wall function for turbulent thermal diffusivity (α_t)	alphat	kg/m/s
Turbulence kinetic energy(k)	k	m^2/s^2
Turbulence viscosity (ν_t)	nut	m^2/s
Specific turbulence dissipation rate (ω)	omega	1/s
Static pressure (p)	p	$kg/m/s^2$
Static temperature (T)	T	K
Velocity (U)	U	m/s

The solution field is initialized with zero value for α_t. The boundaries except the wall region has been appointed with the boundary condition named *zeroGradient*, which means that the quantity is developed in space and its gradient is equal to zero in direction perpendicular to the patch. Typical Neumann boundary condition implementation in OpenFOAM® is *zeroGradient*. A standard wall function for alphat is applied to the walls, called *alphatWallFunction*. Slip boundaries are set to be *symmetry* boundary condition.

For turbulence kinetic energy (k), one of the default wall functions that is defined in OpenFOAM® is used for the wall, named *kqRWallFunction*. The internal field and the inlet are initiliazed with the following formula given in equation 4.1:

$$k = \frac{3}{2}(UI)^2 \tag{4.1}$$

where I is the turbulence intensity of the flow and U is the freestream velocity.
The turbulence viscosity (ν_t) is also one of the turbulence related parameters that needs to be defined in ***0*** directory in a compressible turbulent simulation. The field is initialized with the value of 1.79×10^{-5} m^2/s. A wall function is defined for the wall boundary, called *nutkWallFunction*. The inlet and outlet boundaries are assigned to *zeroGradient* boundary condition.

The specific dissipation rate (ω) in the internal field and the inlet is initiliazed with the following formula given in equation 4.2:

$$\omega = \frac{\rho k}{\mu}\left(\frac{\mu_t}{\mu}\right)^{-1} \tag{4.2}$$

where ρ is the freestream density, μ is the dynamic viscosity and μ_t/μ is the eddy viscosity ratio which is the ratio of turbulent viscosity to molecular dynamic viscosity of the fluid. For the wall boundary, a standard wall function named *omegaWallFunction* is imposed.

Primitive variables of the flow (pressure, temperature and velocity) are also defined in ***0*** time directory. For the pressure, since strong pressure waves exist, a non-reflecting boundary condition is used to ensure that the outgoing acoustic waves can travel outside of the domain e.g., absorbed, when reached to the boundaries, without reflecting and truncating additional non-physical numerical errors. The non-reflecting boundary condition of OpenFOAM® is called *waveTransmissive* and is used in the present study. The internal field is initialized with the freestream value of static pressure. The generic Neumann boundary condition of OpenFOAM® *(zeroGradient)* is used for the walls. The internal field is initiliazed with the freestream temperature as well as the inlet boundary where Dirichlet boundary condition is applied. Outlet and walls are set to be Neumann type boundary conditions. As for the velocity parameter, the internal field is initialized with the freestream value and the inlet is set to be Dirichlet boundary condition. The outlet section is set to be Neumann type boundary and the walls are set to be adiabatic, as mentioned before. The slip boundaries which are placed upstream, sidestream and downstream of the cavity region are set to be *symmetry* boundary condition which enforces a symmetry constraint. Cavity-adjacent walls are defined as adiabatic walls boundaries. Sea level properties of flow variables are used for the initialization for the analyses. Applied initial conditions are presented in Table 4.3.

Table 4.3 : Initial conditions of the problem.

Parameter	α_t	k	ν_t	ω	p	T	U
Initial Value	Uniform 0	Uniform 12.56	Uniform $1.79\text{x}10^{-5}$	Uniform 856000	Uniform 101325	Uniform 288.15	Uniform (289.32 0 0)

Applied boundary conditions and corresponding boundary values for each boundaries are given in Table 4.4-Table 4.6.

Table 4.4 : Applied boundary conditions for outlet boundary.

Outlet		
Parameter	Boundary Condition	Boundary Value
α_t	zeroGradient	--
k	zeroGradient	--
ν_t	zeroGradient	--
ω	zeroGradient	--
p	waveTransmissive	Uniform 101235
T	zeroGradient	--
U	zeroGradient	--

Table 4.5 : Applied boundary conditions for inlet boundaries.

Inlet		
Parameter	Boundary Condition	Boundary Value
α_t	zeroGradient	--
k	fixedValue	Uniform 12.56
ν_t	fixedValue	Uniform 1.79×10^{-5}
ω	fixedValue	Uniform 856000
p	waveTransmissive	Uniform 101235
T	fixedValue	Uniform 288.15
U	fixedValue	Uniform (289.32 0 0)

Table 4.6 : Applied boundary conditions for wall boundaries.

Wall		
Parameter	Boundary Condition	Boundary Value
α_t	compressible::alphatWallFunction	Uniform 0
k	kqRWallFunction	Uniform 12.56
ν_t	nutkWallFunction	Uniform 1.79×10^{-5}
ω	omegaWallFunction	Uniform 856000
p	zeroGradient	--
T	zeroGradient	--
U	fixedValue	Uniform (0 0 0)

Simulations are conducted at sea level and reference sea level freestream values for the specified problem are presented in Table 4.7.

Table 4.7 : Sea level freestream values of flow properties.

Property	Value
Velocity (m/s)	289.325
Mach	0.85
Pressure (Pa)	101325
Temperature (K)	288.15
Reynolds Number	$1x10^7$
Turbulence kinetic energy (m^2/s^2)	12.56
Specific dissipation rate (1/s)	$8.56x10^4$

It should be noted that transient analyses are conducted throughout this thesis. Aforementioned initial and boundary values are evolved with the advancement in time and lost the importance especially in wall functions. Also, only M219CC case is initiliazed with the settings given above. The rest of simulations are initialized with the last time step data of the M219CC.

Once ***0*** time directory is constituted, physical properties of the fluid and turbulence properties of the simulation are set in ***constant*** directory. For compressible flows, physical properties are specified in *thermoPhysicalProperties* file. The turbulence is also set in the same directory in a file named *turbulenceProperties*. In this simulation, $k-\omega SSTDES$ turbulence model is applied.

The information about mesh is kept in a sub-directory named *polyMesh* which consists of seven different files for the present problem named *boundary*, *cellZones*, *faces*, *faceZones*, *neighbour*, *owner* and *points*, respectively. The information of boundary conditions are kept inside the file *boundary*.

Lastly, the necessary arrangements in ***system*** directory are performed. In this directory, six files are present which are given in Table 4.8.

Table 4.8 : *system* directory files and their content.

File Name	Content
controlDict	Solver, simulaton time, Courant number, time step spesifications, additional functions
decomposeDict	Parallelization settings
fvOptions	Additional settings such as temperature limiter
fvSchemes	Discretization specifications
fvSolutions	Linear matrix solver spefications
mapFieldsDict	Mapping of a previous solution

The *controlDict* file contains information related to the solver and simulation time as well as the functions that may be used for the simulation. As mentioned in previous chapters, implicit solver rhoPimpleFoam is used. The simulations are run for 50 CTS where 1 CTS corresponds to the one passage of a flow particle through the cavity length. CTS is calculated as shown in equation 4.3.

$$1\ CTS = L/U_{\infty} \tag{4.3}$$

For the current problem, 1 CTS corresponds to 1.76×10^{-3} seconds. Simulations are run for 50 CTS where the first 10 CTS is used to settle the flow down and then the average of data of last 40 CTS is taken for the solution. The flowfield data of each 0.1 CTS is written and stored inside time directories. Maximum Courant number is set to 1 since a DES is performed in a turbulent compressible region. The residuals are both stored and plotted using the relevant function and flow variable Mach number, additional to the main variables is computed for each time step. Probes that are placed on cavity floor are defined in this file as shown in Figure 4.5. Pressure data at each probe is stored for each 0.001 CTS.

```
probes_floor
{
    type            probes;
    libs            ("libsampling.so");
    writeControl    runTime;
    writeInterval   1.76e-6; // cts 0.001
    fields
    (
  p
    );
probeLocations
    (
        (0.0254 -0.1016 0) // 5%
        (0.0762 -0.1016 0) // 15%
        (0.1270 -0.1016 0) // 25%
        (0.1778 -0.1016 0) // 35%
        (0.2286 -0.1016 0) // 45%
        (0.2794 -0.1016 0) // 55%
        (0.3302 -0.1016 0) // 65%
        (0.3810 -0.1016 0) // 75%
        (0.4318 -0.1016 0) // 85%
        (0.4826 -0.1016 0) // 95%
    );
}
```

Figure 4.5 : Probes placed on cavity floor.

As for the averaging of the flow variables (pressure and velocity) that has been started after the first 10 CTS, *fieldAverage* function of OpenFOAM® is used and both mean and the RMS values of each variable are computed. A sample *fieldAverage* function definition is shown in Figure 4.6.

```
fieldAverage
{
    type            fieldAverage;
    libs            ("libfieldFunctionObjects.so");
    writeControl    writeTime;
    fields
    (
        U
        {
            mean        on;
            prime2Mean  on;
            base        time;
        }
        p
        {
            mean        on;
            prime2Mean  on;
            base        time;
        }
    );
}
```

Figure 4.6 : Field averaging in OpenFOAM®.

To observe the qualitative evolution of unsteadiness behavior of the cavity flow, surface sampling is also done for velocity and pressure. Surfaces at each 0.1 CTS for three different locations (central xy-plane cut where probes are placed, xz-plane cut at a 0.01L distance from the cavity mouth, yz-plane cut at a 0.5L distance from cavity start).

Lastly, iso-surfaces of Q which calculates and stores the second invariant of the velocity gradient tensor [139] are sampled for a proper visualization of turbulent structures present in the flow.

In *decomposeParDict* file, number of processors to be used for parallel simulations and the technique for the parallelization is defined. In most of the cases, 224 processors are used and the "*scotch*" technique which aims to minimize the number of processor boundaries is applied for parallelization of the simulations.

The limits of temperature, to avoid possible non-physical values, are defined in *fvOptions* file. The minimum temperature is set to $100\ K$, whereas the maximum is set to $500\ K$.

The file named as *fvSchemes* is the key aspect of the numerical discretization and finite volume solution. In this file, discretization method of terms of governing equations are specificied both in space and in time. The generic *fvSchemes* file that has been set up for the present simulations is shown in Figure 4.7.

```
ddtSchemes
{
    default         Euler;
}

gradSchemes
{
    default         Gauss linear;
}

divSchemes
{
    default         Gauss upwind;
    div(phi,U)      Gauss limitedCubicV 1;
    div(((rho*nuEff)*dev2(T(grad(U))))) Gauss linear;
}

laplacianSchemes
{
    default         Gauss linear limited 1;
}

interpolationSchemes
{
    default         linear;
}

snGradSchemes
{
    default         limited 1;
}

wallDist
{
    method      meshWave;
}
```

Figure 4.7 : *fvSchemes* file used for the simulations.

In Figure 4.7, the keyword *ddtSchemes* corresponds to the discretization of time. In this study, time discretization is applied via Euler scheme. Euler scheme is a first order, bounded time discretization scheme that is used for transient simulations. The keyword *gradSchemes* corresponds to the gradient term discretization. The discretization of gradient terms of governing equations are done via Gauss linear technique which is second order accurate. In OpenFOAM®, there are many discretization options available for convective term discretization. The most common schemes are first order upwind differencing, central differencing, total variation diminishing (TVD) schemes and normalized variable diagram (NVD) schemes. Convective term discretization is specified under the keyword *divSchemes*. In most of the cases, the velocity is discretized via Gauss *limitedCubicV* with a limiter of 1. This scheme is a TVD scheme and prevents the generation of local undershoots and/or overshoots in the solution. Specification of discretization of Laplacian terms are made in *laplacianSchemes* section. Surface normals (*snGradSchemes*) are discretized in the same manner with Laplacian terms. The term *wallDist* is needed when wall functions are used and the wall is modeled.

Solution strategy of linear algebraic equations, solver tolerances and algorithms are specified and controlled in the *fvSolution* file. For each equation that needs to be solved in the system, a solver must be defined. Solvers distinguish from each other depending on the quantity that needs to be solved. For instance, time derivatives and Laplacian terms form a symmetric matrix whilst an advective derivative forms an asymmetric matrix Pressure is a symmetric, velocity is an asymmetric matrix. In OpenFOAM®, while some solvers use smoother functions and some others use preconditioner functions and explicit system solvers require neither of them. For a comprehensive information, user guide of OpenFOAM® is strongly advised [125]. In the present study, generalized geometric algebraic multi grid (GAMG) solver with the diagonal incomplete lower-upper (DILU) smoother is applied for the pressure solution. For other quantities that exist in flow (velocity, internal energy and turbulence related parameters) stabilized preconditioned bi-conjugate gradient (PBiCGStab) solver with DILU smoother is applied. Lastly, for the computation of density, diagonal solver is used. Solution algorithm PIMPLE which is a combination of pressure implicit with splitting operator (PISO) algorithm and semi-implicit method for presure linked equations (SIMPLE) is used as a requirement of rhoPimpleFoam solver.

The file *mapFieldsDict* is used for mapping of solution field from one case to another. It has the advantage of generating the desired flow domain much more quicker than the standart initialization. In most of the cases, solution field of the M219CC case is mapped to the initial ***0*** time directory of the current case. This mapping has contributed vanishing of divergence errors and greatly reduced required computational time for the desired solution.

5. RESULTS AND DISCUSSIONS

Obtained results of conducted simulations are presented in this chapter. Results of grid convergence study, clean cavity case and passive flow control methods will be given in detail. Comparisons and conclusions from instantaneous field contours, mean field contours of Mach, pressure and turbulence kinetic energy intensity, PSD graphs, OASPL distributions, and so on will be made.

Firstly, the effect of grid density and dimensionless wall distance y^+ are investigated. Validation through available experimental [38] and numerical [67] data is also conducted.

5.1 Validation of the Model

Validation of the current model is conducted prior to investigations of passive flow control techniques, to ensure that the model is valid. As given in Table 4.1, six different grids are constructed. For the grid convergence study, results are given as two parts. Results of the first part where cell number is changed but the y^+ value kept constant are given together. Similar to that, results of the second part where the cell number is kept constant but the y^+ value is altered are presented together. This discrimination is done to ease the readability of grid convergence investigation results.

Discrete acoustic tones seen in open cavities (Rossiter modes) are compared with the experimental and theoretical findings (Figure 5.1). A set of pressure data obtained from the probe placed at 0.95 x/L of the cavity floor is used for the PSD measurement. In other words, pressure data of last 40 CTS of simulations which approximately corresponds to ~40000 data are used for these measurements. It is seen that Rossiter modes were captured well for all grid convergence study cases. The highest power density is seen in case VF1 which is the finest grid. Although some delusive peaks are observed, first three modes of Rossiter are captured well. Fourth mode, which is seen approximately at 800 Hz is captured but since the magnitude of the tone is smaller than the others, it is difficult to see. Also, the most dominant Rossiter mode is observed as

the 2nd one which occurs approximately at 380 Hz. Figure 5.1 reveals that the presence of Rossiter modes are not primarily depend on the y^+ value of the upstream wall.

a

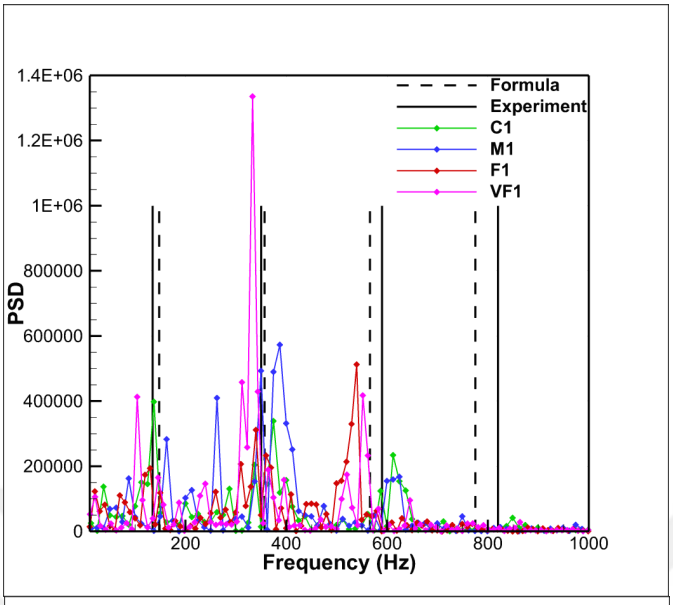

b

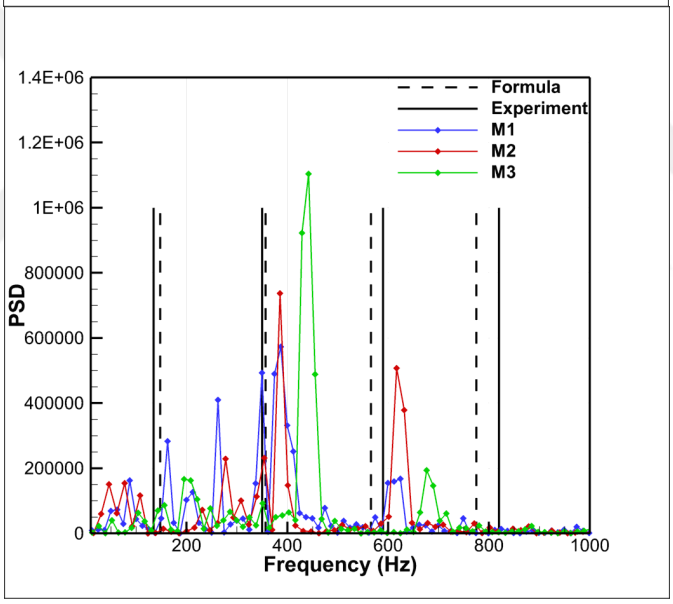

Figure 5.1 : Spectral analysis (at x/L=0.95) on cavity floor for grid convergence study for M219CC with Rossiter's acoustic tones. a) Comparison for different grid numbers b) Comparison for different y^+ values.

Normalized longitudinal velocity profiles on the central xy-plane are also compared with each other and with the reference numerical data (Figure 5.2). Velocity profiles from six equally distant different locations are extracted starting from the cavity leading edge up until the cavity aft edge. It is seen that the velocity profile of C1 is slightly shifted from the reference data and from other cases. The main reason of the shifted profile C1 case is considered to be the too coarse grid structure. Figure 5.2 shows that the velocity profile of M1 case is well-suited to the reference data. Profile

of F1 seems to fit well except the lower part of the cavity. A similar situation is also observed in the VF1 case (Figure 5.2a). It may be viewed that the velocity profile of M3 shifted a lot more than others. Although the spectral analysis (Figure 5.1) gave satisfactory results for M3 case, the expected similar results are not present for velocity profiles (Figure 5.2b). Velocity profiles of M1, as mentioned previously, are well-suited to reference data, whereas a small distortion for M2 on lower part of the cavity is observed.

a

b

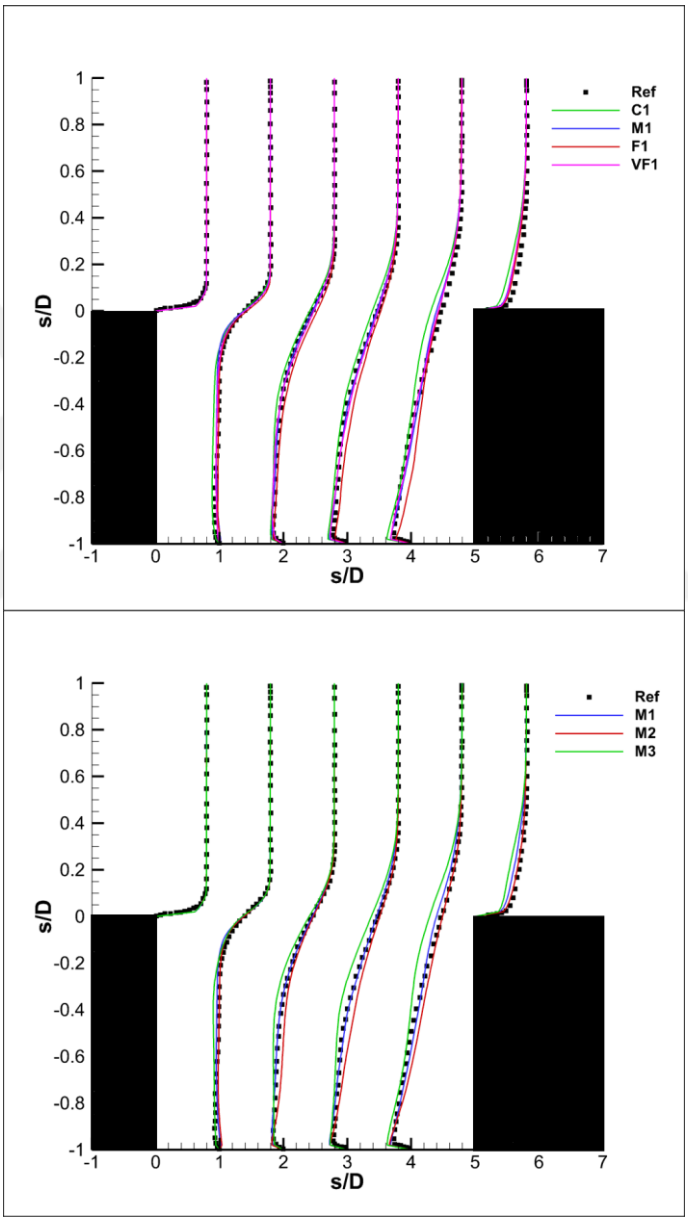

Figure 5.2 : Mean longitudinal velocity analysis for grid convergence study for M219CC. a) Comparison of different grid resolutions b) Comparison of different y^+ resolutions.

Mean contours of Mach number, turbulence intensity and OASPL are presented respectively in Figure 5.3 and Figure 5.4. In Figure 5.3, mean Mach number contour

for each case are found to be similar. The behavior of mean shear layer is almost identical for each case. For VF1, the shear layer seems to be more oscillatory than the others. The turbulence intensity of C1 is also the lowest. The main reason for this difference is thought to be the coarse grid structure. As expected, turbulence intensity increases going from C1 to VF1. Maximum turbulence intensity seen in cavity region is also approximately ~23%. As for the OASPL contours of Figure 5.3, a similarity for each grid convergence case is present.

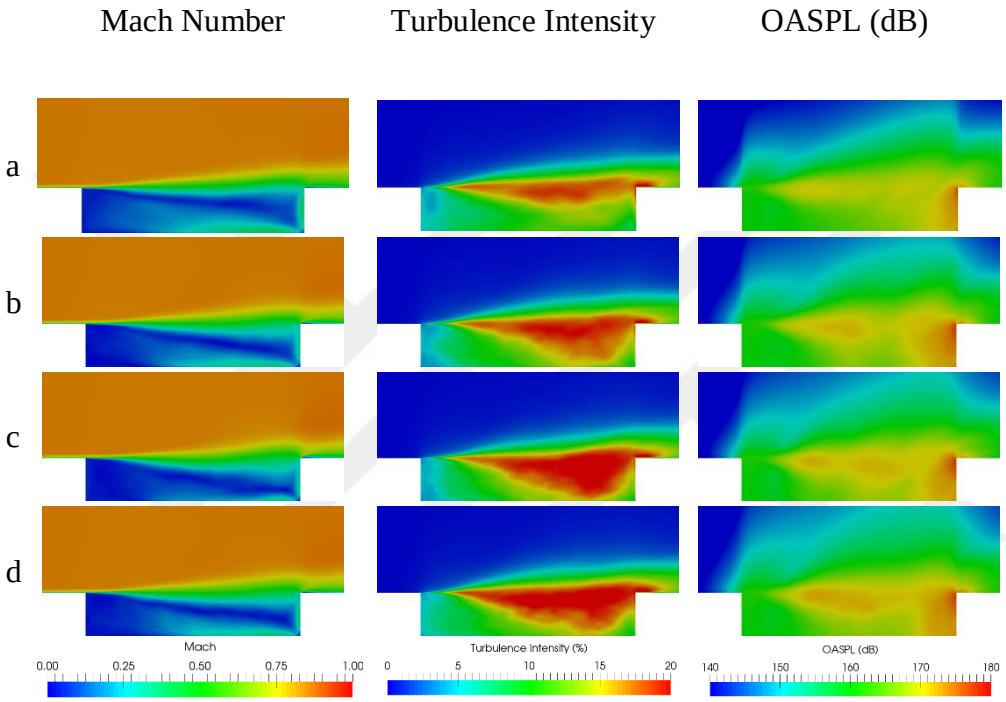

Figure 5.3 : Mean Mach, turbulence intensity and OASPL (dB) contours for different grid numbers: a) C1 b) M1 c) F1 d) VF1.

Figure 5.4 represents the mean flow contours of grid convergence study for cases where y^+ value is changed. Mean Mach number contours reveal that the mean shear layer in M3 case tends to go slightly downward compared to M1 and M2. The mean impingement location of M3 is slighly closer to the cavity floor. The propagation of turbulence intensity is smaller on M2 and M3 cases than M1. Analogous to Figure 5.3, a similarity is of the case for OASPL contours.

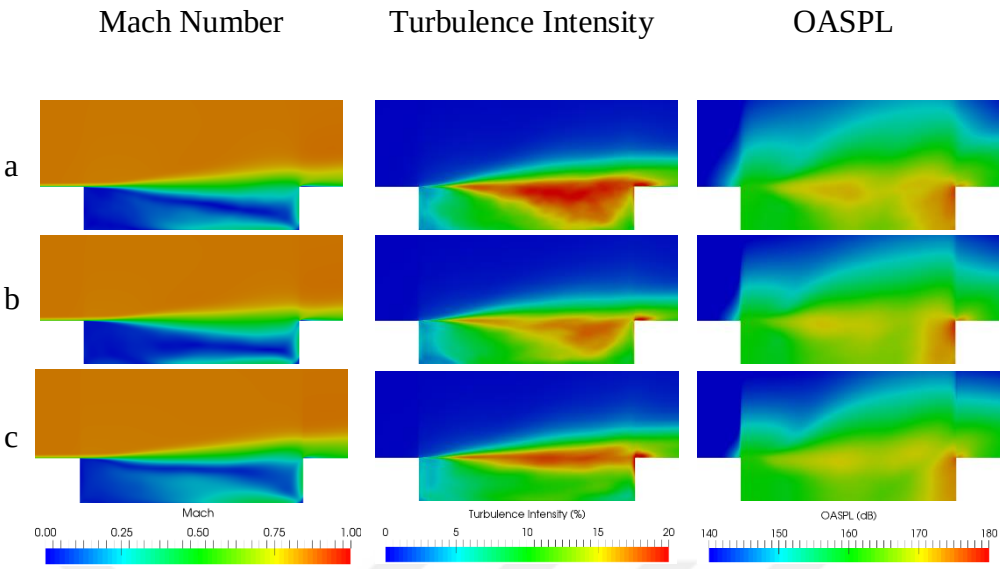

Figure 5.4 : Mean Mach, turbulence intensity and OASPL (dB) contours for different y^+ values: a) M1 b) M2 c) M3.

OASPL distribution on the cavity floor is obtained through pressure probes located equidistantly along the cavity floor at central xy plane. The results in Figure 5.5a shows that an overprediction for all cases is present. C1 case is failed to capture the general OASPL distribution profile along the cavity floor. C1, being too dissipative, is proven to be an undesirable selection for the following simulations. However, all cases show a similar profile at the start and at the end of the floor. The differences seen in mid-section of the cavity floor are negligible for F1 and VF1 cases. OASPL distribution of M1 case is observed to catch the general trend of the experimental data. In Figure 5.5b, M1, M2 and M3 cases are compared in terms of OASPL distribution. Distributions of M1 and M2 are very similar except that the slope of increment at 30% of the cavity is higher for M2 than M1 and experimental data.

As a conclusion to grid convergence study, six different grids are investigated. The grid resolution and the y^+ variation are examined. It is seen that the y^+ dependency is not crucial for cavity investigations when the y^+ value is higher than 1. According to the results, usage of wall functions are sufficient in terms of spectral analyses. Since the flow is governed by the behavior of the shear layer and by large-scale coherent structures, resolving the wall is not the first priority. It is believed that the grid convergence is completed and M1 case is decided to be used for the remaining simulations.

a

b

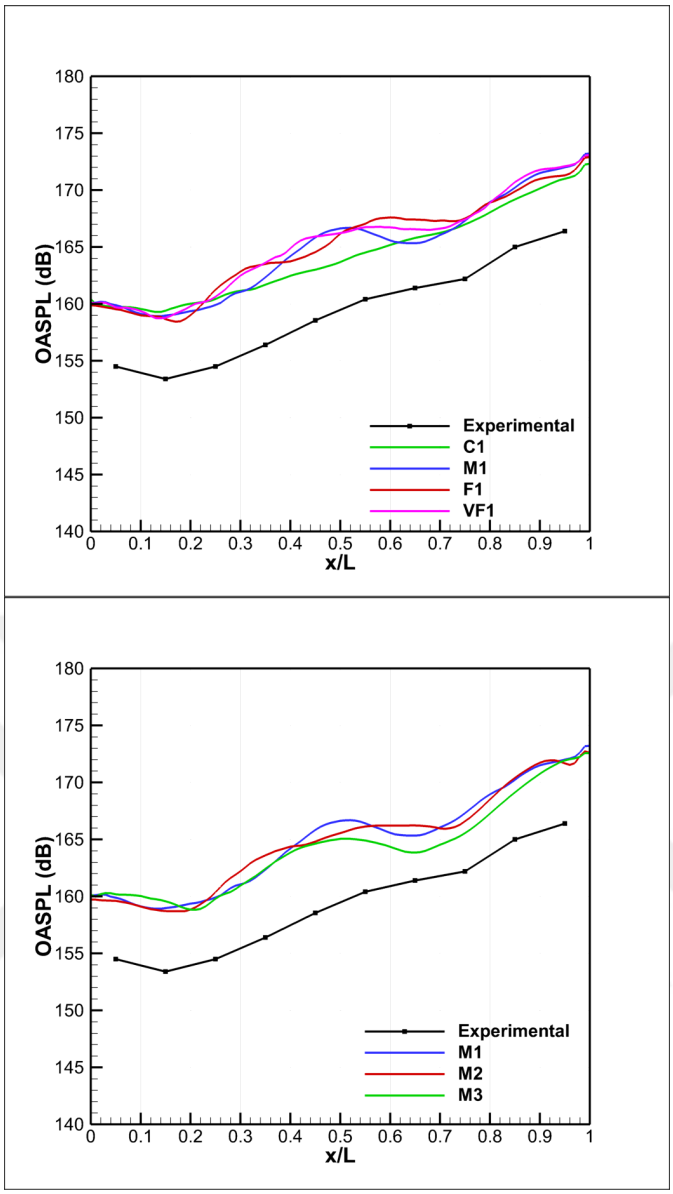

Figure 5.5 : OASPL distribution at the mid-section of the cavity floor for grid convergence study a) For different cell numbers b) For different y^+ values.

5.2 Clean Cavity

Instantaneous flow contours of clean cavity are inspected in order to visualize the feedback mechanism and complex unsteady flow behavior. Figure 5.6 shows the evolution of a main streamwise vortex within the cavity as an expected result of feedback mechanism. The contours are taken at equally divided instantaneous time of the 2nd Rossiter mode period which is represented as t_{R2}. It is also noticed that the flow is highly unsteady which has several vortices at different locations of the cavity. It is also a fact that since DES technique is applied, the instantaneous flow has a highly rotational behavior where both small and large vortices present.

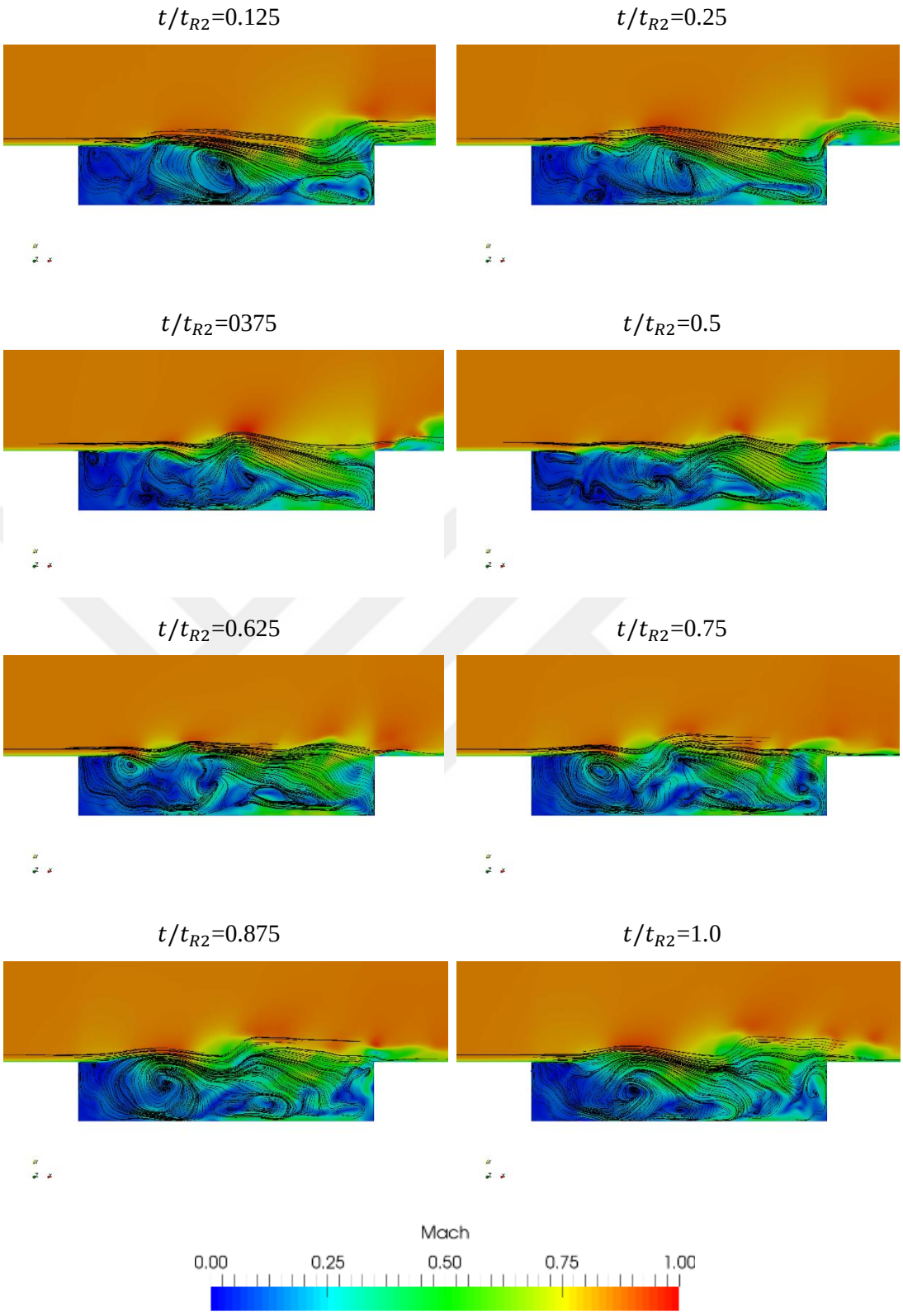

Figure 5.6 : Instantaneous Mach contours of M219CC for one period of 2nd Rossiter mode.

Similar to instantaneous Mach contours, instantaneous pressure contours are also sampled and represented for one dominant Rossiter mode (2nd mode) in Figure 5.7.

The legend ‘pNon’ represents the deviation from freestream pressure where red coloring shows the positive deviation and the blue shows the negative deviation. The fluctuant, time-dependent pressure profile, high pressure levels resulting from the impingement of shear layer to cavity aft wall can easily be seen by inspecting Figure 5.7.

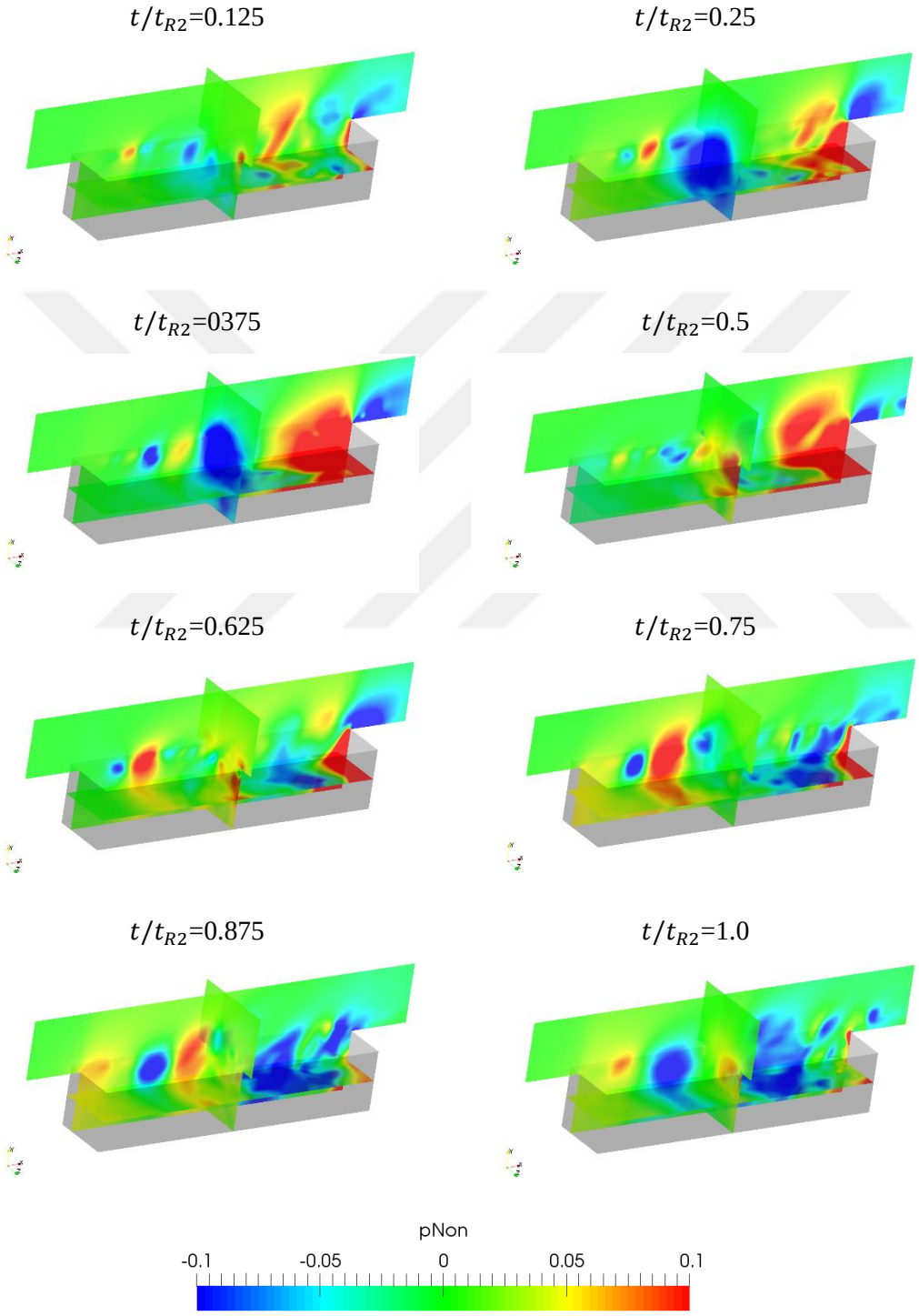

Figure 5.7 : Instantaneous pressure contours of M219CC for one period of Rossiter mode.

Isosurfaces of Q-criterion for clean cavity configuration are represented in Figure 5.8. The result shows that the flow within the cavity is governed by large-scale coherent structures which are formed by the separation of shear layer from cavity leading edge and these structures densify near the cavity aft wall where the interaction of shear layer with the cavity aft wall occurs.

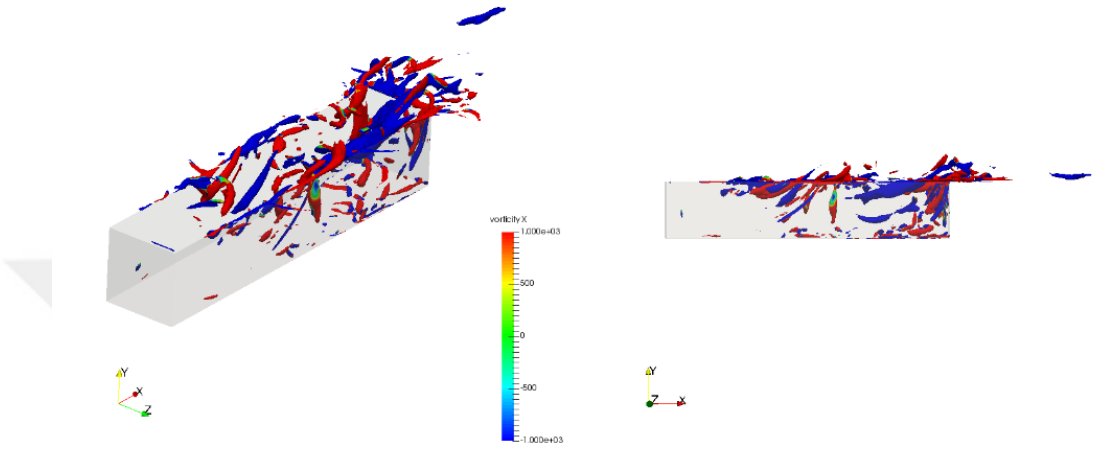

Figure 5.8 : Isosurfaces of Q-criterion for colored by x-vorticity for clean cavity configuration, t=0.88 s.

Planes normal to x-direction at various locations (0.2, 0.5 and 0.8 of x/L) are also extracted and colored by instantaneous x-vorticity with streamlines of instantaneous velocity. This representation visualizes of three dimensional, highly rotational and unsteady behavior of cavity flows and may be examined in Figure 5.9.

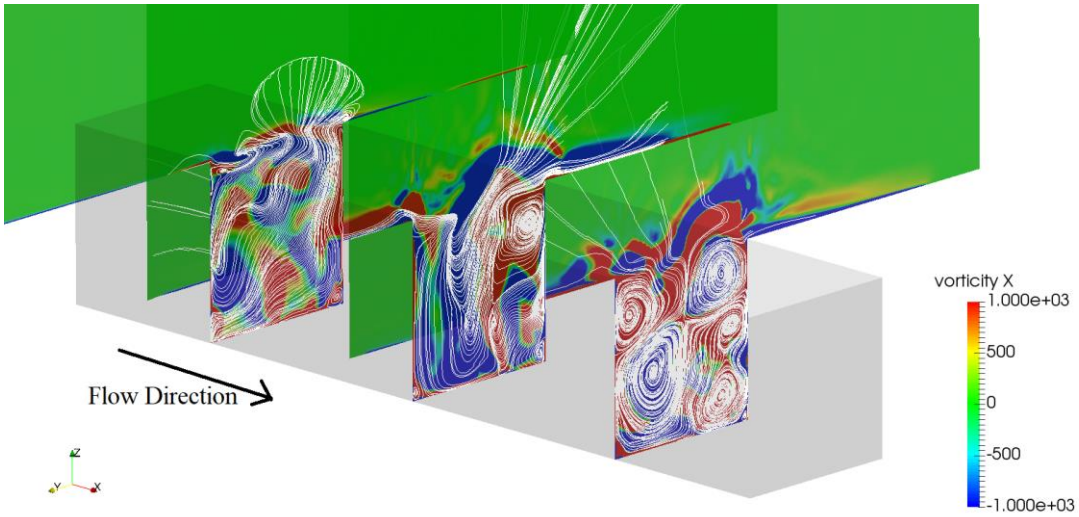

Figure 5.9 : x-vorticity contours at different planes for M219CC, t=0.88 s.

5.3 Aft Wall Configurations

Mean flow contour results of cavity aft wall configurations are presented in Figure 5.10. It is observed that the general behavior of the shear layer shows almost no change whereas the turbulence intensity inside the cavity decreases slightly when an aft wall passive flow control method is applied. This alleviation is thought to be arise from the smoother collision of the shear layer with the aft wall. The highest reduction in turbulence intensity is seen in PAW1 configuration where the aft wall was inclined by 45°. As for the OASPL, all aft wall configurations reduced the OASPL distribution especially near the cavity front side. OASPL intensity at cavity aft wall are higher for PAW3 and PAW4 configurations compared to PAW1 and PAW2. Expansion of high OASPL values to out of the cavity was lowered when a passive flow control is applied. The difference in the acoustic propagation is seen obviously for each aft wall control technique. Figure 5.11 represents the OASPL distribution along the cavity floor at the mid-plane for aft wall configurations. Aft wall configurations have proven to be effective in terms of OASPL reduction. Since the main source of the noise generation is aft wall, changing the geometry of aft wall has decreased OASPL. PAW1 configuration is the best applied configuration in terms of OASPL reduction. Reduction was measured as ~10 dB at the front half of the cavity floor. All configurations have given similar OASPL results near the cavity aft wall. Isosurfaces of Q-criterion for aft wall configurations colored by x-vorticity are shown in Figure 5.8. It can be examined that less and smaller structures are present for aft wall configurations compared to M219CC. Chaotic structures that are seen in front half of M219CC are no longer present for PAW1, PAW2 and PAW4 configurations. It is also noticed that the flow tends to be more rotational in aft wall configurations, especially in PAW3, than M219CC.

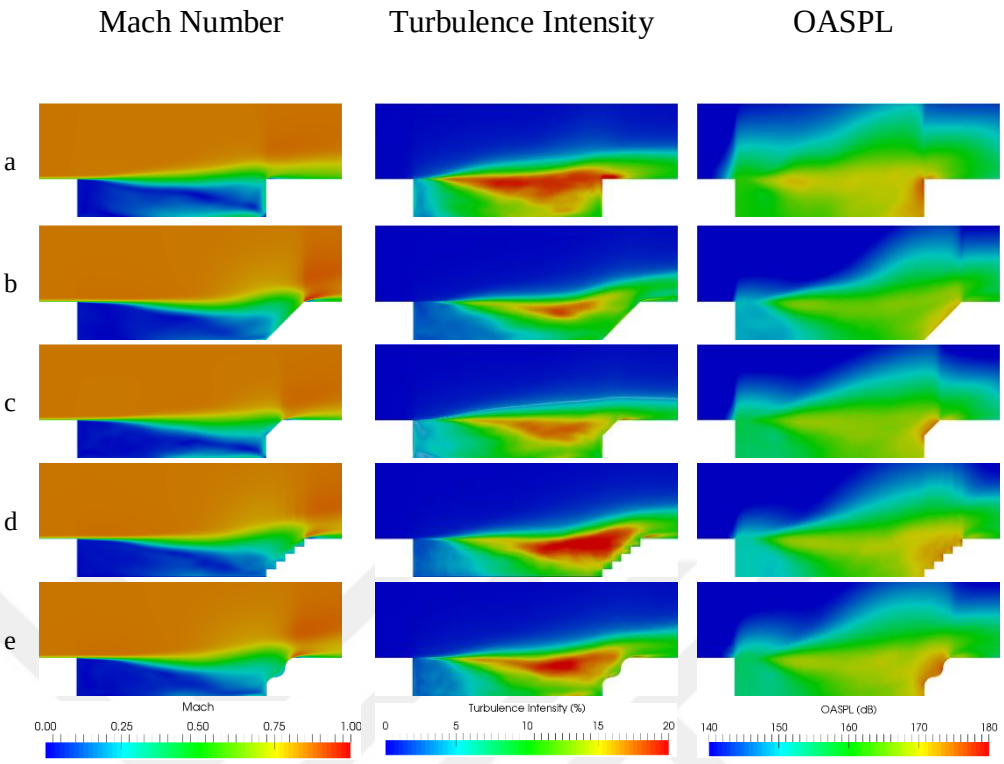

Figure 5.10 : Mean Mach, turbulence intensity and OASPL (dB) contours for aft wall configurations (close-up, side view of the cavity region) a) M219CC b) PAW1 c) PAW2 d) PAW3 e) PAW4.

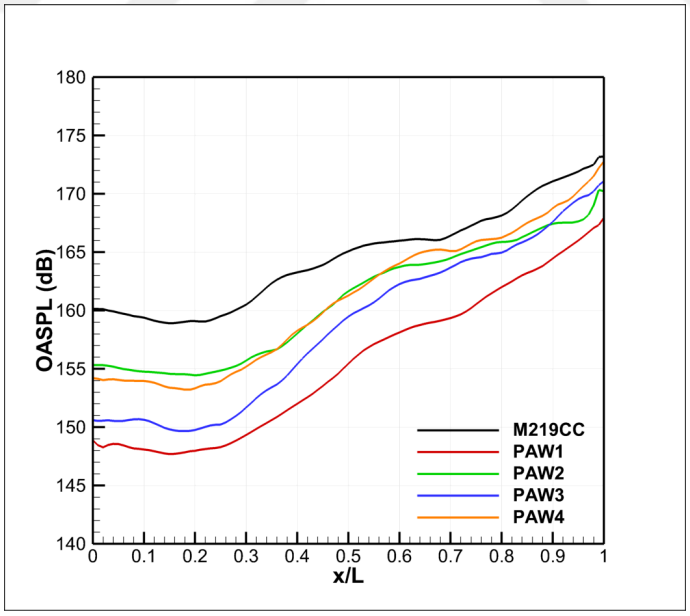

Figure 5.11 : OASPL distribution at the mid-section of the cavity floor for different aft-wall modifications.

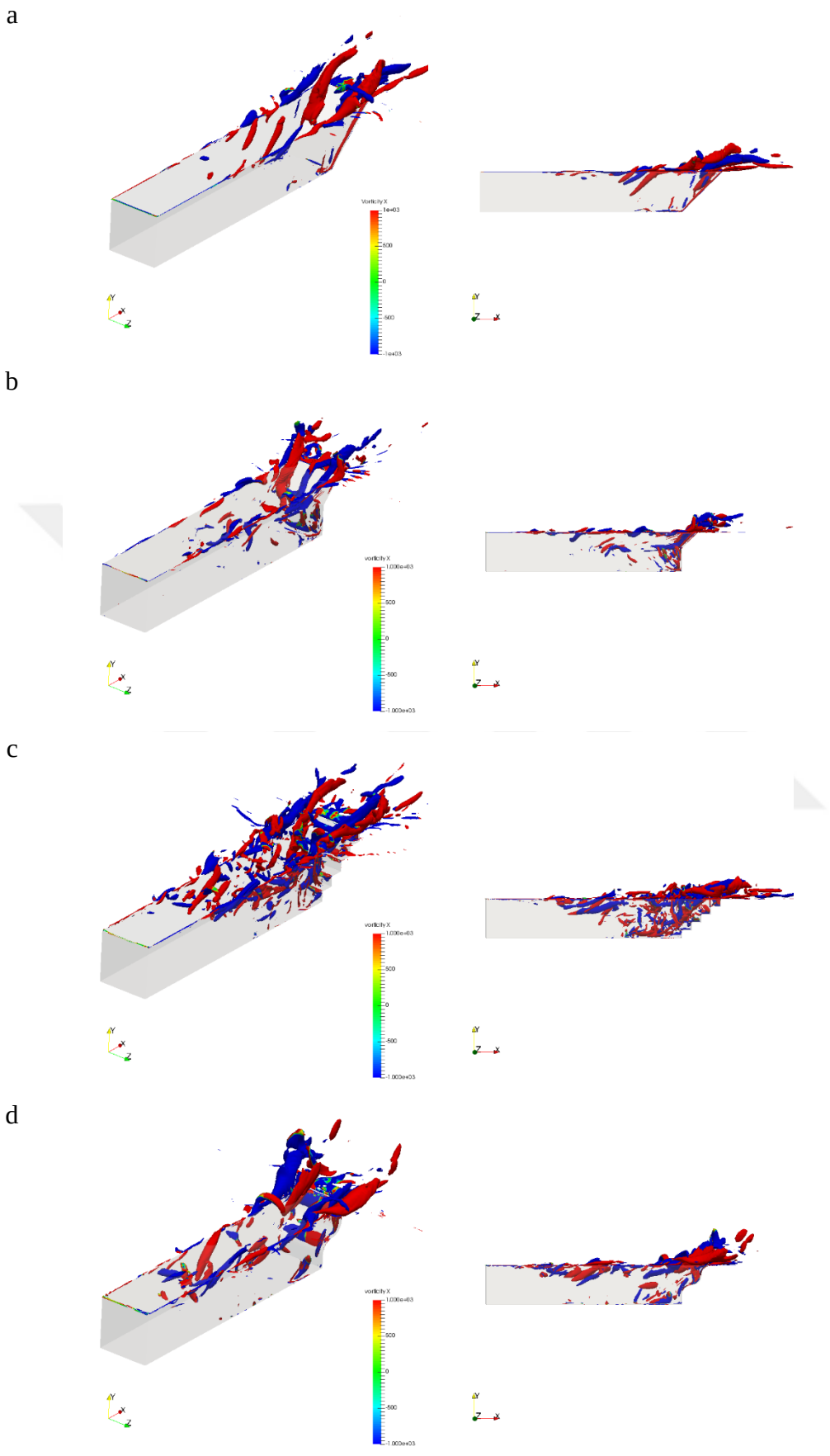

Figure 5.12 : Isosurfaces of Q-criterion colored by Mach number for aft wall configurations a) PAW1 b) PAW2 c)PAW3 d) PAW4, t=0.088 s.

5.4 Front Wall Configurations

Mean flow contour results of cavity front wall configurations are presented in Figure 5.13. As a result of slanting the front wall, the impingement location of shear layer to cavity aft wall has become closer to the bottom of aft wall. Mean turbulence intensity and OASPL contours are similar to those of M219CC. By examining OASPL contours, it may be concluded that the distribution near cavity half region is smoother for front wall configurations.

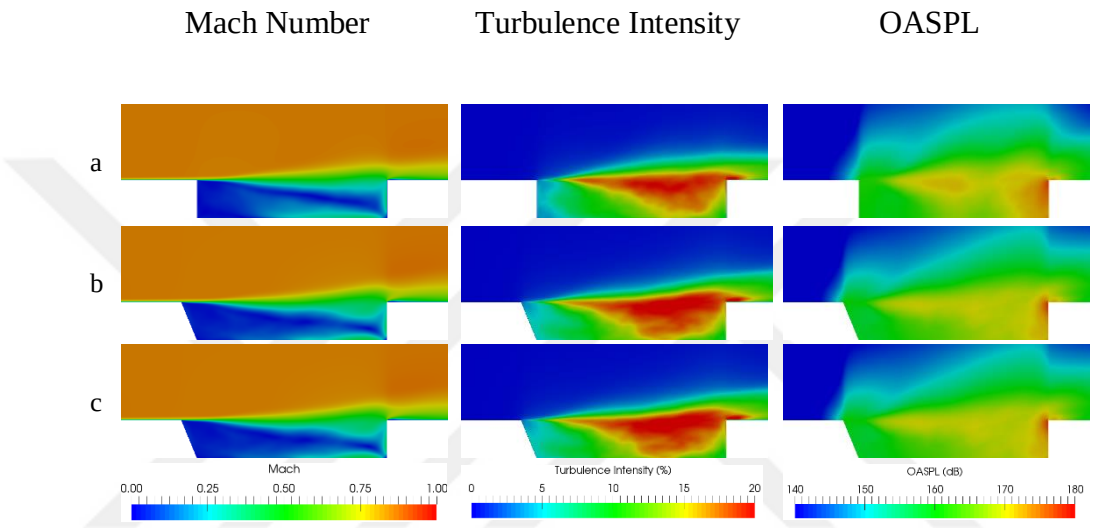

Figure 5.13 : Mean Mach, turbulent intensity and OASPL (dB) contours for front wall configurations a) M219CC b) PFW1 c) PFW2.

Figure 5.14 represents the OASPL distribution along the cavity floor at the mid-plane for aft wall configurations. PFW2 configuration resulted in a noise increment. OASPL distribution and values of PFW1 is obtained similarly to M219CC. Additionally, general trend of distribution is almost identical for PFW1 and PFW2.

Isosurfaces of Q-criterion colored by x-vorticity for front wall configurations are given in Figure 5.15. Similar to M219CC, the flow has large-scale coherent structures at both front half and aft half of the cavity. The structures are seen to be similar to M219CC. The most prominent structures are seen at aft wall region where the shear layer interaction occurs.

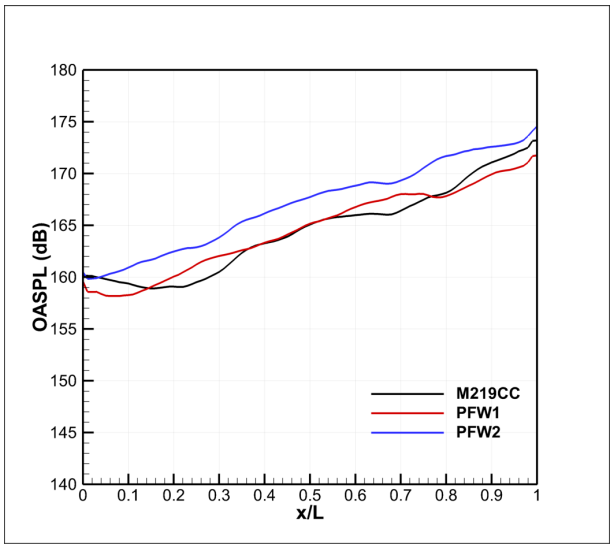

Figure 5.14 : OASPL distribution at the mid-section of the cavity floor for different front-wall modifications.

a

b

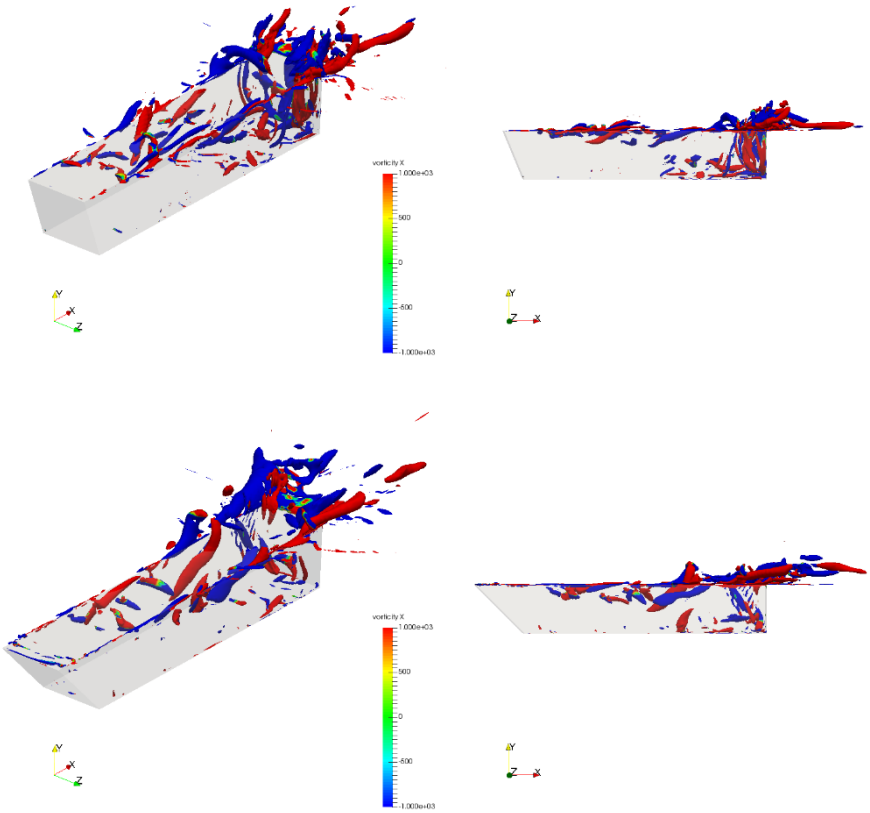

Figure 5.15 : Isosurfaces of Q-criterion colored by Mach number for front wall configurations a) PFW1 c) PFW2, t=0.088 s.

5.5 Passive Injection-Suction Configurations

Two different passive injection-suction cases are applied as passive flow control techniques one playing an injection role whilst the other playing a suction role. The idea was to mimic the active flow control techniques and observe the behavior of the flow. The inclined spoiler and injection to cavity from front wall in PIS1 [137] has changed the shear layer behavior as seen from Figure 5.16. A small reverse flow region leaps to the eye for PIS1 case just after the inclined spoiler. The suction from cavity aft wall has also changed the shear layer behavior which can be seen from Mach contour. Most of the flow passes through the channel on cavity aft wall and continues its way. Another reverse flow region is also seen on the beginning region of suction of PIS2 case. Turbulence intensity is smaller for each case than M219CC while the reduction in PIS1 is higher. OASPL contours show that the intensity and high levels of noise near cavity aft wall region are reduced, too. Propagation of pressure waves for passive injection/suction configurations are also observed to decrease slighlty in the region outside of the cavity.

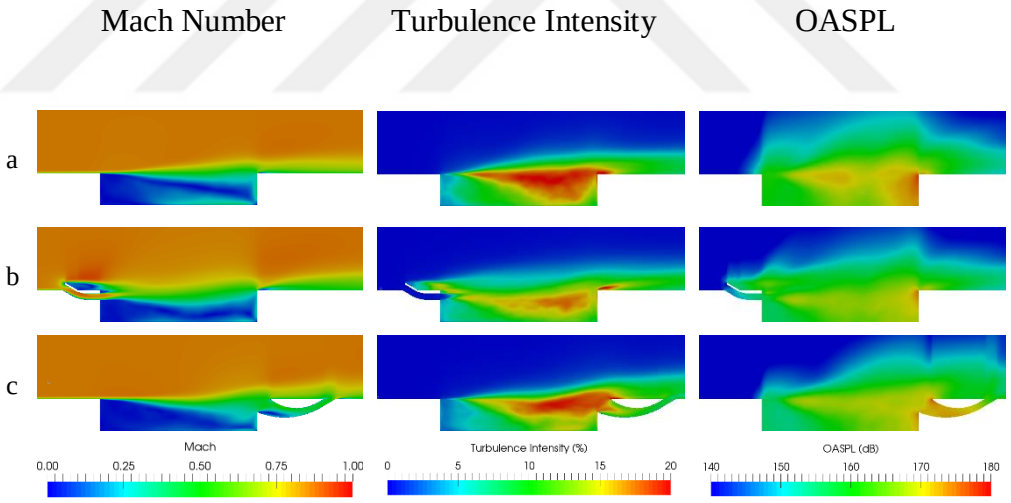

Figure 5.16 : Mean Mach, turbulent intensity and OASPL (dB) contours for spoiler configurations a) M219CC b) PIS1 c) PIS2.

OASPL distribution at mid-plane for cavity floor is presented in Figure 5.17 for passive injection-suction configurations. It is clear that the OASPL is reduced especially at the half front of the cavity extending up to 60% of the floor. PIS2 configuration is proven to be more effective in terms of OASPL reduction than PIS1.

Figure 5.18 gives an insight of the complex flow structure seen in applied configurations where isosurfaces of Q-criterion colored by x-vorticity are presented.

Generally speaking, structures seen in both configurations are scattered compared to M219CC. Due to the usage of an inclined spoiler upstream of the cavity, more structures are seen in cavity front half in PIS1 than PIS2. It can also be seen from Figure 5.18 that the spoiler has divided the flow into two before reaching the cavity. Large-scale turbulent structures are also present on suction channel for PIS2.

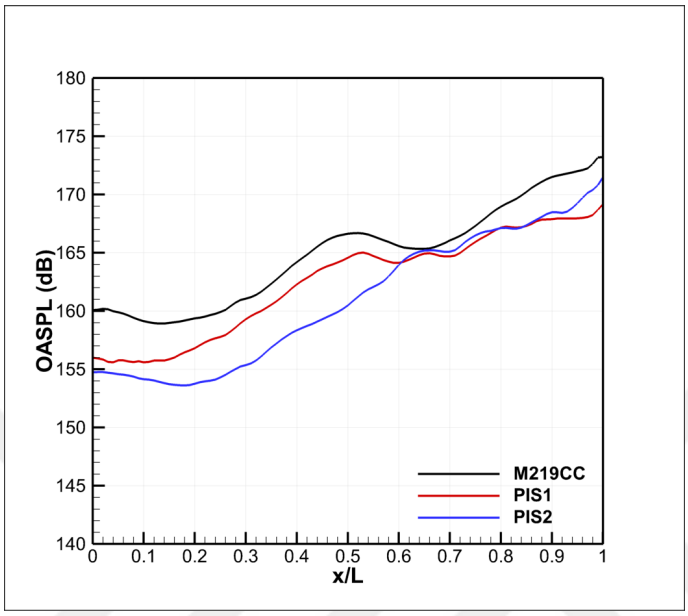

Figure 5.17 : OASPL distribution at the mid-section of the cavity floor for passive injection-suction modifications.

a

b

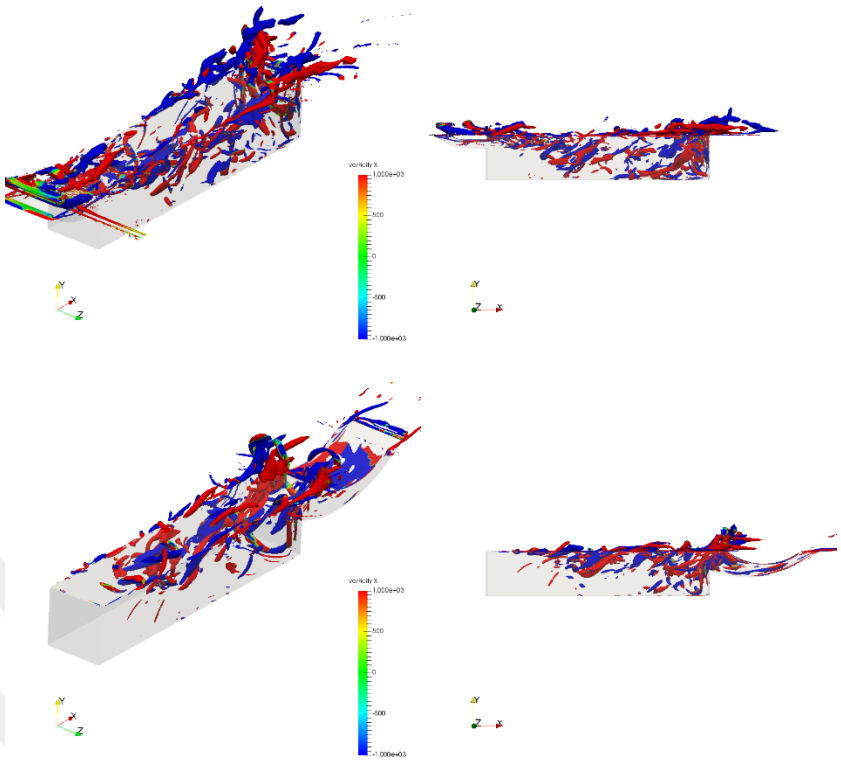

Figure 5.18 : Isosurfaces of Q-criterion colored by Mach number for passive injection-suction configurations a) PIS1 b) PIS2, t=0.088 s.

5.6 Spoiler Configurations

Effects of spoilers located in various positions upstream of the cavity and a wedge-type spoiler are investigated in Figure 5.19. It can be seen from Mach contours that the spoilers have lifted the shear layer along the cavity mouth. Turbulence intensity inside the cavity is smaller for each spoiler configuration than M219CC since the shear layer is lifted up. As for the OASPL reduction, spoiler configurations have proven to be effective. OASPL has smaller values all along the cavity region for each case.

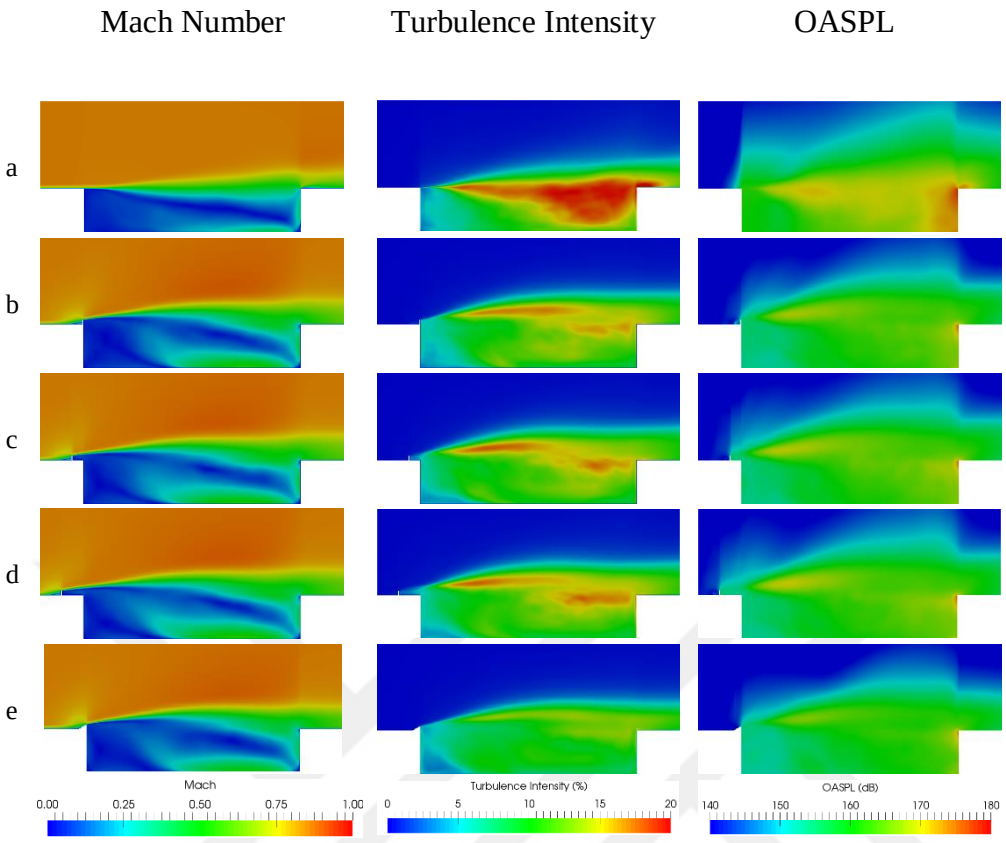

Figure 5.19 : Mean Mach, turbulent intensity and OASPL (dB) contours for spoiler configurations a) M219CC b) PSP1 c) PSP2 d) PSP3 e) PSP4.

Figure 5.20 shows the OASPL distribution at the mid-plane of the cavity walls (front-floor-aft) for spoiler configurations. Since the geometrical change is outside of the cavity, OASPL data for each cavity walls is obtained and processed for comparison. The parameter s/D assigned to x-axis of Figure 5.20 represents a dimensionless distance. The value of s/D from 0-1, 1-6 and 6-7 represents cavity front wall, floor and aft wall, respectively. All configurations have reduced the OASPL. The trend of PSP1, PSP2 and PSP3 are similar to that of M219CC whereas PSP4 has a slightly different behavior starting from 20% of the cavity floor.

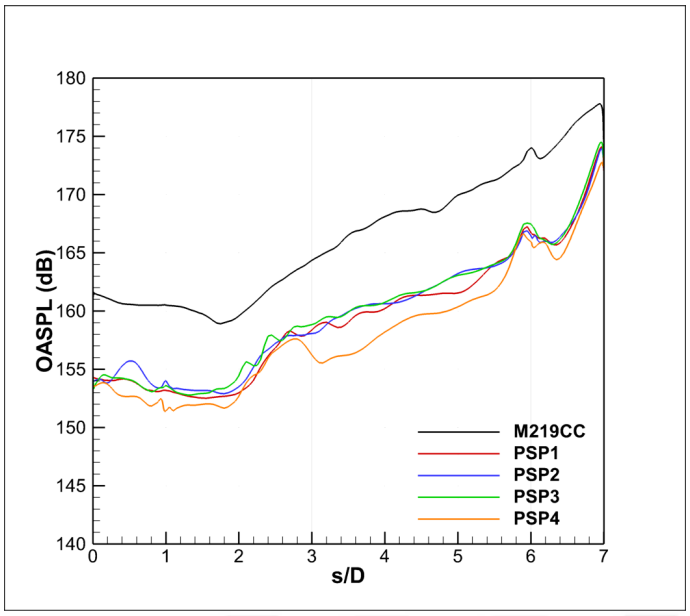

Figure 5.20 : OASPL distribution at the mid-section of the cavity walls (front-floor-aft) for different spoiler configurations.

Isosurfaces of Q-criterion colored by x-vorticity given in Figure 5.21 represent the small structures caused by the placement of a flat spoiler upstream of the cavity. A similarity on isosurfaces of Q for PSP1, PSP2 and PSP3 cases can be observed even though the location of spoiler was different on each configuration. More structures are present compared to M219CC near cavity aft region but they are smaller in size. Structures that exist about the mid-region of the cavity for M219CC do not exist on these cases. At each configuration, existence of spoiler divides the flow into two and creates a rotation that can be seen by looking at the just upstream of the placed spoilers in Figure 5.21.

a

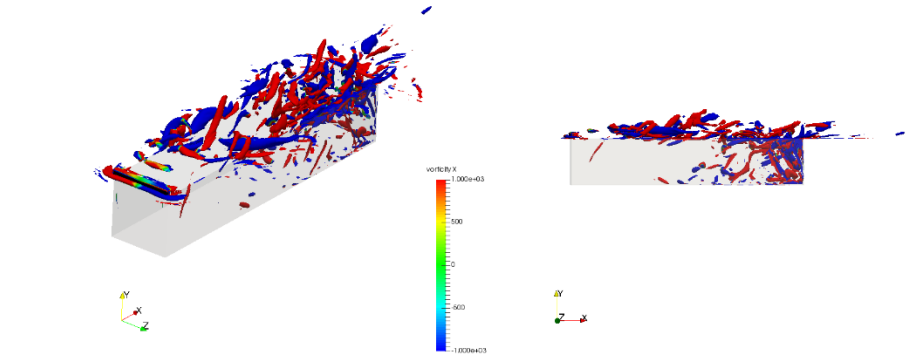

b

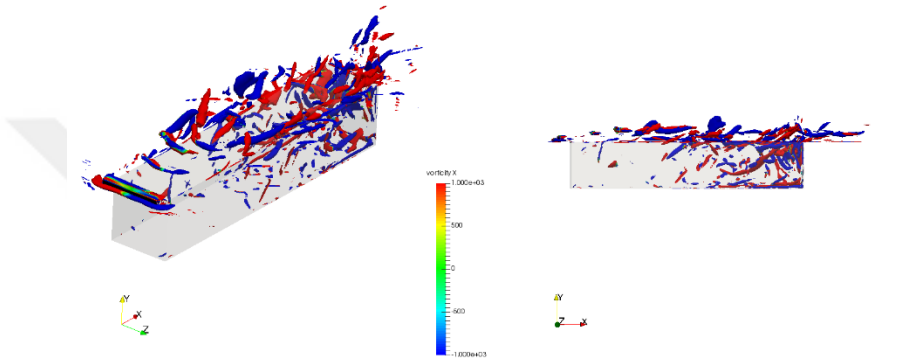

c

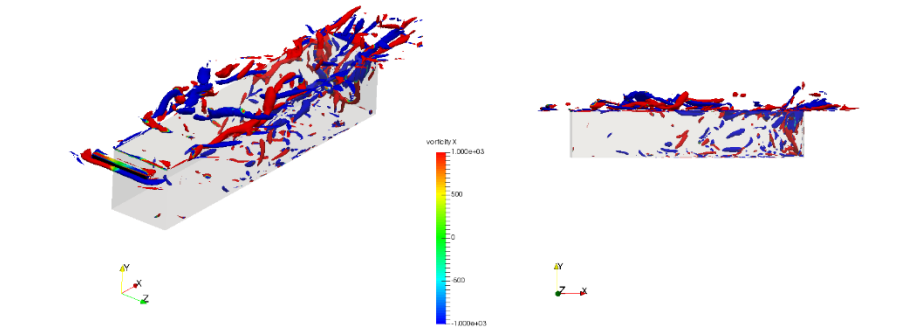

d

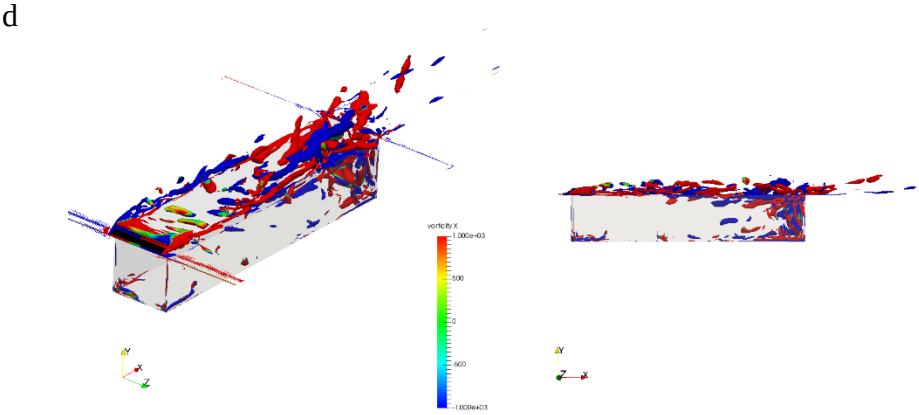

Figure 5.21 : Isosurfaces of Q-criterion colored by Mach number for spoiler configurations a) PSP1 b) PSP2 c) PSP3 d) PSP4, t=0.088 s.

5.7 Vortex Generator Configurations

Four different vortex generator configurations were tested as passive flow control methods with the aim of crumbling the upcoming boundary layer and generating a distrubed shear layer [138]. Figure 5.22 shows that the behavior of mean shear layer is affected as expected. The flow near the cavity aft edge near cavity wall shows a higher profile in magnitude than the M219CC for each configurations. Since the flow is crumbled prior to the separation from the front edge, the intensity of turbulent energy is also reduced for each case. Similar to turbulence intensity reduction, an improvement on noise levels is also achieved. Mean Mach contours show that the shear layer is also lifted similarly to spoiler configurations.

Among all vortex generator cases, PVG4 has the best noise reduction especially near cavity front region which is also presented in Figure 5.23. Mean OASPL distribution along the cavity floors from front to aft are given in Figure 5.23. PVG1 and PVG4 cases are more effective than the others at each point until cavity aft edge. Each configuration shows a similar OASPL profile at cavity aft wall.

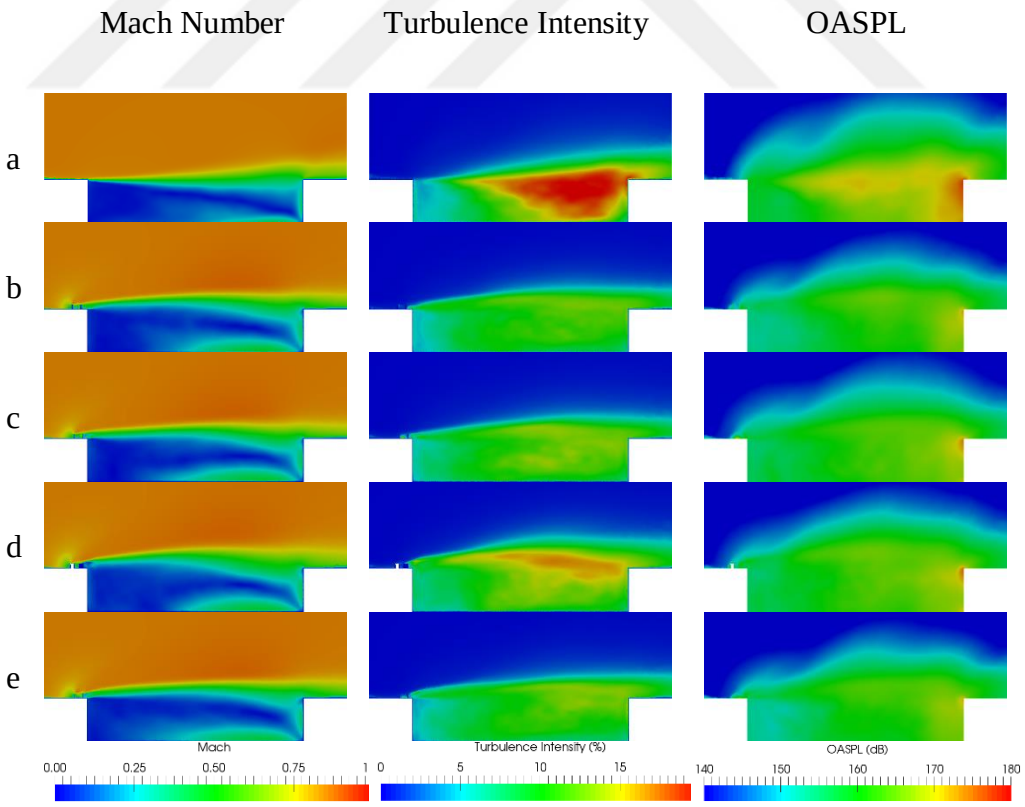

Figure 5.22 : Mean Mach, turbulent intensity and OASPL (dB) contours for vortex generator configurations a) M219CC b) PVG1 c) PVG2 d) PVG3 e) PVG4.

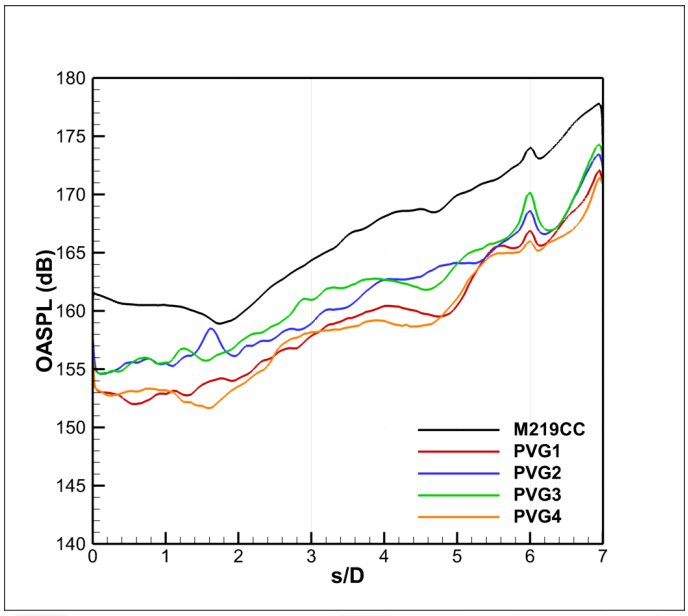

Figure 5.23 : OASPL distribution at the mid-section of the cavity walls (front-floor-aft) for different spoiler configurations.

5.8 Combined Configurations

Combined configurations are tested as the last part of passive flow control methods, to examine the effect of two different control methods when applied simultaneously. Mean flow contours for M219CC, PAW1, PSP1, PSP3, PC1 and PC2 are presented in Figure 5.24. Similar to other shown passive flow control techniques, combined configurations were effectively reduced the turbulence intensity inside the cavity. By examining OASPL contours, it is seen that combined configurations have greatly reduced the OASPL near cavity front region compared to other methods.

OASPL distribution along the cavity floor at mid-plane is given in Figure 5.25 and it is obvious that the combined configurations have reduced the noise generation even further than PAW1 case which was the best method among all other configurations. Despite PAW1 is the best configuration in terms of OASPL reduction at cavity front wall and up to 20% of the cavity floor, PC2 case then reduces the noise significantly starting from 80% of the cavity floor including cavity aft wall. Isosurfaces of Q-criterion for combined configurations represents the rotational behavior of the flow when the attention is focused about the mid-section of the cavity in Figure 5.26. Counter rotating vortices are present as a result of both rotational nature of the flow and usage of spoilers ahead of the cavity. Less structures are also observed compared to M219CC configuration.

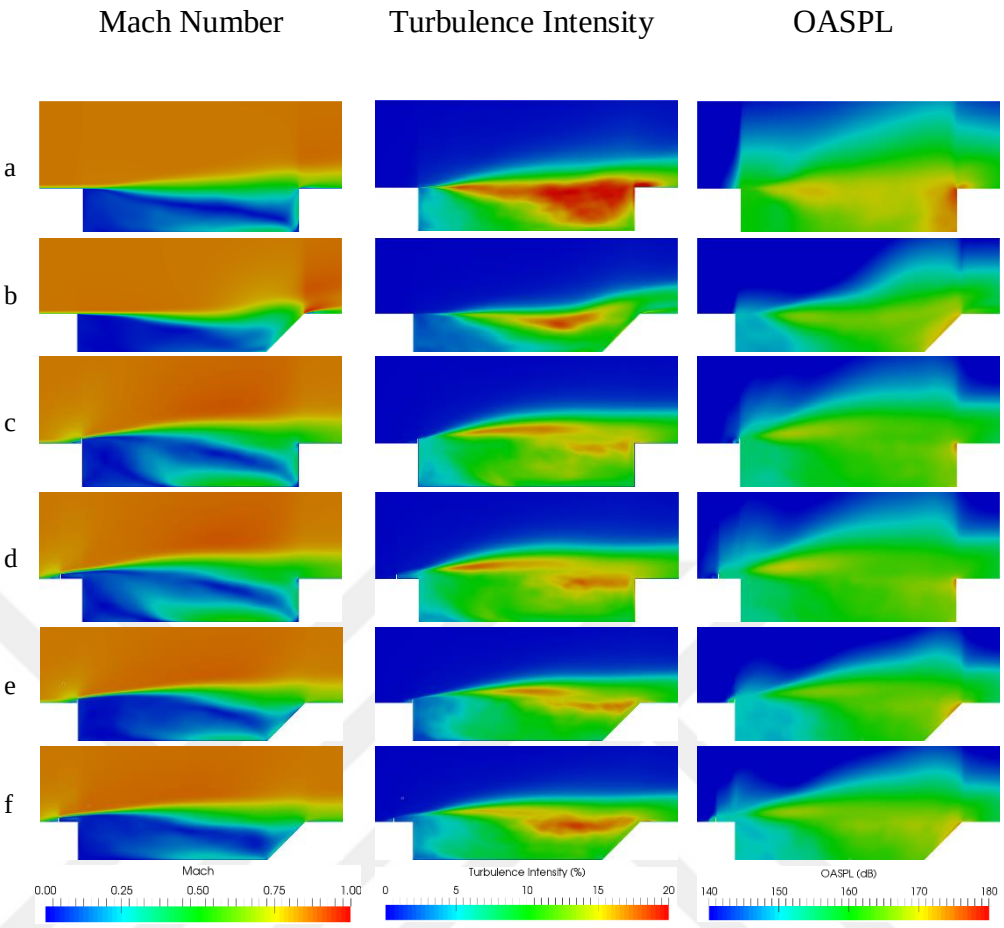

Figure 5.24 : Mean Mach, turbulent intensity and OASPL (dB) contours for combined configurations a) M219CC b) PAW1 c) PSP1 d) PSP3 e) PC1 f) PC2.

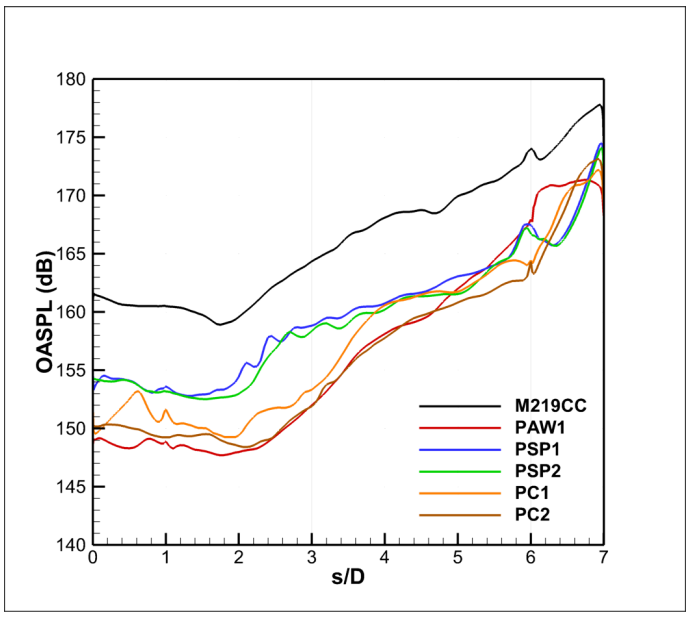

Figure 5.25 : OASPL distribution at the mid-section of the cavity walls (front-floor-aft) for combined passive flow control configurations.

a

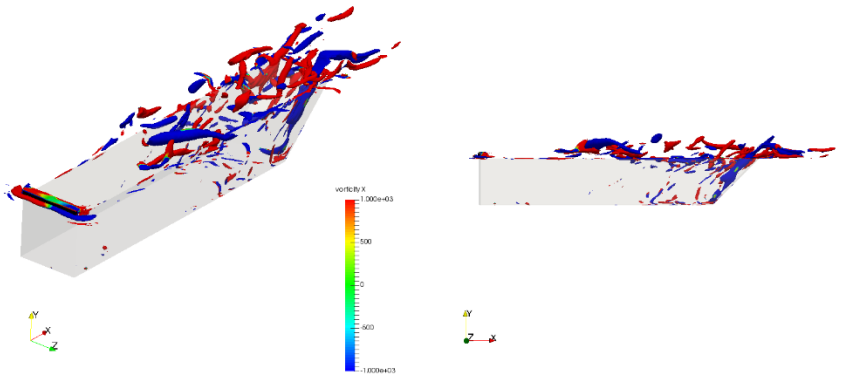

b

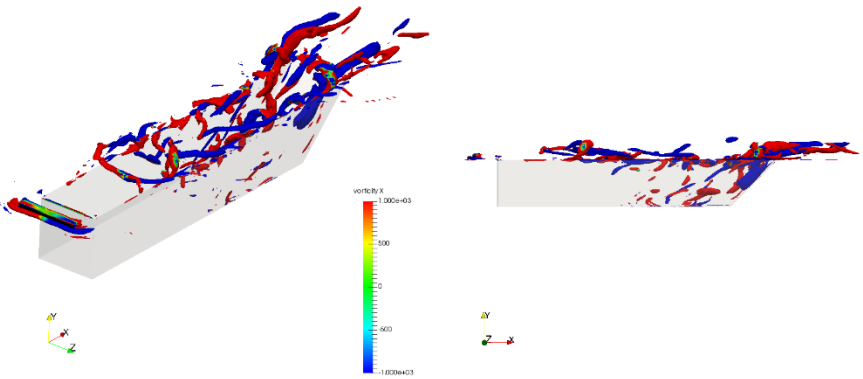

Figure 5.26 : Isosurfaces of Q-criterion colored by Mach number for combined passive flow control configurations a) PC1 b) PC2, t=0.088 s.

5.9 Overall Comparison

In this section, all configurations are gathered for a better comparison. Average OASPL on cavity floor for applied configurations along with the M219CC baseline configuration are computed and listed in Table 5.1. PAW1 configuration where aft wall of cavity is inclined with 45° has reduced the OASPL more than other aft wall configurations. The reduction was approximately 9.4 dB in magnitude and was around 5.7%. PFW1 configuration where the cavity front wall was inclined 22.5° was the best configuration in terms of OASPL reduction on cavity floor for front wall configurations. In fact, PFW2 configuration where the angle of inclination was 45° has increased the general OASPL inside the cavity. Average OASPL on cavity floor was reduced by 0.26 dB in magnitude and about 0.16% for PFW1. PIS2 case where the passive suction methodology from cavity aft wall via a channel to downstream is applied, has reduced the average OASPL by 3.93 dB and around 2.38%. For spoiler configurations, wedge shaped spoiler placed just before the cavity performed better than the other spoiler configurations and a reduction of 7.55 dB in magnitude was obtained which corresponds

to an improvement about 4.58%. PVG4 configuration which implies the usage of delta shaped devices upstream of the cavity effectively reduced the average OASPL by 6.75 dB. Lastly, PC2 configuration where PAW1 and PSP3 cases are combined and applied simultaneously, has reduced the average OASPL on cavity floor by 9.72 dB which corresponds to ~5.9%.

Table 5.1 : Average OASPL along the cavity floor for each configuration.

Configuration	AOASPL (dB)	Noise Reduction (dB)	Noise Reduction (%)
M219CC	164.88	--	--
PAW1	155.48	9.4	5.7011
PAW2	160.82	4.06	2.4624
PAW3	158.59	6.29	3.8149
PAW4	160.95	3.93	2.3836
PFW1	164.92	0.26	0.1577
PFW2	167.05	-2.17	-1.3161
PIS1	162.46	2.42	1.4677
PIS2	160.95	3.93	2.3836
PSP1	158.73	6.15	3.73
PSP2	159.14	5.74	3.4813
PSP3	159.35	5.53	3.354
PSP4	157.33	7.55	4.5791
PVG1	158.67	6.21	3.7664
PVG2	161.23	4.1	2.6624
PVG3	161.61	3.64	2.4329
PVG4	158.73	6.75	4.1717
PC1	156.21	8.67	5.2584
PC2	155.16	9.72	5.8952

Pressure fluctuations of a probe placed at 95% of the cavity floor for a selected configuration of each category are presented in Figure 5.27. In order to ease the visibility, the results are shown differently for each case. In Figure 5.27a, fluctuations of pressure from 10 CTS to 40 CTS for M219CC and PAW1 configurations are compared. It is seen that severe fluctuations observed in M219CC are no longer present in PAW1 case. The level of fluctuations are reduced with the applied flow control method. Fluctuations recorded in PFW1 case are similar to those of M219CC. It should be recalled that the PFW1 were just 0.15% efficient in terms of noise reduction. Therefore, it can be implicated that the reduction in pressure fluctuations can also be a representative notation to noise reduction. Figure 5.27f shows that PC2 configuration were significantly attenuated the oscillatory behavior of pressure. Generally, other

than PFW1, each passive flow control method have successively suppressed the pressure oscillations compared to M219CC case.

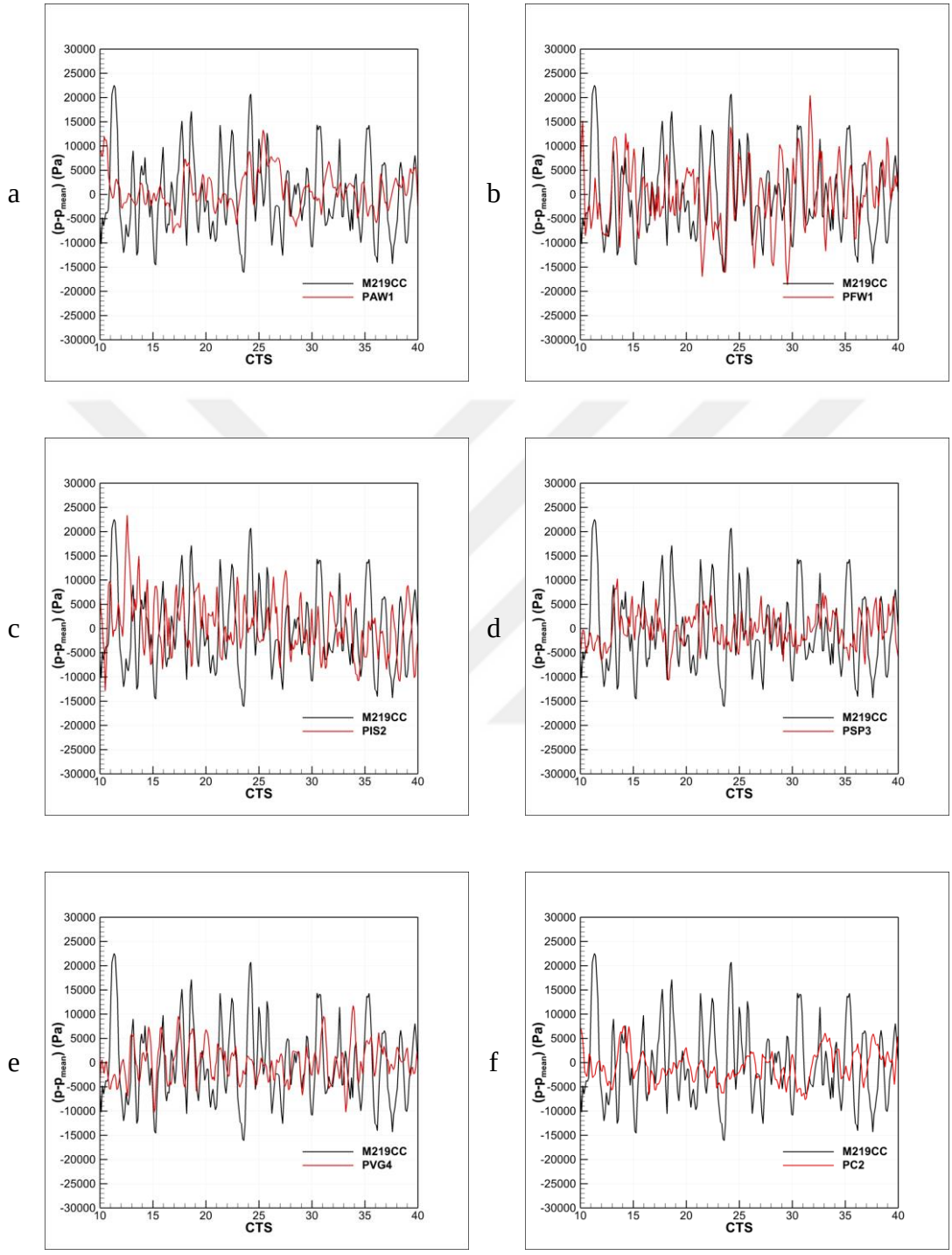

Figure 5.27 : Comparison of pressure fluctuations at 0.95 x/L of cavity floor for selected cases with clean cavity configuration: a) M219CC-PAW1 b) M219CC-PFW1 c) M219CC-PIS2 d) M219CC-PSP3 e) M219CC-PVG4 f) M219CC-PC2.

6. CONCLUSION AND DISCUSSIONS

Numerical simulations of an open cavity at a transonic speed where freestream Mach number was 0.85 were performed throughout this thesis. Various passive flow control techniques were applied with the aim of reducing OASPL and suppressing severe pressure oscillations. Analyses were conducted via pressure-based transient flow solver rhoPimpleFoam of OpenFOAM® with $k-\omega SSTDES$ turbulence model.

A grid convergence study were conducted prior to passive flow control simulations to validate the simulation model and investigate the effects of y^+ and mesh resolution. The influence of y^+ was proven to be small since the flow is governed by large-scale coherent structures. Since formation of shear layer over cavity mouth and its interaction with cavity aft wall are main source of the noise generation, wall functions are used on the walls. As a result of grid convergence study, a y+ value within the limitations of log-law of the wall and a structured grid consisting of approximately 3 million cells are selected for the simulations except for the vortex generator simulations. For vortex generator cases, an unstructured grid were constructed.

M219CC analyses have shown that the flow is highly transient and unsteady which were not possible to examine using URANS methods. Due to this problem, DES methodology is followed.

Aft wall modifications were effective in terms of reducing OASPL and pressure fluctuations on cavity floor. PAW1 configuration decreased the average OASPL about ~9 dB. Large turbulent structures seen on M219CC were also vanished in PAW1 configuration. Slanting the cavity front wall with 22.5° slightly decreased the average OASPL, about ~0.26 dB.

Passive injection and suction flow controls were applied with the intent of creating an alternative way to flow into/from the cavity. These configurations have reduced the OASPL generation inside the cavity.

Spoilers and vortex generators were placed upstream wall of the cavity on the purpose of lifting or scattering the incoming boundary layer. These methods were successfully reduced the OASPL up to 7.5 dB.

Lastly, combined configurations where spoiler and aft wall flow controls were applied simultaneously were investigated. Obtained results proved that the large-scale coherent structures were diminished since the flow were stabilized much more than the clean cavity configuration. Oscillations of pressure were also become less in parallel with this stabilization.

All simulations presented in this thesis were run in parallel. Most of the cases were run using 224 processors and 43461 cpu-hour is consumed in total, except PIS1 and PIS4 cases.Due to the corruption of solution log files of PIS1 and PSP4 configurations, consumed cpu-hour for these simulations were not gathered. Cpu-hour is calculated as the multiplication of clock time of the simulation and number of processors used for that specific case.

As a future work, active flow control methods coupled with passive flow control methods may be investigated to examine the hybrid effects of both control techniques. LES simulations using denser grids could be performed with more computational resources. By this way, a more sophisticated in-depth acoustic field analysis might be performed. Doors of the cavity might be included in the simulations in order to see the integrated effect of an internal weapon bay door to cavity flowfield. Store separation studies might also be conducted alongside the cavity studies. Doing so, separation of a bomb/missile from an internal weapon bay might be simulated with the aim of a reliable/acceptable separation.

Additionally, an optimization procedure focusing on the reducing the aft wall-shear layer interaction to achieve lower acoustic propagation could be also be created.

REFERENCES

[1] Url-1 *<https://www.quora.com/What-is-the-%E2%80%9Cinternal-weapons-bay%E2%80%9D-in-aircraft>*, date retrieved 20.04.2019.

[2] Wieghardt, K. (1942). *Erhöhung des turbulenten Reibungswiderstandes durch Oberflächenstörungen*. Göttingen.

[3] Tillmann, W. (1951). *Additional measurements of the drag of surface irregularities in turbulent boundary layers*. Washington, DC: National Advisory Committee for Aeronautics.

[4] Norton, D. A. (1952) Investigation of B47 bomb bay buffet, Boeing Airplane Co., Doc. No. D12675.

[5] Fail, R., Owen, T. B., and Eyre, R. C. N. (1954) Low Speed Wind Tunnel Tests on the Flow in Bomb bays and its Effect on Drag and Vibration. Aero Report 2511, Royal Aircraft Establishment.

[6] Stallings Jr, R. L., and Wilcox Jr, F. J. (1987). *Experimental cavity pressure distributions at supersonic speeds*. Washington, DC: National Aeronautics and Space Administration, Scientif. and Techn. Information Branch.

[7] Plentovich, E.B., Stallings, R. L., and Tracy, M. B. (1993). *Experimental cavity pressure measurements at subsonic and transonic speeds: Static-pressure results*. Washington, D.C.: National Aeronautics and Space Administration, Office of Management, Scientific and Technical Information Program.

[8] Syed, S. A. (2010). *Detached eddy simlation of turbulent flow over an open cavity with and withour cover plates* (Master's Thesis). Retrieved from http://soar.wichita.edu//

[9] ESDU. (2005) *Aerodynamics and aero-acoustics of rectangular planform cavities. Part II: unsteady flow and aero-acoustics*. Technical Report 04023, ESDU International.

[10] Lawson, S., and Barakos, G. (2011). Review of numerical simulations for high-speed, turbulent cavity flows. *Progress in Aerospace Sciences,47*(3), 186-216.

[11] Freitas, P. G. F. E. (2014). *Numerical simulation of compressible flow over a deep cavity* (Master's thesis). Retrieved from http://fenix.tecnico.ulisboa.pt/

[12] Rizzetta, D. P. (1988). Numerical simulation of supersonic flow over a three-dimensional cavity. *19th AIAA, Fluid Dynamics, Plasma Dynamics, and Lasers Conference*.

[13] Tracy, M. B., and Plentovich, E. B. (1997). *Cavity unsteady-pressure measurements at subsonic and transonic speeds*. Hampton, VA: National Aeronautics and Space Administration, Langley Research Center.

[14] Url-2 <*https://earthsky.org/earth/kelvin-helmholzt-clouds*>, date retrieved 20.04.2019.

[15] **Izawa, S.** (2011). Active and Passive Control of Flow Past a Cavity. In *Wind Tunnels and Experimental Fluid Dynamics Research*. INTECH Open Access Publisher.

[16] Rossiter, J. E. (1964). *Wind-tunnel experiments on the flow over rectangular cavities at subsonic and transonic speeds*. London: H.M.S.O.

[17] Hirschberg, A., and Rienstra, S. W. (2004). *An introduction to aeroacoustics*. Eindhoven.

[18] Pierce, A. D. (1995). *Acoustics: An introduction to Its physical principles and applications*. New York: Acoustical Society of America.

[19] Tam, C., Orkwis, P., and Disimile, P. (1996). Supersonic open cavity flow physics ascertained from algebraic turbulence model simulations. *34th Aerospace Sciences Meeting and Exhibit*.

[20] Charwat, A. F., Roos, J. N., Dewey, F. C., and Hitz, J. A. (1961). An Investigation of Separated Flows - Part I: The Pressure Field. *Journal of the Aerospace Sciences,28*(6), 457-470.

[21] Henderson, J., Badcock, K., and Richards, B. (2000). Understanding subsonic and transonic open cavity flows and supression of cavity tones. *38th Aerospace Sciences Meeting and Exhibit*.

[22] Rossiter, J. E. (1962). The Effect of Cavities on the Buffeting of Aircraft. Technical Memorandum 754, Royal Aircraft Establishment, Farnborough, UK.

[23] Tam, C. K., and Block, P. J. (1978). On the tones and pressure oscillations induced by flow over rectangular cavities. *Journal of Fluid Mechanics,89*(02), 373.

[24] Shaw, L. L., and Shimovetz, R. M. (1994). *Weapons Bay Acoustic Environment. Impact of Acoustic Loads on Aircraft Structures*. AGARD-CP-549.

[25] Alvarez, J., Kerschen, E., and Tumin, A. (2004). A Theoretical Model for Cavity Acoustic Resonances in Subsonic Flow. *10th AIAA/CEAS Aeroacoustics Conference*.

[26] Nayyar, P. (2005). *CFD Analysis of Transonic Turbulent Cavity Flows.* (Doctoral dissertation). Retrieved from http://theses.gla.ac.uk/

[27] Roshko, A. (1955). Some Measurements of Flow in a Rectangular Cut-Out. Technical Report 3488, NACA, California Institute of Technology.

[28] Krishnamurty (1955). Acoustic radiation from two-dimensional rectangular cutouts in aerodynamics surfaces. Technical Note 3487, NACA.

[29] Rossiter, J. E. (1960). A Preliminary Investigation into Armament Bay Buffet at Subsonic and Transonic Speeds. Techical Memorandum 679, Royal Aircraft Establishment, Farnborough, UK.

[30] Rossiter, J. E. (1961). A Note on Periodic Pressure Fluctuations in the Flow over Open Cavities. Technical Memorandum 743, Royal Aircraft Establishment, Farnborough, UK.

[31] Ross, J. A., and Peto, J. W. (1992). Internal Stores Carriage Research at RAE. Technical Memorandum 2223, QinetiQ.

[32] Ross, J. A., and Peto, J. W. (1992). The Unsteady Environment within an Internal Weapon Bay or Cavity. Technical Report, QinetiQ.

[33] Ross, J. A., and Peto, J. W. (1997). The Effect of Cavity Shaping, Front Spoilers and Ceiling Bleed on Loads Acting on Stores, and on The Unsteady Environment within Weapon Bays. Technical Report, QinetiQ.

[34] Ross, J. A., and, Odedra, J., and Peto, J. W. (1998). DERA Bedford Internal Report. MSSA CR980744/1.0.

[35] Esteve, M. J., Reulet, P., and Millan, P. (2000). *Flow Field Characterization within a Rectangular Cavity*. In 10th International Symposium Applications of Laser Techniques to Fluid Mechanics.

[36] Ross, J. A. (2002). PIV Measurements of The Flowfields in an Aerodynamically Deep Cavity, Technical Report, QinetiQ.

[37] Ross, J. A. (2000). Cavity Acoustic Measurements at High Speeds. Technical Report, QinetiQ.

[38] Nightingale, D., Ross, J. A., and Foster, G. (2005). Cavity Unsteady Pressure Measurements-Examples from Wind-Tunnel Tests. Technical Report, QinetiQ.

[39] Karamcheti, K. (1955). Acoustic Radiation from Two-Dimensional Rectangular Cutouts in Aerodynamic Surfaces. Technical Report 3487, NACA.

[40] Karamcheti, K. (1956*). Sound Radiation from Surface Cutouts in High Speed Flow.* (Doctoral dissertation). Retrieved from http://thesis.library.caltech.edu/

[41] Rossiter, J. E., and Kurn, A. G. (1962). Wind Tunnel Measurements of the Unsteady Pressures in and behind a Bomb Bay. Technical Note 2845, Royal Aircraft Establishment, Farnborough, UK.

[42] Powell, A. (1961). On the Edgetone. *The Journal of the Acoustical Society of America*, *33*(4), 395-409.

[43] Rockwell, D., and Naudascher, E. (1978). Review—Self-Sustaining Oscillations of Flow Past Cavities. *Journal of Fluids Engineering, 100*(2), 152.

[44] Heller, H., and Bliss, D. (1975). The physical mechanism of flow-induced pressure fluctuations in cavities and concepts for their suppression. *2nd Aeroacoustics Conference*.

[45] Stallings, R. L. (1983). Store separation from cavities at supersonic flight speeds. *Journal of Spacecraft and Rockets,20*(2), 129-132.

[46] Blair, A. B., and Stallings, R. L. (1989). Cavity door effects on aerodynamic loads of stores separating from cavities. *Journal of Aircraft,26*(7), 615-620.

[47] Gharib, M., and Roshko, A. (1987). The effect of flow oscillations on cavity drag. *Journal of Fluid Mechanics,177*(1), 501-530.

[48] Gharib, M. (1987). Response of the cavity shear layer oscillations to external forcing. *AIAA Journal,25*(1), 43-47.

[49] Ritchie, S., Lawson, N., and Knowles, K. (2003). An Experimental and Numerical Investigation of an Open Transonic Cavity. *21st AIAA Applied Aerodynamics Conference*.

[50] Foster, G. W., Ross, J. A., and Ashworth, R. M. (2005) Wind-Tunnel Trials and CFD Modelling by QinetiQ UK. *RTO/AVT Symposium on "Flow Induced Unsteady Loads and The Impact on Military Applications, NATO*.

[51] Heller, H., Holmes, D., and Covert, E. (1971). Flow-induced pressure oscillations in shallow cavities. *Journal of Sound and Vibration,18*(4), 545-553.

[52] Baysal, O., and Stallings, R. L. (1988). Computational and experimental investigation of cavity flowfields. *AIAA Journal,26*(1), 6-7.

[53] Tracy, M. B., and Plentovich, E. B. (1992). Measurements of Fluctuating Pressure in a Rectangular Cavity in Transonic Flow at High Reynolds Number. Technical Memorandum 4363, NASA.

[54] Tracy, M. B., and Plentovich, E. B. (1993) Characterization of Cavity Flow Fields Using Pressure Data Obtained in the Langley 0.3-Meter Transonic Cryogenic Tunnel. Technical Memorandum 4436, NASA.

[55] Stallings Jr, R. L., Plentovich, E. B., Tracy, M. B., and Hemsch, M. J. (1994). Effect of Passive Venting on Static Pressure Distributions in Cavities at Subsonic and Transonic Speeds. Technical Memorandum 4549, NASA.

[56] Forestier, N., Jacquin, L., and Geffroy, P. (2003). The mixing layer over a deep cavity at high-subsonic speed. *Journal of Fluid Mechanics,475*.

[57] Kegerise, M. A., Spina, E. F., Garg, S., and Cattafesta, L. N. (2004). Mode-switching and nonlinear effects in compressible flow over a cavity. *Physics of Fluids,16*(3), 678-687.

[58] Ukeiley, L. S., Ponton, M. K., Seiner, J. M., and Jansen, B. (2004). Suppression of Pressure Loads in Cavity Flows. *AIAA Journal,42*(1), 70-79.

[59] Unalmis, O. H. (2004). Cavity Oscillation Mechanisms in High-Speed Flows. *AIAA Journal,42*(10), 2035-2041.

[60] Chandra, B. U., and Chakravarthy, S. R. (2005). Experimental Investigation of Cavity-Induced Acoustic Oscillations in Confined Supersonic Flow. *Journal of Fluids Engineering,127*(4), 761.

[61] Zhuang, N., Alvi, F. S., Alkislar, M. B., and Shih, C. (2006). Supersonic Cavity Flows and Their Control. *AIAA Journal,44*(9), 2118-2128.

[62] Hirahara, H., Kawahashi, M., Khan, M. U., and Hourigan, K. (2007). Experimental investigation of fluid dynamic instability in a transonic cavity flow. *Experimental Thermal and Fluid Science,31*(4), 333-347.

[63] Malone, J., Debiasi, M., Little, J., and Samimy, M. (2009). Analysis of the spectral relationships of cavity tones in subsonic resonant cavity flows. *Physics of Fluids,21*(5), 055103.

[64] Hankey, W. L., and Shang, J. S. (1980). Analyses of Pressure Oscillations in an Open Cavity. *AIAA Journal,18*(8), 892-898.

[65] Shih, S. H., Hamed, A., and Yeuan, J. (1994). Unsteady supersonic cavity flow simulations using coupled k-epsilon and Navier-Stokes equations. *AIAA Journal,32*(10), 2015-2021.

[66] Zhang, X., and Edwards, J. A. (1999). Pressure over a dual-cavity cascade at supersonic speeds. *The Aeronautical Journal,103*(1019), 45-54.

[67] Larchevêque, L., Sagaut, P., Lê, T., and Comte, P. (2004). Large-eddy simulation of a compressible flow in a three-dimensional open cavity at high Reynolds number. *Journal of Fluid Mechanics,516*, 265-301.

[68] Peng, S., & Leicher, S. (2008). DES and Hybrid RANS-LES Modelling of Unsteady Pressure Oscillations and Flow Features in a Rectangular Cavity. *Notes on Numerical Fluid Mechanics and Multidisciplinary Design Advances in Hybrid RANS-LES Modelling,*132-141.

[69] Atalay, Selçuk (2010). *The transient cavity flow.* (Master's thesis). Retrieved from http://theses.gla.ac.uk/2373/

[70] Elsayed, M. F. M. (2013). *Effect of Upstream Edge Geometry on The Trapped Mode Resonance of Ducted Cavities*. (Master's Thesis). Retrieved from http://macsphere.mcmaster.ca/

[71] Omer, A. (2014). *Passive Methods for Suppressing Acoustic Resonance Excitation in Shallow Rectangular Cavities*. (Master's Thesis). Retrieved from http://ir.library.dc-uoit.ca/

[72] Url-3 <*http://www.razvanapetrei.com/summary-of-cfd-mdo-conference-2017*/>, date retrieved 29.04.2019.

[73] Rowley, C. W., Colonius, T., and Basu, A. J. (2002). On self-sustained oscillations in two-dimensional compressible flow over rectangular cavities. *Journal of Fluid Mechanics,455*.

[74] Cebeci, T., and Smith, A. M. (1990). *Analysis of turbulent boundary layers*. San Diego: Acad. Press.

[75] Baldwin, B., and Lomax, H. (1978). Thin-layer approximation and algebraic model for separated turbulentflows. *16th Aerospace Sciences Meeting*.

[76] Baysal, O., Srinivasan, S., and Stallings, R. (1988). Unsteady viscous calculations of supersonic flows past deep and shallow three-dimensional cavities. *26th Aerospace Sciences Meeting*.

[77] Lamp, A. M., and Chokani, N. (1997). Computation of Cavity Flows with Suppression Using Jet Blowing. *Journal of Aircraft,34*(4), 545-551.

[78] Jones, W., and Launder, B. (1972). The prediction of laminarization with a two-equation model of turbulence. *International Journal of Heat and Mass Transfer,15*(2), 301-314.

[79] Wilcox, D. C. (1988). Reassessment of the scale-determining equation for advanced turbulence models. *AIAA Journal,26*(11), 1299-1310.

[80] Zhang, X., and Edwards, J. A. (1988). Computational analysis of unsteady supersonic cavity flows driven by thick shear layers. *The Aeronautical Journal,92*(919), 365-374.

[81] Zhang, X., and Edwards, J. A. (1988). Computational analysis of unsteady supersonic cavity flows driven by thick shear layers. *The Aeronautical Journal,92*(919), 365-374.

[82] Henderson, J. (2001). *Investigation of Cavity Flow Aerodynamics using Computational Fluid Dynamics.* (Doctoral Dissertation). Retrieved from http://theses.gla.ac.uk/

[83] Morgenstern, A., and Chokani, N. (1994). Hypersonic flow past open cavities. *AIAA Journal,32*(12), 2387-2393.

[84] Lawrie, D., Nayyar, P., Badcock, K.J., Barakos, G.N., and Richards, B.E. (2003) A CFD Study of Cavity Flows. In RAeS/CEAS Aerospace Research Conference, London, UK. Royal Aeronautical Society.

[85] Stanek, M. J., Visbal, M. R., Rizzetta, D. P., Rubin, S. G., and Khosla, P. K. (2007). On a mechanism of stabilizing turbulent free shear layers in cavity flows. *Computers & Fluids,36*(10), 1621-1637.

[86] Colonius, T. (2001). An overview of simulation, modeling, and active control of flow/acoustic resonance in open cavities. *39th Aerospace Sciences Meeting and Exhibit*.

[87] Deardorff, J. W. (1970). A numerical study of three-dimensional turbulent channel flow at large Reynolds numbers. *Journal of Fluid Mechanics,41*(02), 453.

[88] Schumann, U. (1975). Subgrid scale model for finite difference simulations of turbulent flows in plane channels and annuli. *Journal of Computational Physics,18*(4), 376-404.

[89] Smith, B.R., Welterlen, T.J., and Domel, N.D. (2001) Large eddy-simulation for the analysis of weapon bays flows. Technical report, Lockheed Martin Aeronautics Company.

[90] Larchevêque, L., Sagaut, P., Mary, I., Labbé, O., and Comte, P. (2003). Large-eddy simulation of a compressible flow past a deep cavity. *Physics of Fluids,15*(1), 193-210.

[91] Rizzetta, D. P., and Visbal, M. R. (2003). Large-Eddy Simulation of Supersonic Cavity Flowfields Including Flow Control. *AIAA Journal,41*(8), 1452-1462.

[92] Spalart, P. R., Jou, W. H., Strelets, M., and Allmaras, S. R. (1997). Comments on the feasibility of LES for wings, and on a hybrid RANS/LES approach. 1st AFOSR Int. In *Symp. Eng. Turb. Modelling and Measurements.*

[93] Bush, R., and Mani, M. (2001). A two-equation large eddy stress model for high sub-grid shear. *15th AIAA Computational Fluid Dynamics Conference*.

[94] Travin, A., Shur, M., Strelets, M., and Spalart, P. R. (2002). Physical and Numerical Upgrades in the Detached-Eddy Simulation of Complex Turbulent Flows. *Fluid Mechanics and Its Applications Advances in LES of Complex Flows,*239-254.

[95] Mendonca, F., Allen, R., Charentenay, J. D., and Kirkham, D. (2003). CFD Prediction of Narrowband and Broadband Cavity Acoustics at M=0.85. *9th AIAA/CEAS Aeroacoustics Conference and Exhibit*.

[96] Hamed, A., Basu, D., and Das, K. (2003). Detached Eddy Simulations of Supersonic Flow over Cavity. *41st Aerospace Sciences Meeting and Exhibit*.

[97] Ashworth, R. M. (2005). Prediction of acoustic resonance phenomena for weapon bays using detached eddy simulation. *The Aeronautical Journal,109*(1102), 631-638.

[98] Lawson, S. J., and Barakos, G. N. (2009). Assessment of Passive Flow Control for Transonic Cavity Flow Using Detached-Eddy Simulation. *Journal of Aircraft,46*(3), 1009-1029.

[99] Togiti, V., Lüdeke, H., and Breuer, M. (2010). Detached-Eddy and Delayed Detached-Eddy Simulation of Supersonic Flow over a Three-Dimensional Cavity. *Direct and Large-Eddy Simulation VII ERCOFTAC Series,*555-561.

[100] Togiti, V., Breuer, M., and Longo, J. (2010). Detached-Eddy Simulation of Supersonic Separated Flows. *Progress in Hybrid RANS-LES Modelling Notes on Numerical Fluid Mechanics and Multidisciplinary Design,*77-86.

[101] Hamed, A., Basu, D., Mohamed, A., and Das, K. (2001). *Direct Numerical Simulations of High Speed Flow Over Cavity*. Ft. Belvoir: Defense Technical Information Center.

[102] Gloerfelt, X., Bailly, C., and Juve, D. (2001). Computation of the noise radiated by a subsonic cavity using direct simulation and acoustic analogy. *7th AIAA/CEAS Aeroacoustics Conference and Exhibit*.

[103] Gloerfelt, X., Bogey, C., Bailly, C., and Juve, D. (2002). Aerodynamic Noise Induced by Laminar and Turbulent Boundary Layers over Rectangular Cavities. *8th AIAA/CEAS Aeroacoustics Conference & Exhibit*.

[104] Gloerfelt, X., Bogey, C., and Bailly, C. (2003). Numerical Investigation of the Coexistence of Multiple Tones in Flow-induced Cavity Noise. *9th AIAA/CEAS Aeroacoustics Conference and Exhibit*.

[105] Arunajatesan, S., Kannepalli, C., Sinha, N., Sheehan, M., and Shumway, G. (2008). Suppression of Cavity Loads Using Leading Edge Blowing Concepts. *46th AIAA Aerospace Sciences Meeting and Exhibit*.

[106] Lai, H., and Luo, K. H. (2007). A Three-Dimensional Hybrid LES-Acoustic Analogy Method for Predicting Open-Cavity Noise. *Flow, Turbulence and Combustion,79*(1), 55-82.

[107] Levasseur, V., Sagaut, P., Mallet, M., and Chalot, F. (2008). Unstructured Large Eddy Simulation of the passive control of the flow in a weapon bay. *Journal of Fluids and Structures,24*(8), 1204-1215.

[108] Barakos, G. N., Lawson, S. J., Steijl, R., and Nayyar, P. (2009). Numerical Simulations of High-Speed Turbulent Cavity Flows. *Flow, Turbulence and Combustion,83*(4), 569-585.

[109] Cattafesta, L. N., Song, Q., Williams, D. R., Rowley, C. W., and Alvi, F. S. (2008). Active control of flow-induced cavity oscillations. *Progress in Aerospace Sciences,44*(7-8), 479-502.

[110] DiStefano, J. J., Stubberud, A. R., and Williams, I. J. (1995). *Schaums outline of theory and problems of feedback and control systems*. New York: McGraw-Hill.

[111] Cattafesta, L., Alvi, F., Williams, D., and Rowley, C. (2003). Review of Active Control of Flow-Induced Cavity Oscillations (Invited). *33rd AIAA Fluid Dynamics Conference and Exhibit*.

[112] Wang, Y., Li, S., and Yang, X. (2016). Numerical investigation of the passive control of cavity flow oscillations by a dimpled non-smooth surface. *Applied Acoustics,111*, 16-24.

[113] Shaw, L., Clark, R., and Talmadge, D. (1988). F-111 generic weapons bay acoustic environment. *Journal of Aircraft,25*(2), 147-153.

[114] Smith, B., Welterlen, T., Maines, B., Shaw, L., Stanek, M., and Grove, J. (2002). Weapons bay acoustic suppression from rod spoilers. *40th AIAA Aerospace Sciences Meeting & Exhibit*.

[115] Bruggeman, J., Hirschberg, A., Dongen, M. V., Wijnands, A., and Gorter, J. (1991). Self-sustained aero-acoustic pulsations in gas transport systems: Experimental study of the influence of closed side branches. *Journal of Sound and Vibration,150*(3), 371-393.

[116] Karadogan, H., and Rockwell, D. (1983). Toward Attenuation of Self-Sustained Oscillations of a Turbulent Jet Through a Cavity. *Journal of Fluids Engineering,105*(3), 335.

[117] Bolduc, M., Elsayed, M., and Ziada, S. (2013). Effect of Upstream Edge Geometry on the Trapped Mode Resonance of Ducted Cavities. *Volume 4: Fluid-Structure Interaction*.

[118] Saddington, A. J., Thangamani, V., and Knowles, K. (2016). Comparison of Passive Flow Control Methods for a Cavity in Transonic Flow. *Journal of Aircraft,53*(5), 1439-1447.

[119] Wilcox Jr, F. J. (1990). Experimental measurements of internal store separation characteristics at supersonic speeds.

[120] Baysal, O., Yen, G., and Fouladi, K. (1994). Navier-Stokes Computations of Cavity Aeroacoustics with Suppression Devices. *Journal of Vibration and Acoustics,116*(1), 105.

[121] Sarno, R. L., and Franke, M. E. (1994). Suppression of flow-induced pressure oscillations in cavities. *Journal of Aircraft,31*(1), 90-96.

[122] Arunajatesan, S., Shipman, J., and Sinha, N. (2002). Hybrid RANS-LES simulation of cavity flow fields with control. *40th AIAA Aerospace Sciences Meeting & Exhibit*.

[123] Comte, P., Daude, F., and Mary, I. (2008). Simulation of the reduction of unsteadiness in a passively controlled transonic cavity flow. *Journal of Fluids and Structures,24*(8), 1252-1261.

[124] Ashworth, R. (2008). DES of a Cavity with Spoiler. In *Advances in Hybrid RANS-LES Modelling* (pp. 162-171). Springer, Berlin, Heidelberg.

[125] Greenshields, C. J. (2015). OpenFOAM user guide. *OpenFOAM Foundation Ltd, version*, *3*(1), 47.

[126] Garnier, E., Adams, N., and Sagaut, P. (2013). *Large eddy simulation for compressible flows*. Beijing: World Publishing Corporation.

[127] McDonough, J. M. (2007). Introductory lectures on turbulence: physics, mathematics and modeling.

[128] Bingham, R. (2007). On the crest of a wake. *Nature,445*(7129), 721-722.

[129] Versteeg, H. K., and Malalasekera, W. (2011). *An introduction to computational fluid dynamics: The finite volume method*. Harlow: Pearson Education.

[130] Lindblad, D., Jareteg, A., and Petit, O. (2014). Implementation and run-time mesh refinement for the k− ω SST DES turbulence model when applied to airfoils. *Chalmers University of Technology*.

[131] Menter, F. R., Kuntz, M., and Langtry, R. (2003) Ten years of industrial experience with the SST turbulence model. *Turbulence, Heat and Mass Transfer,4*(1), 625-632.

[132] Moukalled, F. H., Mangani, L., and Darwish, M. (2016). *The finite volume method in computational fluid dynamics: An advanced introduction with OpenFOAM® and Matlab®*. Springer.

[133] Matteo. (n.d.). Wolf Dynamics - Multiphysics simulations, optimization, and data analytics. Retrieved from http://www.wolfdynamics.com/tutorials.html?layout=edit&id=50

[134] Guleren, K. M., Turk, S., Demircan, O. M., and Demir, O. (2018). Numerical Analysis of the Cavity Flow subjected to Passive Controls Techniques. *IOP Conference Series: Materials Science and Engineering,326*, 012015.

[135] Jasak, H. (1996). *Error analysis and estimation for the finite volume method with applications to fluid flows* (Doctoral Disseration). Retrieved from http://spiral.imperial.ac.uk

[136] OpenCFD. (2019). ESI-OpenCFD. Retrieved from https://www.openfoam.com/about/

[137] Demircan, O. M., Demir, O., Turk, S., and Guleren, K. M. (2018). Aeroacoustics Analysis of a Hybrid Control Method for the Flow-Induced Noise Generation of Transonic Cavity Flows. *Tenth International Conference on Computational Fluid Dynamics (ICCFD10)*.

[138] Demir, O., Çelik, B., and Guleren, K. M. (2018). Transonik Akışlarda Girdap Üreteçlerinin Kavite Gürültüsüne Etkisi. *VII. Ulusal Havacılık ve Uzay Konferansı.*

[139] Dubief, Y., and Delcayre, F. (2000). On coherent-vortex identification in turbulence. *Journal of turbulence*, *1*(1), 011-011.

APPENDICES

APPENDIX A: Grids of Passive Flow Control Methods

APPENDIX A

Structured grids are generated for each configuration used in this thesis except for the vortex generators. Due to the complex geometrical shapes, an unstuctured meshing is used for those configurations. Grids generated for each passive flow control method simulation are represented in Figure A.1-Figure A.6.

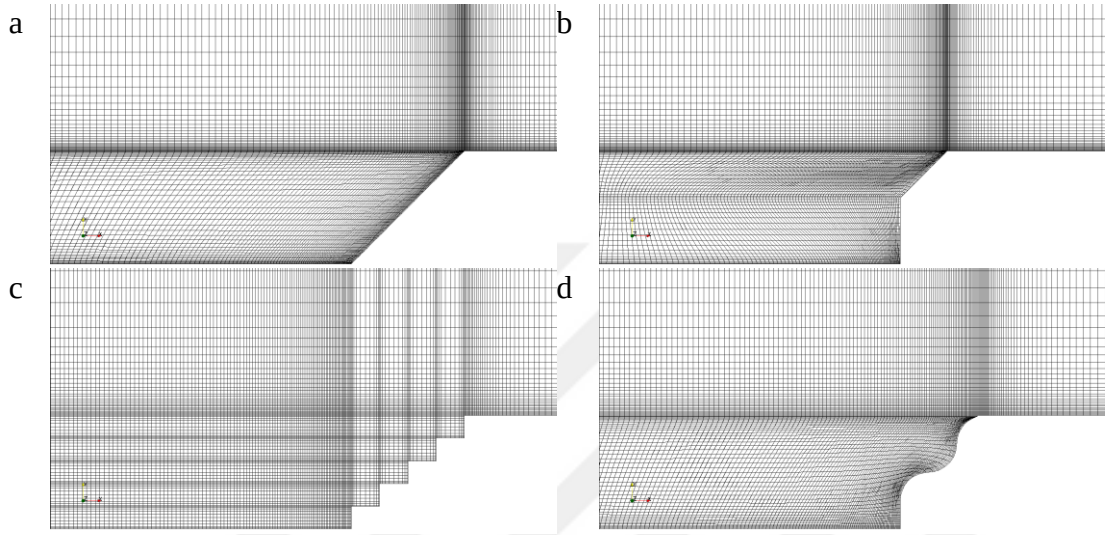

Figure A.1 : Aft wall configurations, close up side view of cavity aft region. a) PAW1 b) PAW2 c) PAW3 d) PAW4.

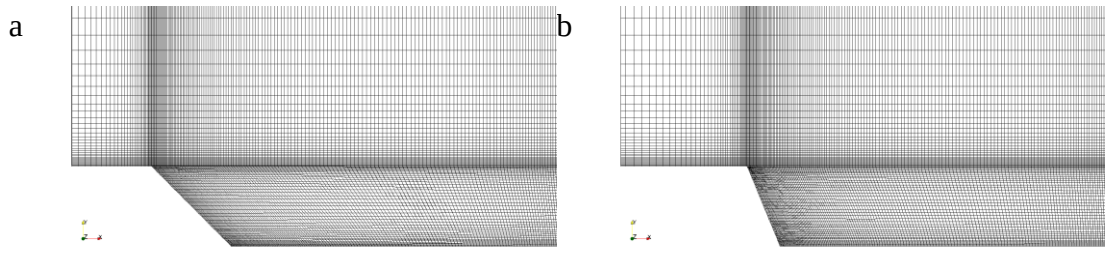

Figure A.2 : Front wall configurations, close up side view of cavity front region. a) PFW1 b) PFW2.

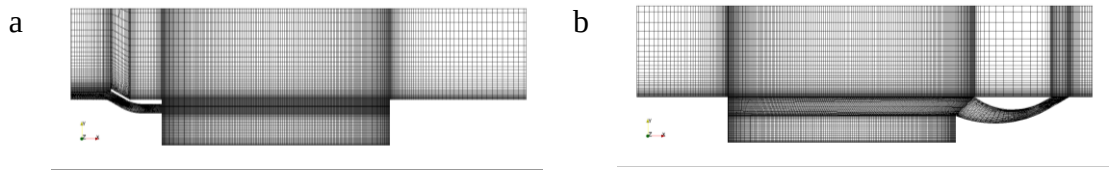

Figure A.3 : Passive injection-suction configurations, close up side view of cavity region. a) PIS1 b) PIS2.

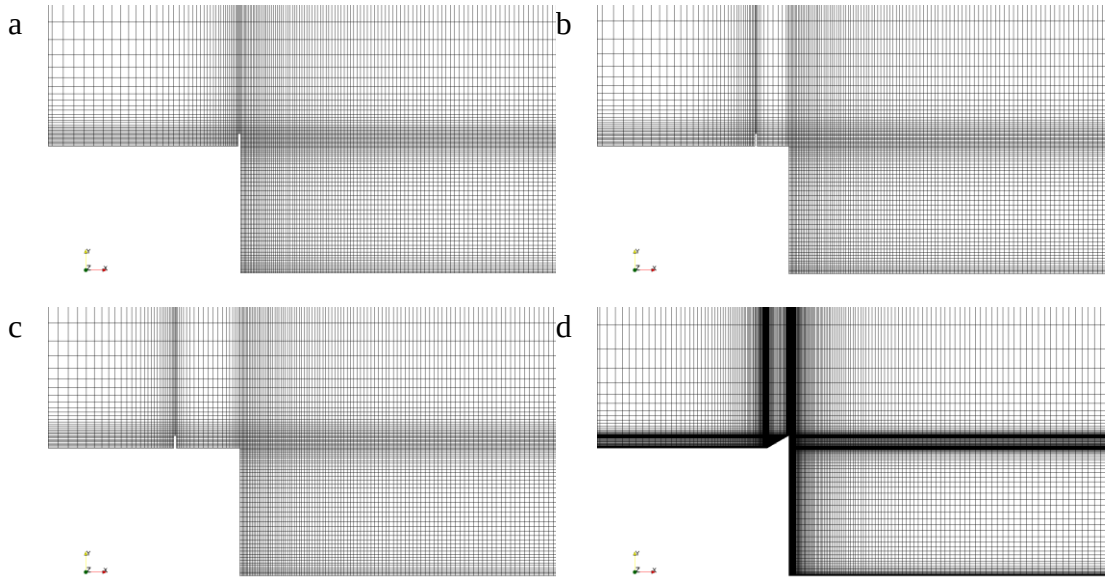

Figure A.4 : Spoiler configurations, close up side view of cavity front region. a) PS1 b) PS2 c) PS3 d) PS4.

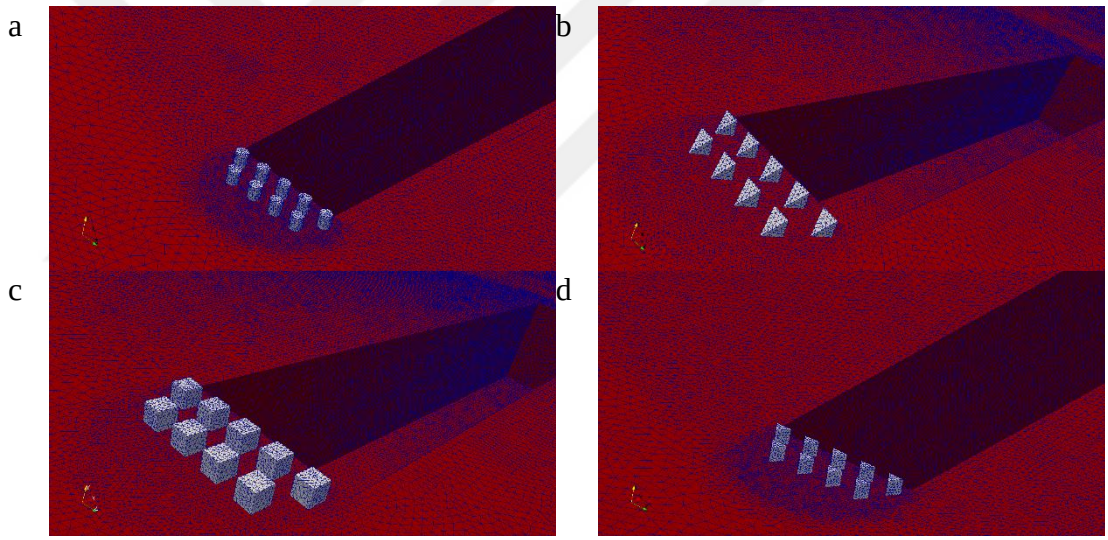

Figure A.5 : Vortex generator configurations, close up view cavity upstream region. a) PVG1 b) PVG2 c) PVG3 d) PVG4.

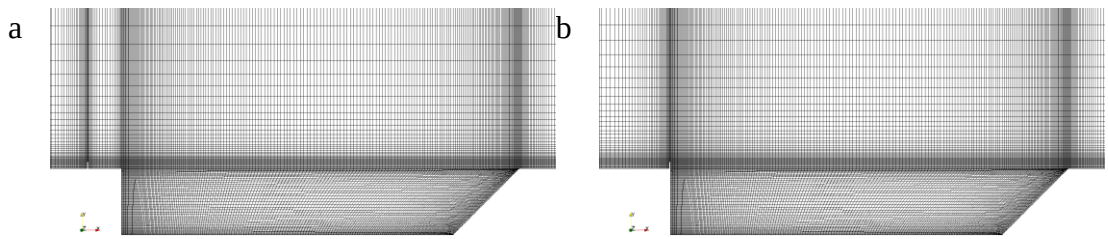

Figure A.6 : Combined configurations, close up side view of cavity region. a) PC1 b) PC2.

CURRICULUM VITAE

Name Surname **:** Oğuzhan Demir

Place and Date of Birth **:** Macon/France, 05/06/1993

E-Mail **:** demirog16@itu.edu.tr

EDUCATION:

- **B.Sc.** **:** 2016, University of Turkish Aeronautical Association, Faculty of Aeronautics and Astronautics, Aeronautical Engineering
- **M.Sc.** **:** 2019, Istanbul Technical University, Department of Aeronautical and Astronautical Engineering, Aeronautical and Astronautical Engineering Program

PROFESSIONAL EXPERIENCE AND REWARDS:

- 2017-2018: ANATEK Technology Transfer Industry and Trade Inc., R&D Engineer
- 2018-Present: Roketsan Missiles Inc., R&D Engineer

PUBLICATIONS, PRESENTATIONS AND PATENTS ON THE THESIS:

Guleren, K. M., Turk, S., Demircan, O. M., and Demir, O. 2018. Numerical Analysis of the Cavity Flow subjected to Passive Controls Techniques. *IOP Conference Series: Materials Science and Engineering,326*, 012015.

Demircan, O. M., Demir, O., Turk, S., and Guleren, K. M. 2018. Aeroacoustics Analysis of a Hybrid Control Method for the Flow-Induced Noise Generation of Transonic Cavity Flows. *Tenth International Conference on Computational Fluid Dynamics (ICCFD10),* July 9-13, 2018 Barcelona, Spain.

Demir, O., Çelik, B., and Guleren, K. M. 2018. Transonik Akışlarda Girdap Üreteçlerinin Kavite Gürültüsüne Etkisi. *VII. Ulusal Havacılık ve Uzay Konferansı*, September 12-14, 2018 Samsun, Turkey.

Demir, O., Çelik, B., and Guleren, K. M. 2019. Noise Reduction of Open Cavities by Passive Flow Control Methods at Transonic Speeds using OpenFOAM. *31st International Conference on Parallel Computational Fluid Dynamics (ParCFD'2019)*, May 14-17 Antalya, Turkey.

OTHER PUBLICATIONS, PRESENTATIONS AND PATENTS